University of Alberta

Design, Fabrication and Characterization of Surface Acoustic Wave Filters with Linewidths of 0.25 down to 0.1 μm

By

Yunlei Li

A thesis submitted to the faculty of Graduate Studies and Research in partial fulfillment of the requirements for the degree of Master of Science

Department of Electrical Engineering

Edmonton, Alberta

Fall 1996

National Library
of Canada

Acquisitions and
Bibliographic Services Branch

395 Wellington Street
Ottawa, Ontario
K1A 0N4

Bibliothèque nationale
du Canada

Direction des acquisitions et
des services bibliographiques

395, rue Wellington
Ottawa (Ontario)
K1A 0N4

Your file Votre référence

Our file Notre référence

The author has granted an irrevocable non-exclusive licence allowing the National Library of Canada to reproduce, loan, distribute or sell copies of his/her thesis by any means and in any form or format, making this thesis available to interested persons.

L'auteur a accordé une licence irrévocable et non exclusive permettant à la Bibliothèque nationale du Canada de reproduire, prêter, distribuer ou vendre des copies de sa thèse de quelque manière et sous quelque forme que ce soit pour mettre des exemplaires de cette thèse à la disposition des personnes intéressées.

The author retains ownership of the copyright in his/her thesis. Neither the thesis nor substantial extracts from it may be printed or otherwise reproduced without his/her permission.

L'auteur conserve la propriété du droit d'auteur qui protège sa thèse. Ni la thèse ni des extraits substantiels de celle-ci ne doivent être imprimés ou autrement reproduits sans son autorisation.

ISBN 0-612-18289-4

Canada

University of Alberta

Library Release Form

Name of Author: Yunlei Li

Title of Thesis: Design, Fabrication and Characterization of Surface Acoustic Wave Filters with Linewidths of 0.25 down to 0.1 μm

Degree: Master of Science

Year this degree Granted: 1996

Permission is hereby granted to the University of Alberta Library to reproduce single copies of this thesis and to lend or sell such copies for private, scholarly, or scientific research purposes only.

The author reserves all other publication and other rights in association with the copyright in the thesis, and except as hereinbefore provided, neither the thesis nor any substantial portion thereof may be printed or otherwise reproduced in any material form whatever without the author's prior written permission.

Yunlei Li

Dept. of Electrical Engineering
University of Alberta
Edmonton, T6G 2G7
Canada

Date: Sept. 25, 1996

University of Alberta

Faculty of Graduate Studies and Research

The undersigned certify that they have read, and recommend to the Faculty of Graduate Studies and Research for acceptance, a thesis entitled **Design, Fabrication and Characterization of Surface Acoustic Wave Filters with Linewidths of 0.25 down to 0.1 μm** submitted by **Yunlei Li** in partial fulfillment of the requirements for the degree of **Master of Science**.

Robert Fedosejevs
Dr. R. Fedosejevs (Supervisor)

Ronald P.W. Lawson
Dr. R.P.W. Lawson

M R Freeman
Dr. M. R. Freeman

Date: Oct. 3, 1996

To the Lord

The fear of the God is the beginning of knowledge (proverbs 1:7)

Abstract

This project investigates the design, fabrication and characterization of Surface Acoustic Wave (SAW) filters with linewidths of 0.25 down to 0.1 μm. The filters consist of two identical unapodized interdigital transducers on 128° rotated YX-cut $LiNbO_3$ substrate. To eliminate finger reflections from second order effects, a split-finger geometry was used in the transducer design. The center frequencies of the filters designed are 2 and 5 GHz for 0.25 and 0.1 μm linewidth devices, respectively, which cover the current most interesting frequency range in mobile telecommunications worldwide. The filters were fabricated using laser plasma X-ray lithography with the masks made by E-beam lithography using a SEM interfaced with a personal computer. The E-beam lithography processing was characterized, and X-ray lithography applied with the results that the 0.25 μm linewidth device was produced and the 0.1 μm linewidth mask achieved. The SAW filters were bonded to Aluminum transmission lines on $LiNbO_3$ and then mounted onto a circuit board having Copper impedance matched microstrip lines for testing. The 0.25 μm linewidth filter was tested using a HP 8510 Network Analyzer and the time gating technique was employed to eliminate electromagnetic feedthrough signals. The final frequency response of the filter showed a center frequency of 1.93 GHz with 30 dB insertion loss and 3 dB bandwidth of 95 MHz, close to the expected performance of our simple design.

Acknowledgment

I am greatly indebted to my supervisor Professor Robert Fedosejevs. First, this is because he provided me with this graduate study opportunity with financial assistantships. Also, I benefited a lot from his guidance, encouragement, advice, discussions. His support and help have made my graduate study easier. His success and attitude towards science have inspired me and will continue to guide me through my future career.

I would like to give my deep thanks to Dr. Romauld Bobkowski for his collaboration in my thesis project. His many valuable explanations, suggestions, and discussions have helped the solutions of problems in my experimental work. He also gave many good suggestions to my thesis writing.

I wish to give my special thanks to Professor RPW Lawson for his encouragement, support and a lot of help in my graduate study.

I would also like to acknowledge the Alberta Microelectronic Centre Fellowship to support my research, and special thanks are given to Graham Mckinnon and Glen Fizpatrick for their help when I was working at AMC for this thesis project.

I would like to acknowledge help from Dr. Tinga in providing access to the HP 8756A network analyzer and Telecommunications Research Laboratories for providing access to the HP 8510B network analyzer.

I give thanks to Dr. James N. Broughton for preparing the low stress Si_3N_4 thin film, Barry Arnold for doing the gold electroplating, and Blair Harwood for a lot of technical help. I also appreciate the help from Yanmin Li and Ying Tusi during this graduate study.

Finally, I would like to thank my dear wife Xiaoqing Luo for her love, understanding, patience and company, and my parents for their continuing encouragement and support throughout of my study.

Table of contents

1. Introduction 1

2. The Surface Acoustic Wave Band Pass Filter 5

2.1 Linear Phase SAW Filters 5

2.2 The Delta Function Model 7

2.3 The Impulse Response and IDT Weighting Methods 9

2.3.1 Impulse Response and Fourier Transform 9

2.3.2 Apodization Weighting 10

2.3.3 Withdrawal Weighting 12

2.4 Window Function Technique 12

2.5 SAW Bandpass Filter Parameters 15

3. GHz Range Linear Phase SAW Filter Design 17

3.1 Introduction 17

3.2 Transducer Analysis 18

3.2.1 Equivalent Circuit Model 18

3.2.2 Three Port Network Model 21

3.3 Second Order Effects 25

3.3.1 Finger Reflections 25

3.3.2 Electromagnetic Feedthrough 27

3.3.3 Acoustic Attenuation 27

3.4 SAW Filter Design 28

3.4.1 2 GHz Filter 28

3.4.2 5 GHz Filter 34

3.5 SPUDT and IIDT Configurations 36

3.5.1 Single Phase Unidirectional Transducer (SPUDT) 36

3.5.2 Interdigited Interdigital Transducer (IIDT) 38

4. Fabrication of 0.25 and 0.1 μm Linewidth SAW Filters 40

4.1 E-beam Lithography-Making the Mask 40

4.1.1 Electron Beam Lithography 40

4.1.2 NPGS 44

4.1.3 Mask Making Process 47

4.1.4 Characterization of 0.25 and 0.1μm Linewidth Mask Making Process 48

4.1.5 Proximity Effect 59

4.1.6 Masks 62

4.2 X-ray Lithography-producing the Device 64

4.2.1 Laser Plasma X-ray Lithography 64

4.2.2 Device Production 66

5. Characterization of the 0.25 μm Linewidth SAW Filter 69

5.1 Filter Testing 69

5.1.1 Packaging Design 69

5.1.2 Testing 71

5.2 Time Gating 71

5.3 Characterization of the 0.25 μm Linewidth Filter 72

6. Conclusion 82

References 84

Appendix 1 The SAW Filter Layout Generating Program--SAWF.BSC 90

Appendix 2 Stereoscan SEM 250-Operating Procedures for E-beam Writing 97

A2.1 Preparations 97

A2.2 E-beam Writing Procedures 97

List of Tables

		Page
Chapter 1		
Table 1.1	Basic properties of some SAW substrates	2
Chapter 3		
Table 3.1	Substrate parameters used in determination of acoustic radiation conductance	29
Chapter 4		
Table 4.1	PMMA thickness and preparation for different feature size masks	49
Table 4.2	Exposures for writing different feature size IDT finger patterns	54
Chapter 5		
Table 5.1	The configuration parameters for the 1.0 μm linewidth SAW filter	73
Table 5.2	Characteristic parameters of the 1.0 μm linewidth SAW filter	73
Table 5.3	The configuration parameters for the 0.5 μm linewidth SAW filter	75
Table 5.4	Characteristic parameters of the 0.5 μm linewidth SAW filter	76
Table 5.5	The configuration parameters for the 0.25 μm linewidth SAW filter	77
Table 5.6	Characteristic parameters of the 0.25 μm linewidth SAW filter with spurious responses removed	80

List of Figures

		Page
Chapter 1		
Figure 1.1	Schematic of a SAW device	1
Figure 1.2	Orientation of 128^0 rotated lithium niobate cut given in Table 1-1 **n** is surface normal, **p** is surface-wave propagation direction	3
Chapter 2		
Figure 2.1	A SAW filter employing uniform finger spacing and constant finger overlap length IDTs	5
Figure 2.2	Transfer function components for the SAW filter with uniform IDTs and symmetric apodization patterns	6
Figure 2.3	IDT Delta function model with one source for each excited electrode	7
Figure 2.4	Calculated magnitude response $\|H_1(f)\|$ of uniform IDT with 20 finger pairs and center frequency f_0=100 MHz using delta-function model	9
Figure 2.5	Transversal filter	11
Figure 2.6	Bandpass filter using apodized transducer and its impulse response	11
Figure 2.7	An example of withdrawal weighting	12
Figure 2.8	Window functions in both the frequency and time domains and their influence on overall filter response. Note that a SAW filter has a "built-in' rectangular window in the time domain associated with the finite length of an IDT along a piezoelectric substrate.	13
Figure 2.9	An additional time-domain cosine-weighting function is used, in addition to the "built-in" rectangular window of the SAW IDT, to reduce the ripple in the passband amplitude response of the SAW filter in Figure 2.8	14
Figure 2.10	Some parameters required for specifying the desired performance of a SAW bandpass filter. Shown are the amplitude and phase responses as a function of frequency	15
Chapter 3		
figure 3.1	Side view of one finger period section of an IDT, showing electric field patterns. (a) Actual field pattern (b) "Crossed-field" approximation (c) "In-line-field" approximation	19
Figure 3.2	Mason equivalent circuit for one period section. The negative capacitors are short-circuited for the "crossed-field" model	19
Figure 3.3	Transducer composed of N period sections, acoustically in cascade and electrically in parallel	19
Figure 3.4	Overall equivalent circuit for SAW filter in crossed-field model	21

Figure 3.5	Schematic diagram of a three-port network for an interdigital transducer with an arbitrary two-port electric matching network	22
Figure 3.6	Schematic of the shunt matching network for an IDT	24
Figure 3.7	SAW reflections from fingers of split-electrode IDT give resultant minimum at center frequency	26
Figure 3.8	The split-finger IDT with finger width and spacing of $\lambda_0/8$	28
Figure 3.9	Equivalent circuit of the input IDT at center frequency showing the tuning inductor connected in (a) parallel (b) series to tune out the reactance of C_T	30
Figure 3.10	Power flow for triple-transit-interference in bidirectional IDTs	31
Figure 3.11	Plot of amplitude and phase ripples vs. TTI suppression level	32
Figure 3.12	Frequency response of the 2 GHz filter with split fingers calculated by the delta function model	33
Figure 3.13	Frequency response of the 5 GHz filter with split fingers calculated by the delta function model	35
Figure 3.14	Three types of SPUDTs (a) Double-metallization type (b) Lewis type single-metallization type (c) Floating-electrode type	37
Figure 3.15	IIDT SAW filters (a) one track configuration (b) Dual track configuration	39
Chapter 4		
Figure 4.1	Schematic of the electron beam exposure system using the SEM at AMC	41
Figure 4.2	Schematic of (a) electron scattering (b) absorbed electron beam energy distribution of the incident electron beam	42
Figure 4.3	An example of the proximity effect	43
Figure 4.4	Schematic diagram showing the electron beam motion	44
Figure 4.5	E-beam writing for filled polygons with different fill directions andfirst fill side	45
Figure 4.6	The SAW filter layout	46
Figure 4.7	Processing steps for the mask wafer preparation	48
Figure 4.8	Mask making processing steps using the E-beam lithography	49
Figure 4.9	A sample plot of PMMA thickness measurement using Alpha-step 200 profilometer. The thickness and length scales are in microns.	50
Figure 4.10	PMMA thickness vs. spin speed	51
Figure 4.11	A sample test pattern written by the Cambridge Stereoscan 250 SEM	52
Figure 4.12	SEM stage with mask sample mounted on	52
Figure 4.13	Characterization of pattern orientation vs. scan rotation of the SEM	53
Figure 4.14	Plot of linewidth vs. E-beam line dose for writing a 0.25 μm linewidth pattern	55
Figure 4.15	A 0.25 μm line pattern writtern not etched down to the bottom	56

Figure 4.16	Granular structure pattern due to SEM out of focus problem during E-beam writing	56
Figure 4.17	SEM images showing an (a) underexposed (b) overexposed pattern	57
Figure 4.18	A SEM image of a well exposed 0.25 μm linewidth split finger IDT pattern	57
Figure 4.19	A 0.1 μm linewidth mask pattern written under 200X magnification	58
Figure 4.20	A 0.1 μm linewidth mask pattern written under 1000X magnification	58
Figure 4.21	Proximity effect demonstration in writing a 0.1 μm linewidth IDT	59
Figure 4.22	The IDT pattern has been divided into three different regions for proximity effect corrections	60
Figure 4.23	The proximity effect correction for writing a 0.25 μm line-width mask (a) pattern in PMMA before the proximity effect correction (b) mask after the proximity effect correction	60
Figure 4.24	A 0.1 μm linewidth mask written with the same doses but the SEM working at different accelerating voltages (a) 30 kV (b) 40 kV	61
Figure 4.25	The 0.1 μm linewidth mask IDT side bar region is written as a group of lines with the result that (a) single lines were formed when the dose was not enough (b) the IDT finger tips was affected although the exposure for the side was appropriate	62
Figure 4.26	The 0.1 μm linewidth mask IDT side bar region written by polyfill	62
Figure 4.27	SEM images of a (a) 0.25 μm and (b) 0.1 μm linewidth masks	63
Figure 4.28	SEM images of a 0.25 μm linewidth mask in gold pattern	63
Figure 4.29	SEM images of a 0.1 μm mask in gold pattern	64
Figure 4.30	Schematic drawing of the laser plasma X-ray lithography technique	65
Figure 4.31	Device production processing steps by the X-ray lithography	66
Figure 4.32	The full picture of a 0.25 μm linewidth SAW filter fabricated by the laser plasma X-ray lithography technique	67
Figure 4.33	A SEM image of the 0.25 μm linewidth SAW filter showing the Aluminum electrodes	68

Chapter 5

Figure 5.1	A SAW filter mounted on a circuit board with impedance matched microstrip lines and high frequency connectors	70
Figure 5.2	Microstrip line	70
Figure 5.3	Coupled microstrip line	71
Figure 5.4	Power flow in the SAW filter testing using the scalar network analyzer HP 8756A with HP 8350B sweep oscillator	71
Figure 5.5	Frequency response of the 1 μm linewidth SAW filter tested	

Figure 5.9 Time gating is applied to the impulse of Figure 5.8 to remove second order effects caused by electromagnetic feedthrough and triple transit interference. The horizontal and vertical scales are 30 ns and 10 dB per division, respectively 79

Figure 5.10 Amplitude frequency response of the 0.25 μm linewidth filter after spurious responses have been removed. The horizontal and vertical scales are 46 MHz and 6 dB per division, respectively 79

Figure 5.11 The circuitry of the balanced transformer technique for the Electromagnetic feedthrough suppression. Ideally, the transformer converts the unblanced input line to a balanced one 81

List of Abbreviations

Abbreviation	Full Name
COM	Coupling-of-modes
CTC	Center to center
DUV	Deep ultra violet
EBL	Electron beam lithography
EM	Electromagnetic feedthrough
FEUDT	Floating electrode unidirectional transducer
FIR	Finite impulse response
GUDT	Group unidirectional transducer
HMDS	Hexamethylenedisiloxane
IDFT	Inverse discrete Fourier transform
IDT	Interdigital transducer
IF	Intermediate frequency
IIDT	Interdigited interdigital transducer
LS	Line spacing
MSC	Multistrip coupler
NPGS	Nanometer pattern generation system
PECVD	Plasma enhanced chemical vapor deposition
RPM	Revolutions per minute
RF	Radio frequency
SAW	Surface acoustic wave
SEM	Scanning electron microscope
SMT	Surface mount technology
SPUDT	Single-phase unidirectional transducer
TTI	Triple transit interference
TTS	Triple transit suppression
UDT	Unidirectional transducer
UV	Ultra violet
XRL	X-ray lithography
VLSI	Very large scale integrated circuit

List of Symbols

Symbol	Meaning	Unit
A_{p-p}	Peak to peak amplitude ripple	dB
BW_4	4 dB bandwidth	MHz
c	Speed of light	m/s
θ	Transit angle of one period finger section of an IDT	°
C_0	Static electrode capacitance of one period section per unit length	F/pair·cm
C_s	Static electrode capacitance of one period section	F/pair
C_T	IDT capacitance	F
d	Separation between two IDT phase centers	cm
ε_r	Dielectric constant	
f_0	SAW filter center frequency	GHz
Δf	3 dB bandwidth	MHz
ϕ_{p-p}	Peak to peak phase ripple	°
IL	Insertion loss	dB
k	Phase constant	m^{-1}
K^2	Piezoelectric coupling coefficient	
L	IDT finger width	μm
λ_0	Acoustic wavelength at center frequency	μm
N	Number of finger pairs of an IDT	pair
Q_e	External circuit Q of an IDT	
Q_L	Loaded Q of an IDT	
Q_r	Acoustic radiation Q of an IDT	
R_0	Equivalent electrical impedance of the free piezoelectric surface	Ω
α	Surface acoustic wave attenuation coefficient per unit length	cm^{-1}
α_t	Acoustic attenuation	dB/μm
S	IDT finger spacing	μm
SF	Shape factor of the SAW amplitude frequency response	
τ	Time separation between two IDT phase centers	s
v	Surface acoustic wave velocity	m/s
W	IDT finger overlap length	μm
Z_0	Characteristic impedance of a microstrip line	Ω

Symbol	Meaning	Unit
A_{p-p}	Peak to peak amplitude ripple	dB
BW_4	4 dB bandwidth	MHz
c	Speed of light	m/s
θ	Transit angle of one period finger section of an IDT	degree
C_0	Static electrode capacitance of one period section per unit length	F/pair·cm
C_S	Static electrode capacitance of one period section	F/pair
C_T	IDT capacitance	F
d	Separation between two IDT phase centers	cm
ε_r	Dielectric constant	
f_0	SAW filter center frequency	GHz
Δf	3 dB bandwidth	MHz
ϕ_{p-p}	Peak to peak phase ripple	°
IL	Insertion loss	dB
k	Phase constant	m^{-1}
K^2	Piezoelectric coupling coefficient	
L	IDT finger width	μm
λ_0	Acoustic wavelength at center frequency	μm
N	Number of finger pairs of an IDT	pair
Q_e	External circuit Q of an IDT	
Q_L	Loaded Q of an IDT	
Q_r	Acoustic radiation Q of an IDT	
R_0	Equivalent electrical impedance of the free piezoelectric surface	Ω
α	Surface acoustic wave attenuation coefficient per unit length	cm^{-1}
α_t	Acoustic attenuation	dB/μm
S	IDT finger spacing	μm
SF	Shape factor of the SAW amplitude frequency response	
τ	Time separation between two IDT phase centers	s
v	Surface acoustic wave velocity	m/s
W	IDT finger overlap length	μm
Z_0	Characteristic impedance of a microstrip line	Ω

1 Introduction

Surface Acoustic Wave (SAW) devices are now used in a wide range of applications in modern electronics. The theoretical foundation of surface acoustic waves was established as early as the 19th century by Lord Rayleigh when he made his research into earthquakes. He demonstrated that a homogeneous isotropic elastic solid can support mechanical waves which are confined within several wavelengths of the surface, and studied the properties of such waves (also known as Rayleigh waves). However, the real application of this scientific finding to our modern SAW devices remained unexploited until 1965 when White and Voltmer[1] demonstrated the important role of the Interdigital Transducer (IDT) in exciting surface acoustic waves efficiently on piezoelectric substrates such as quartz. The basic configuration of such a device is illustrated schematically in Figure 1.1, in which the surface acoustic wave is launched and received by the two IDTs via the piezoelectric effect, thus realizing signal transfer. Also, since the acoustic wave which carries the energy is within a wavelength of the surface, it is easily intercepted and processed anywhere on its propagation path. Therefore, SAW devices are especially important in signal processing applications, e.g. in radar, fiber optics, mobile radio, cellular phone, TV as delay lines, filters, oscillators, etc.

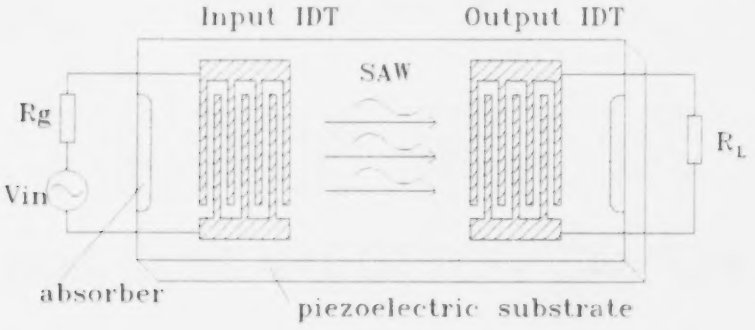

Figure 1.1. Schematic of a SAW device.

The most commonly used piezoelectric crystals are quartz, lithium niobate and lithium tantalate while others have been explored extensively[2]. The basic parameters of these typical substrates are listed in Table 1.1, where K^2 is the electromechanical coupling coefficient, which is a measure of the efficiency of a given piezoelectric in converting an applied electrical signal into mechanical energy associated with a surface acoustic wave. The performance of a device depends on a particular substrate as well as its orientation. Quartz features low cost, high temperature stability (ST-cut), but it has a low electroacoustic coupling coefficient and is only suitable for narrow band applications. Lithium niobate ($LiNbO_3$) and lithium tantalate ($LiTaO_3$) both provide high SAW velocities and strong coupling abilities for certain cuts, so they are among the choices for high frequency and wide band applications while some tradeoffs for temperature stability have to be accepted. Of these two, 128^0 YX-$LiNbO_3$ and 36^0 YX-$LiTaO_3$ have special advantages for GHz range SAW devices. The 128° rot. $LiNbO_3$ orientation is shown in Figure 1.2.

Table 1.1. Basic properties of some SAW substrates[41, 15(p.152)].

Substrate (Cut and propagation direction)	Free surface velocity v	Piezoelectric coupling coefficient K^2	Maximum fractional bandwidth	1st-order temperature coefficient of delay	Attenuation at 1 GHz
	m/s	%	%	$\times 10^6$/C°	dB/μs
Quartz ST,X	3157	0.14	4	0	3.1
$LiNbO_3$ Y,Z	3488	5	24	91	1.07
128°-rot Y,X	3977	5.6	27	72	-
$LiTaO_3$ Y,Z	3254	0.74	10	35	1.14
X,112°Y	3288	0.6	9	18	-
36°Y,X	4216	6.6	34	–30	-

SAW filters are among the most successful SAW devices in modern telecommunications. They have found widespread applications in consumer, commercial

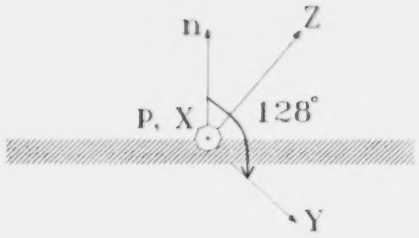

Figure 1.2. Orientation of 128° rotated lithium niobate cut shown in Table 1-1 **n** is surface normal, **p** is surface-wave propagation direction.

and military fields[3]. Compared with conventional L-C filters, SAW filters feature small size, offer wide design flexibility, and more important, can be mass produced by sophisticated semiconductor lithography techniques. As a result, high performance and low cost filters can be easily implemented by SAW technology. In addition, combined with Surface Mount Technology (SMT), these devices are fast replacing their L-C counterparts in mobile and portable equipment [4-6].

In general, SAW filters operate in the frequency range of 10 MHz-1 GHz. The feature sizes of such devices are in microns. Now, intensive research activities have concentrated on pushing them further into the high GHz range to cater for the ever growing demands in such areas as mobile communications[7]. However, the simple scaling of devices to higher frequencies requires smaller separations and narrower linewidth features than available in standard optical lithography processing. This challenge has created two research trends. On the one hand, some researchers tried to utilize harmonic mode operations[8,9] or conventional processing with special design techniques[10], or else choose materials with very high surface wave velocities[11] to make such filters, thus sub-micron lithography processes are avoided. Nevertheless, the penalties paid are the design and processing complexities. On the other hand, all kinds of modern VLSI sub-micron lithography techniques have been explored to fabricate such devices, including E-beam, Ion-beam and X-ray lithography. Up to present, the finest feature sizes in research SAW devices fabricated using these techniques are 50 nm, 0.3 μm and 0.25 μm, respectively[12-14]. It is expected that this trend to higher frequencies and narrow linewidths will continue in the future.

As is well known, although E-beam lithography can produce very fine feature size patterns (less than 0.1 μm), it is not a cost-effective production technique. The same story holds for Ion-beam lithography. Therefore, X-ray lithography is the most promising among the three as a large scale production technique. The main objective of this research project was to show feasibility of the X-ray lithography to mass production of such narrow linewidth SAW devices. The advantage of such a technique is that once a X-ray mask has been fabricated such devices can be manufactured using a single lithographic fabrication step. Therefore, the focus of this project was to design suitable test devices, to fabricate a thin film proximity X-ray exposure mask and to employ the X-ray lithography technique with a laser plasma source to fabricate SAW filters with feature sizes from 0.5 down to 0.1 μm. The results presented here are the design, fabrication and characterization of a SAW filter with 0.25 μm linewidth. In addition, the first stage of a 0.1 μm device fabrication, i.e. a X-ray mask of 0.1 μm linewidth is also demonstrated. In the future, it is hoped that our design can be improved to obtain surface acoustic wave filters with higher performance operating at several GHz.

2 The Surface Acoustic Wave Bandpass Filter

2.1 Linear Phase SAW Filters

As we know, the conventional L-C filter comprises a network of inductors and capacitors. Unlike their L-C counterparts, the SAW filter is implemented by the SAW delay line structure. Figure 2.1 shows a simple SAW filter, which consists of two IDTs with uniform finger period (λ_0) and constant finger overlap length (W). Such a device is fabricated by depositing a thin metal film on a piezoelectric substrate and then patterning it using photolithography techniques.

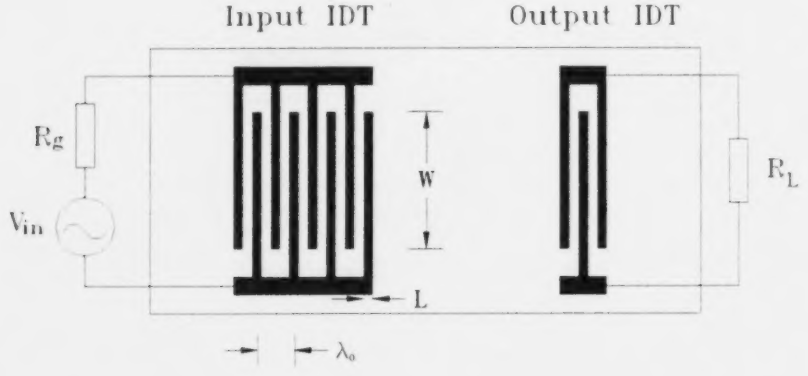

Figure 2.1. A SAW filter employing uniform finger spacing and constant finger overlap length IDTs.

The operation of the SAW filter is as follows: When an oscillatory voltage is applied to the input IDT, the transducer generates a periodic electric field corresponding to its periodic finger positions. A surface acoustic wave is then excited and launched due to the piezoelectric effect. At the output transducer, the surface acoustic wave is converted back to a voltage signal. The detailed mechanism of the SAW propagation on the surface of an unbound piezoelectric elastic surface involves solving the acoustic and electromagnetic wave equations and can be found in a number of text books such as [15].

To efficiently generate the acoustic wave, the finger width L is usually made equal to the finger spacing, and the finger period is kept constant, equal to the wavelength λ_o.

Then, the center frequency of such a filter is given by $f_o = v/\lambda_o = v/4L$, where v is the surface acoustic wave velocity. So the operating frequency is related to the feature size of the finger widths, which are determined by the lithography technique. The advantages of such filters include that they can achieve impressive band pass performances, such as very flat pass-bands, sharp band edges and high stop-band rejection ratios. However, since the surface wave transducers give zero response at zero frequency, SAW devices can not be used for low pass filtering.

In Figure 2.1, both of the two IDTs are unapodized, which means that the finger overlap length within each IDT is a constant. In addition, the finger spacing is uniform. For such a filter, the transfer function can be divided into four components as illustrated in Figure 2.2 , which is[19]:

$$H(f) = \frac{V_{out}}{V_{in}} = H_1(f)H_2^*(f)e^{-jkd}\, e^{-\alpha d} \qquad (2.1)$$

where $H_1(f)$ and $H_2(f)$ are the frequency responses corresponding to the input and output IDTs, respectively. The third term e^{-jkd} is the phase delay between the two IDTs,

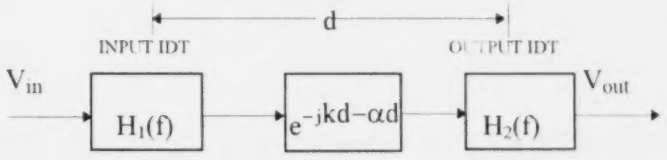

Figure 2.2. Transfer function components for the SAW filter with uniform IDTs and symmetric apodization patterns.

where $k = 2\pi/\lambda = 2\pi f/v$ is the phase constant related to the signal frequency f , and d is the separation between the phase centers of the two IDTs. The fourth term $e^{-\alpha d}$ is introduced here to describe the acoustic wave attenuation, where α is the attenuation coefficient per unit length. $H_2^*(f)$ is the complex conjugate response of $H_2(f)$, with

$$|H_2(f)| = |H_2^*(f)|$$

Since the delay term varies linearly with the frequency, this filter gives a linear phase response. A key feature of a linear phase filter is that all of the frequency

components of an input signal would experience the same time delay and attenuation in passing through the filter without distortion. It can be proven that: if either or both IDTs are apodized, the filter still produces a linear phase response as long as the apodization pattern is symmetric about the IDT vertical central axis. Here, the apodization means the finger overlap width as a function of the finger positions. In this project, only linear phase filters are considered and discussed.

2.2 The Delta Function Model

The Delta function model was proposed by Tancrell and Holland[16]. Although it is an over-simplified model, it provides important information on the transfer function of a SAW filter. Consider the input uniform transducer as shown in Figure 2.3. When a voltage is applied to the two bus bars of the IDT, an electric field is set up under the transducer and surface waves are launched. The wave amplitude is proportional to the wave surface potential Φ and electric field E. The delta function model approximates the complex electric field distribution between adjacent fingers of an excited IDT as a discrete number

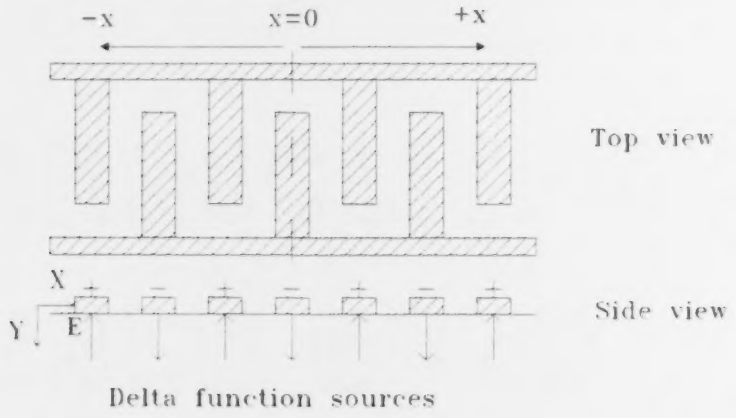

Figure 2.3. IDT Delta function model with one source for each excited electrode.

of delta function sources as shown in Figure 2.3. Let us take x = 0 at the center of the IDT, and assume the IDT has M electrodes. For the frequency response of the IDT, each individual source contributes the same amplitude, but a different phase term e^{-jkx_n},

where x_n corresponds to the position for each source. If we sum up the contributions of all the delta sources along the length of the IDT, the resultant frequency response is[19]:

$$H_1(f) = \sum_{n=-(M-1)/2}^{(M-1)/2} (-1)^n A_n \exp(-jkx_n) \qquad (2.2)$$

where the term $(-1)^n$ relates the alternating electrode polarity, and A_n is an amplitude parameter corresponding to the finger apodization. Since delta function model only gives the relative insertion loss, A_n can be taken to be unity for the uniform finger apodization. In equation (3.2), the wave number k is related to the frequency f by $k = \omega/v = 2\pi f/v$. Close to the center frequency f_0, equation (3.2) can be expanded into a cosine series and finally yields a sinc function response given by[17]

$$|H_1(f)| \cong M \left| \frac{\sin\{M\pi(f - f_0)/2f_0\}}{M\pi(f - f_0)/2f_0} \right| \qquad (2.3)$$

where the term in the absolute sign is the sinc function defined as $\mathrm{sinc}(X) = (\sin X)/X$, with $X = M\pi(f-f_0)/2f_0$.

A calculated example frequency response for one excited IDT with 20 finger pairs (M = 40) and central frequency 100 MHz is shown in Figure 2.4. The first main peak occurs at frequency f_0, and this is called the fundamental response. The zeros nearest to f_0 are at $f = f_0 \pm 2f_0/M$. Roughly speaking, the transducer works effectively within a 4 dB bandwidth below its main peak bounded by the points $f = f_0 \pm f_0/M$. Thus, the fractional bandwidth $BW_4 = (100/N)\%$, where N = M/2 is the number of finger pairs in the IDT.

As shown in Figure 2.4, the first sidelobes are approximately 12 dB below the main peak, which is typical for sinc function responses. It can be shown that the output IDT has the same sinc function response as the input IDT. The total response of the filter is determined by equation (2.1), which gives 24 dB sidelobe rejection. Often, the bandwidth of one IDT is made much wider than that of the other so that the frequency response of the filter is only determined by the narrower bandwidth IDT.

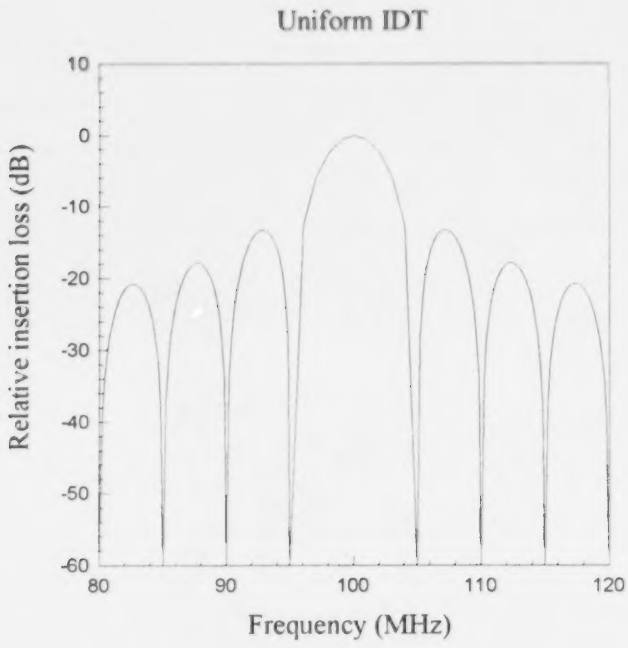

Figure 2.4. Calculated magnitude response $|H_1(f)|$ of uniform IDT with 20 finger pairs and center frequency f_0 = 100 MHz using the delta-function model.

2.3 The Impulse Response and IDT Weighting Methods

2.3.1 Impulse Response and Fourier Transform

When a very short electrical pulse approximating a δ-function is applied to the input of a filter, the output is its impulse response h(t). The impulse response describes the "memory" of the filter, which tells us how the output at the present time is affected by an input at a past time. The impulse response h(t) and frequency response H(f) consist of a pair of Fourier transforms

$$H(f) = \int_{-\infty}^{+\infty} h(t)e^{-j2\pi ft}dt \tag{2.4a}$$

$$h(t) = \int_{-\infty}^{+\infty} H(f)e^{j2\pi ft}df \tag{2.4b}$$

and either can be derived if the other is known. There are certain properties that hold for all Fourier transform pairs, the following two are very useful in relating h(t) and H(f).

1. Shifting Theorem

If h(t) is shifted in time by t_0, the magnitude of H(f) is not affected but its phase is changed by $(-2\pi ft)$. If H(f) is shifted by f_0, the impulse response h(t) is multiplied by $e^{+j2\pi f_0 t}$.

2. Convolution Theorem

Suppose that two filters are cascaded together. The overall frequency response is the product of the individual responses $H_1(f)$ and $H_2(f)$

$$H(f) = H_1(f) \cdot H_2(f) \tag{2.5}$$

The convolution theorem states that the overall impulse response h(t) is related to the individual responses $h_1(t)$ and $h_2(t)$ by

$$h(t) = h_1(t) * h_2(t) \tag{2.6}$$

where * denotes the convolution product , which is defined as

$$h_1(t) * h_2(t) = \int_{-\infty}^{+\infty} h_1(\tau) h_2(t-\tau) d\tau \tag{2.7}$$

The same property also holds; that is, if

$$h(t) = h_1(t) \cdot h_2(t) \tag{2.8}$$

then

$$H(f) = H_1(f) * H_2(f) \tag{2.9}$$

2.3.2 Apodization Weighting

In fact, SAW filters realize the concept of the transversal filter proposed by Kallman in 1940. As shown in Figure 2.5, an ideal transversal filter is a tapped delay line. The input is sampled at the delayed times τ_s by the taps , and the output is the weighted sum of the signals at different taps.

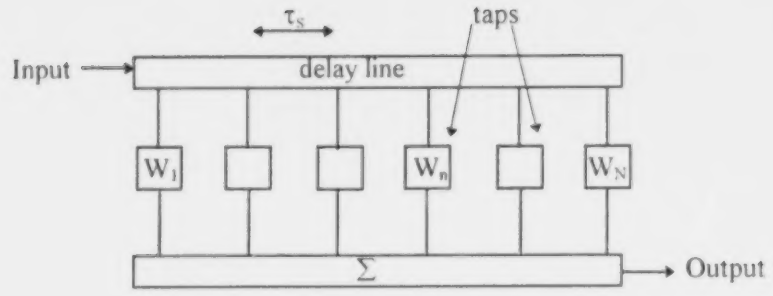

Figure 2.5. Transversal filter.

Figure 2.6 shows a bandpass filter using an apodized transducer with regular electrodes and its impulse response, which behaves exactly like a transversal filter[15].

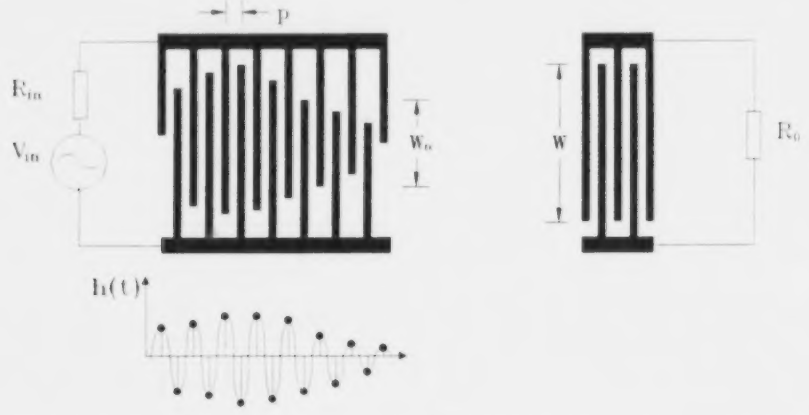

Figure 2.6. Bandpass filter using an apodized transducer and its impulse response.

The delay $\tau_s = p/v$ corresponds to the distance p between the adjacent fingers, where v is the free wave velocity. As shown in Figure 2.6, the impulse response of such a filter is related to the geometry of the apodized transducer. This is manifested by the fact that the impulse response consists of a sequence of discrete delta functions at different finger locations, with amplitudes given by the electrode overlaps W_n. This impulse response is a sampled version of the actual response expected, that is, the envelope of the impulse response shown in Figure 2.6, and its inverse Fourier transform gives its frequency response. Since the filter response is essentially the product of the two transducer

responses, only one transducer is apodized while the other is unapodized with a smooth response function. As a result, the design problem of such a transversal filter is simplified to the design of the apodized transducer.

2.3.3 Withdrawal Weighting

As is well known, one disadvantage of apodization weighting is that the transducer response may suffer the effect of diffraction from narrow fingers, a second order effect. To solve this problem, an alternative technique of withdrawal weighting can be used to achieve the required frequency response. This technique applies to the transducer by selectively omitting some fingers from the transducer, and was first demonstrated by Hartmann[17]. One example of withdrawal weighting is illustrated in Figure 2.7. Withdrawal weighting is only suitable for transducers with relatively narrow bandwidths. Another negative effect is that it may result in poor stop band attenuation. In practical devices, a withdrawal-weighted transducer is often used in conjunction with an apodized transducer, with the latter designed such that adequate stop-band attenuation is obtained.

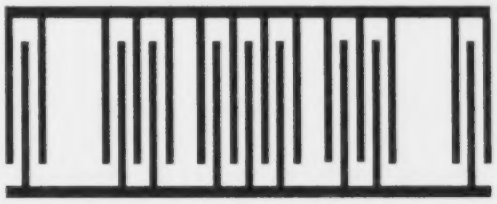

Figure 2.7. An example of withdrawal weighting[15].

2.4 Window Function Technique

Given a frequency response, the corresponding impulse response is infinite in the time domain according to the Fourier transform. Whereas, its realization by a SAW filter has to be cut off in length, resulting in a finite impulse response (FIR) filter. Such an abrupt truncation of the impulse response would produce large ripples in the frequency response, and window functions are often employed to get a good approximation of the required response.

Window function technique was first used in FIR digital filter design to improve the shape of the passband response[18]. Although the frequency response accuracy can be obtained by increasing the duration of the impulse response in space, the window function technique seeks a gradual cutoff instead of an abrupt truncation. For the desired box frequency response as shown in Figure 2.8, the resultant frequency response has a large ripple in the passband because of the straight cutoff by the 'built in' rectangular window function. As shown in Figure 2.9, this ripple can be greatly reduced by the additional cosine window, which provides a smooth truncation to the impulse response. The truncated impulse response is given by

$$h_1(t) = h(t) \cdot w(t) \tag{2.10}$$

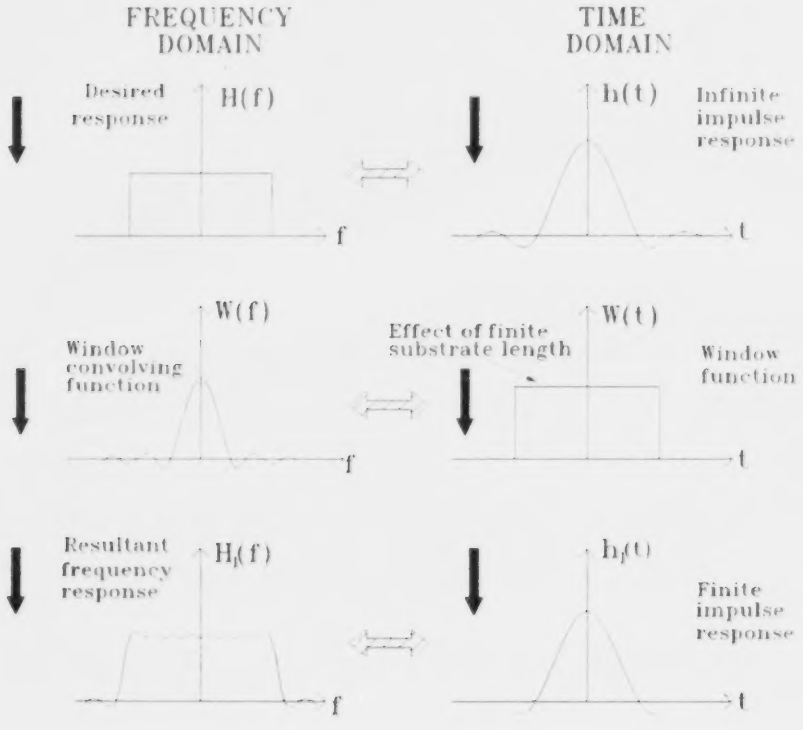

Figure 2.8. Window functions in both the frequency and time domains and their influence on overall filter response. Note that a SAW filter has a " built-in" rectangular window in the time domain associated with the finite length of an IDT along a piezoelectric substrate[19].

while the resultant frequency response $H_1(f)$ is governed by the convolution theorem

$$H_1(f) = H(f) * W(f)$$
$$= \int_{-\infty}^{+\infty} df' W(f') H(f - f') \qquad (2.11)$$

where W(t) is the window function. In addition to cosine weighting, many other widow

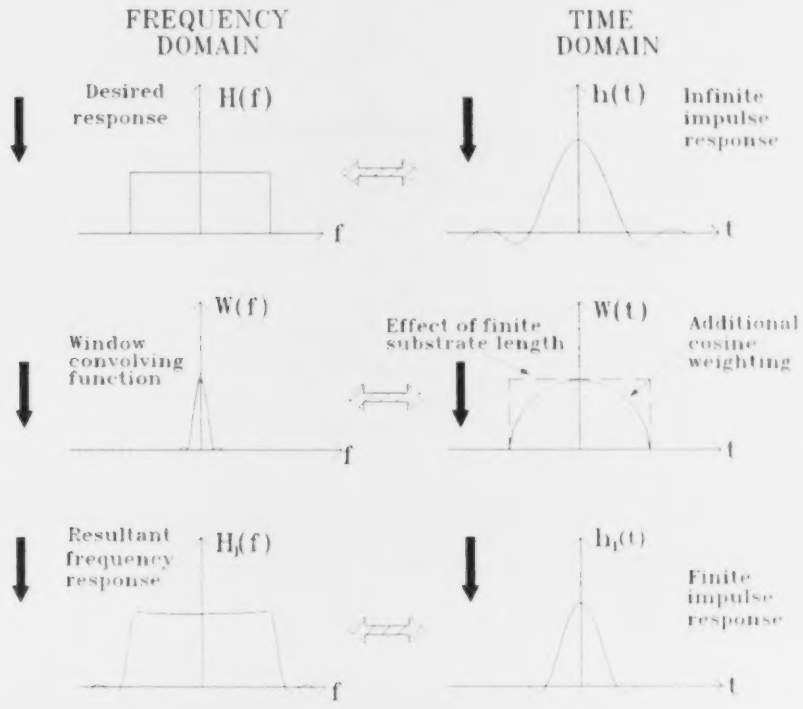

Figure 2.9. An additional time-domain cosine-weighting function is used, in addition to the "built-in" rectangular window of the SAW IDT, to reduce the ripple in the passband amplitude response of the SAW filter in Figure 2.8[19].

functions exist for different design purposes, such as Hamming, Taylor and Dolph-Chebyshev, etc[19]. The drawback of using window functions is that they may produce the largest error in the frequency response around the passband edges. In such cases, an optimization algorithm that spreads out the error uniformly over the frequency can be

used, such as the program by McClellan et al for FIR linear phase digital filter design[20], which is also suitable for applications to SAW filter design after some small modifications.

2.5 SAW Bandpass Filter Parameters

Although there are a variety of design parameters for different applications, the typical SAW bandpass filter frequency response is shown in Figure 2.10. The ideal bandpass response is a rectangular wall with a shape factor SF = 1.0. The actual response has a shape SF > 1.0, and always has amplitude and phase ripples in the passband. The group delay $\tau = -d\phi/d\omega$ describes the linearity of the phase response, where $\phi(\omega)$ is the

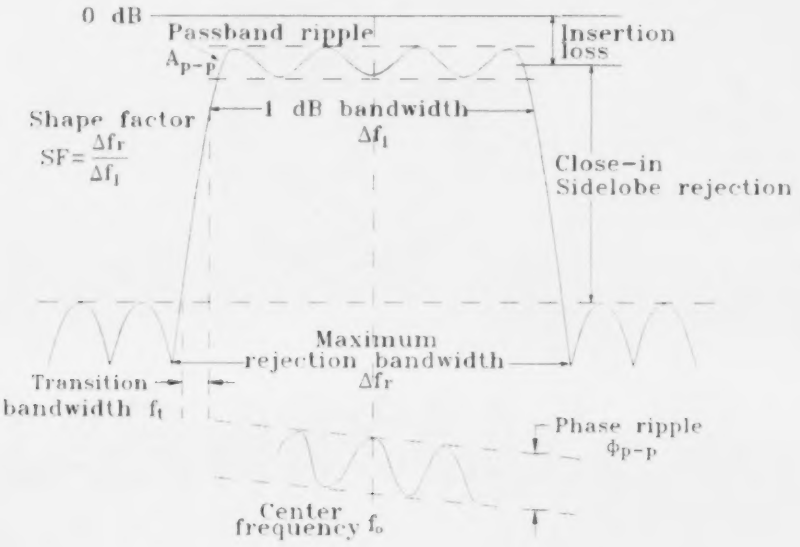

Figure 2.10. Some parameters required for specifying the desired performance of a SAW bandpass filter. Shown are the amplitude and phase responses as a function of frequency[42].

phase angle frequency response of the SAW filter. As shown in Figure 2.10, the definitions of these parameters are as follows:

f_0: the center frequency of the transfer response.

Close-in sidelobe rejection: the amplitude difference between the main peak at center frequency and the first sidelobes in dB.

Insertion loss: $IL = 10\log_{10}\frac{(power\ at\ load\ with\ no\ device\ present)}{(power\ at\ load\ with\ device\ inserted)}dB$

Fractional bandwidth: $BW\% = \frac{\Delta f}{f_0} \times 100\%$,(Δf may be designated at 1 dB, 3 dB or 4 dB amplitude response levels to midband)

Shape factor: $SF = \Delta f_r/\Delta f_1$, (where Δf_r is the maximum filter rejection bandwidth and Δf_1 is the bandwidth measured to the 1-dB amplitude points

Passband ripple $A_{p\text{-}p}$: the peak to peak amplitude ripple in the passband of the SAW filter amplitude frequency response.

Phase ripple $\phi_{p\text{-}p}$: the peak to peak phase ripple of the SAW filter phase frequency response.

3 GHz Range Linear Phase SAW Filter Design

3.1 Introduction

The modern surface acoustic wave filters work in the frequency range of 10 MHz to 1 GHz, which covers a wide range of applications in radio frequency (RF) filtering and signal processing. Currently, GHz SAW filters are in great demand in new telecommunication systems all around the world[7]. Especially, low-loss, wide bandwidth, cost-effective and high performance devices are required[21,22].

The simple SAW filter structure sketched in Figure 2.1 consists of two IDTs facing each other on the surface of a piezoelectric substrate. When an RF voltage is attached to the input IDT, only half of the acoustic energy produced travels towards the output IDT while the other half will be launched in the opposite direction. This causes an intrinsic minimum insertion loss of 3 dB for one transducer and 6 dB for the filter. The other problem associated with this configuration is that the filter will suffer a large amplitude ripple in the pass band and phase ripple. This is related to the Triple Transit Interference (TTI) phenomenon, which will be discussed later. The solution to this problem is to sacrifice insertion loss for a large TTI suppression. Consequently, this kind of filter is often used in the intermediate frequency (IF) section of cellular radio systems, and not suitable for applications to the front-ends , where low insertion loss filters are required.

Many schemes have been developed to reduce the TTI signal. Unidirectional transducers (UDT) provide an effective solution, and have the extra advantage of reducing the insertion loss at the same time. The earliest UDT was the three phase type[23,24], but this implementation involves a cross-over technology, in which metal fingers must run across an insulating dielectric, and also requires complicated matching networks. Subsequently, two phase group type unidirectional transducers (GUDT) were proposed to overcome these difficulties[25-30], however, they still require more than one tuning component per transducer. The most recent development in unidirectional transducers is centered on the new single-phase unidirectional transducers (SPUDT) invented by Hartmann, et al[31]. The initial realization involved a double metallization process. Later, the single metallization SPUDT structure was reported by Lewis[32], and followed by the

floating electrode type UDT (FEUDT) proposed by Yamanouchi et al[33]. Of these three, the Lewis type SPUDT was studied most often due to its design versatility through the Coupling-of-modes (COM) theory[34].

At present, it seems that the most attractive low-loss GHz filter is the interdigited interdigital transducer (IIDT) type presented by Lewis[35]. In this configuration, many bi-directional input and output IDTs are connected in parallel and interleaved together so that the bidirectionality loss can be minimized. The IIDT proposed by Lewis is the one track structure, the dual track configuration was reported later by Hikita to introduce a new coupling scheme for passband ripple suppression[36]. One main problem of IIDT structure is its poor stopband rejection, however, this can be overcome by withdrawal-weighting design approach[37], and a recent 1.9 GHz filter with 30 dB stopband rejection and 1.6 dB insertion loss was reported by Yatsuda[38]. Up to now, the major difficulty of IIDT filter development lies in its design, computer aided design has to be used via mixed scattering matrix approach or equivalent circuit model[39, 40]. Nevertheless, there has been a successful example of 2 GHz low-loss IIDT filter used in the front-ends of an antenna-duplexer in radio communication systems[7].

In this project, the simple bidirectional transducer design was followed. To give a suggestion of the future design work, the layouts and designs of SPUDT and IIDT will be discussed later in this chapter.

3.2 Transducer Analysis

3.2.1 Equivalent Circuit Model

In transducer analysis, the actual electric field distribution in the substrate for one finger period section is often simplified as the crossed field or in-line field model as shown in Figure 3.1. The crossed field model is suitable for describing IDTs fabricated on high K^2 piezoelectric substrates such as lithium niobate while the in-line model is appropriate for IDT designs on low K^2 substrates such as quartz. For either of these two models, the Mason equivalent circuit can be applied to derive the equivalent circuit for the whole IDT. Figure 3.2 shows the Mason equivalent circuit for one period section. The equivalent electrical impedance of the free piezoelectric surface R_0 is derived as[43]:

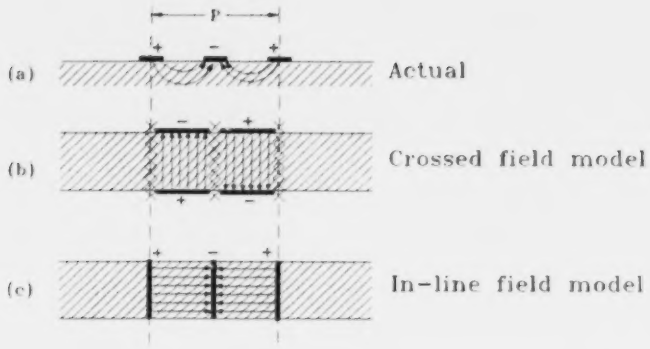

Figure 3.1.Side view of one finger period section of an IDT, showing electric field patterns. (a) Actual field pattern (b) "Crossed-field" approximation (c) "In-line field" approximation[43].

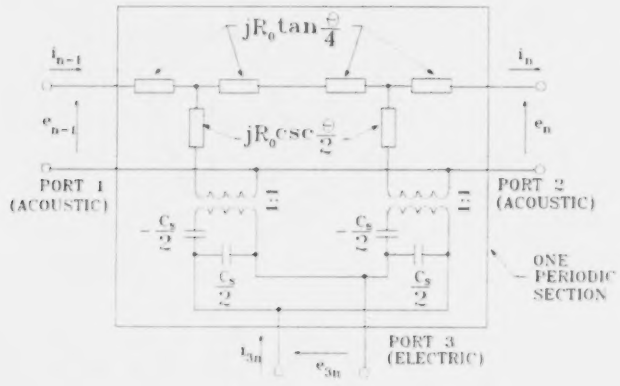

Figure 3.2. Mason equivalent circuit for one period section. The negative capacitors are short-circuited for the "crossed-field" model [43].

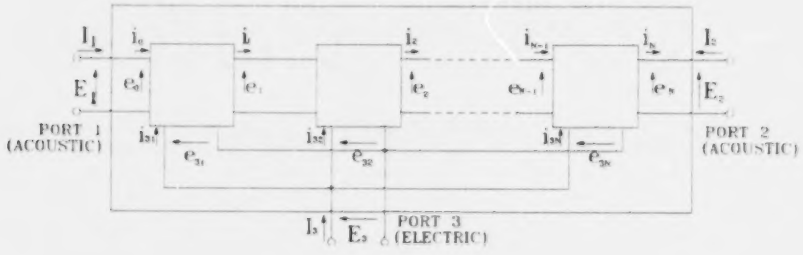

Figure 3.3. Transducer composed of N period sections, acoustically in cascade and electrically in parallel[43].

$$R_0 = \frac{2\pi}{\omega_0 C_s K^2} \tag{3.1}$$

where K^2 is the electromechanical coupling constant, $C_s = C_0 W$ = capacitance/finger pair with C_0 = capacitance/finger pair/unit finger length, W = acoustic aperture of the IDT fingers. And the period section transit angle is defined as:

$$\theta = 2\pi\omega / \omega_0 \tag{3.2}$$

where $\omega_0 = 2\pi f_0$ is the synchronism frequency defined by $f_0 = v/P$ with v the wave velocity and P the period length.

The equivalent circuit of the entire IDT is formed by connecting the electrical ports in parallel and acoustic ports in cascade as shown in Figure 3.3. The standard network analysis and algorithms can be applied to the three port network of the finger section[43,44]. Taking into account of the symmetry of the two acoustic ports with respect to the electric port, we have the following transducer 3-port equation and admittance matrix for unapodized uniform finger spacing IDT using the crossed field model:

$$\begin{bmatrix} I_1 \\ I_2 \\ I_3 \end{bmatrix} = [Y] \cdot \begin{bmatrix} E_1 \\ E_2 \\ E_3 \end{bmatrix} \tag{3.3}$$

$$[Y] = \begin{bmatrix} Y_{11} & Y_{12} & Y_{13} \\ Y_{12} & Y_{11} & -Y_{13} \\ Y_{13} & -Y_{13} & Y_{33} \end{bmatrix} \tag{3.4}$$

and

$$\begin{aligned} Y_{11} &= -jG_0 \cot N\theta \\ Y_{12} &= jG_0 \csc N\theta \\ Y_{13} &= -jG_0 \tan \theta/4 \\ Y_{33} &= j\omega C_T + 4jNG_0 \tan \theta/4 \end{aligned} \tag{3.5}$$

where $G_0 = 1/R_0$, $C_T = NC_s$ = total IDT capacitance (F), N = number of electrode pairs.

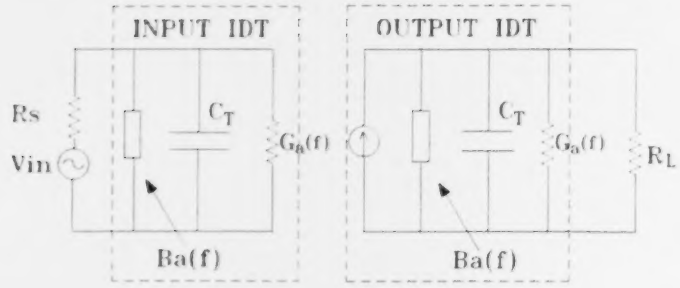

Figure 3.4. Overall equivalent circuit for SAW filter in crossed-field model[19].

From the above derivation, the overall equivalent circuit for a SAW filter, including both IDTs and source and load resistances is shown in Figure 3.4. Note that the equivalent excitation source for the output IDT has been realized as a current source. For the frequencies at the acoustic synchronism f_0, the radiation conductance is[19] :

$$G_a(f_0) = 8K^2 f_0 C_S N^2 \tag{3.6}$$

and for the frequencies near the center frequency, Ga(f) may be generalized as:

$$G_a(f) \approx G_a(f_0)\left|\frac{\sin X}{X}\right|^2 \approx 8N^2 G_0\left|\frac{\sin X}{X}\right|^2 \tag{3.7}$$

where $X = N\pi(f - f_0)/f_0$. In the equivalent circuit, $B_a(f)$ is called the radiation susceptance, which results from the Impulse Response Model[45] and can be expressed as:

$$B_a(f) = \frac{8N^2 G_0\{\sin(2X) - 2X\}}{2X^2} \tag{3.8}$$

Radiation susceptance is a reactive parameter (i.e., $\pm jB$) which goes to zero at center frequency. Near center frequency it is normally quite small compared to the IDT capacitance C_T and is often omitted in calculations as a result.

3.2.2 Three Port Network Model

The three port network model introduced by Smith allows us to derive expressions for transfer functions and take the matching circuit into account in the IDT analysis. In the three port network model as shown in Figure 3.5, each of the two acoustic ports is

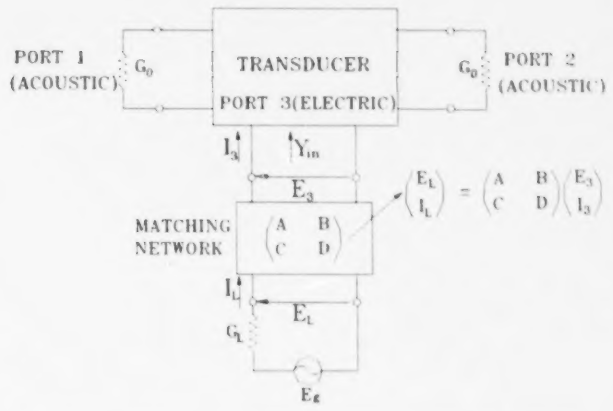

Figure 3.5. Schematic diagram of a three-port network for an interdigital transducer with an arbitrary two-port electric matching network[46].

terminated by a matched admittance G_0 to represent the reflectionless acoustic ends, and there is an impedance matching network connected between the transducer and the electrical terminal driven by the signal source. For this network, a set of complex transfer functions T_{ij} can be defined as[47]:

$$T_{ij} = 2\sqrt{\frac{G_i}{G_j}}\frac{E_i}{E_j} \tag{3.9}$$

where E_i is the "voltage" of the transmitted or reflected wave delivered to load G_i at port i when a Thevenin generator of voltage E_j and a series conductance G_j drives the transducer at port j. The power scattering coefficients are:

$$P_{ij} = \frac{P_i}{(P_{avail})_j} = \left|T_{ij}\right|^2 \tag{3.10}$$

where P_i is the power transmitted or reflected from port i ,and $(P_{avail})_j$ is the power available from a matched generator at port j. Therefore, p_{ii} represents the fraction of power reflected when power is incident at port i, and p_{ij} is the fraction of power transmitted from port i when power is incident at port j. The definition of the scattering loss in dB follows:

$$L_{ij} = -10\log_{10}\left(P_{ij}\right) \tag{3.11}$$

Among these scattering parameters, the most important are the electroacoustic transfer function T_{13}, T_{23} and the acoustic reflection coefficient T_{11}, T_{22}. The symmetry of the acoustic ports dictates: $T_{13} = T_{23}$ and $T_{11} = T_{22}$, which are given by[46]:

$$T_{13}(f) = \sqrt{\frac{2Q_L}{Q_r}} \frac{A(f)}{C(f)} \tag{3.12}$$

and

$$T_{11}(f) = \frac{Q_L [A(f)]^2}{Q_r \quad H(f)} \tag{3.13}$$

where

$$Q_L = 2\pi f_0 C_T / G_L \tag{3.14}$$

and

$$Q_r = 2\pi f_0 C_T / G_a(f_0) \tag{3.15}$$

are the loaded Q and acoustic radiation Q, respectively. G_L is the conductance in series with the voltage source Eg in Figure 3.5, and $R_L = 1/G_L$. The quantity A(f) is the well known array factor, which depends on the transducer geometry and can be calculated by the crossed field model or the delta function model. C(f) and H(f) are the two circuit factors, which determine the frequency dependence caused by the matching network. For the circuit in Figure 3.5, C(f) and H(f) are derived to be:

$$C(f) = A + BY_{in} + R_L(C + DY_{in}) \tag{3.16}$$

and

$$H(f) = R_L \left[Y_{in} + \frac{A + CR_L}{B + DR_L} \right] \tag{3.17}$$

where the ABCD matrix elements of an arbitrary matching circuit are defined as:

$$\begin{pmatrix} E_L \\ I_L \end{pmatrix} = \begin{pmatrix} A & B \\ C & D \end{pmatrix} \begin{pmatrix} E_3 \\ I_3 \end{pmatrix} \tag{3.18}$$

and the transducer admittance Y_{in} is given by:

$$Y_{in} = j2\pi fC_T + G_a(f) + jB_a(f) \tag{3.19}$$

The matching circuit often used is shown in Figure 3.6, which uses a shunt tuned resistor and inductor. The optional transformer is introduced for the purpose of matching

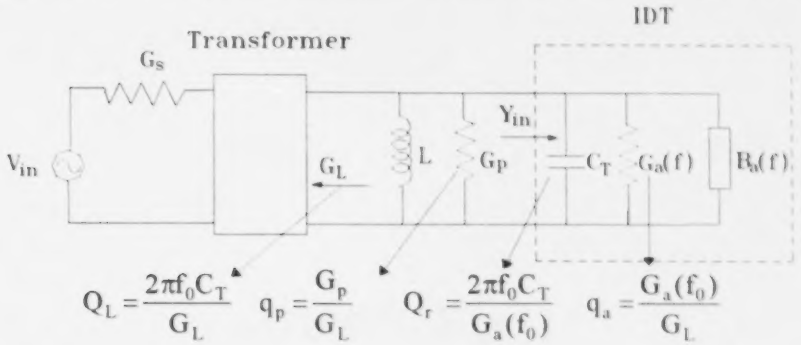

Figure 3.6. Schematic of the shunt matching network for an IDT [46].

the input impedance to 50 Ω. For this shunt matching circuit, T_{11} and T_{13} are related by

$$T_{11}(f) = \frac{|T_{13}(f)|^2}{2} C(f) \qquad \text{(for B=0, D=1)} \tag{3.20}$$

Further, two other parameters $q_p = G_p / G_L$ and $q_a = G_a(f_0) / G_L$ can be defined to facilitate the expressions of insertion loss

$$|T_{13}(f_0)|^2 = \frac{2q_a}{(1+q_a+q_p)^2} \tag{3.21}$$

and the acoustic reflection coefficient

$$|T_{11}(f_0)|^2 = \frac{{q_a}^2}{(1+q_a+q_p)^2} \tag{3.22}$$

For a filter with two transducers, $|T_{11}(f_0)|^2$ and $|T_{13}(f_0)|^2$ are related to the triple transit suppression (TTS) and insertion loss, respectively, and have the relationship

$$TTS \cong IL - 20\log_{10} q_a + 6 \quad \text{(dB)} \tag{3.23}$$

while the whole frequency response of the filter is

$$H(f) = CT_{32}^{(e1)}(f) \cdot T_{13}^{(e2)}(f)\exp(-j2\pi f\tau) \qquad (3.24)$$

where $T_{32}^{(e1)}(f)$ and $T_{13}^{(e2)}(f)$ are the electroacoustic transfer functions of the two transducers, and C is a multiplicative constant and τ the constant delay.

3.3 Second Order Effects

In linear phase SAW filter design, many factors contribute to the frequency response of the filter. The filter performance is often influenced or corrupted by some second order effects , which include a) electrode finger reflections b) electromagnetic feedthrough c) acoustic attenuation d) diffraction e) beam steering f) bulk waves. Also among them are circuit loading and triple-transit interference (TTI). Circuit loading has been discussed in the last section, and TTI will be covered in the design. In this part, only the first three effects will be described since they turned out to be the major factors for GHz filter operation.

3.3.1 Finger Reflections

The mass of the IDT electrodes fabricated onto the piezoelectric substrate will dampen the surface acoustic wave and change the wave velocity. This second order effect is called mass loading. To reduce this effect, the finger electrodes should be made as thin as possible with a light metal (such as aluminum instead of gold). However, if the film is too thin, the resistance of the fingers will increase greatly and contribute to circuit-factor loading and insertion loss increase. Typical aluminum film thicknesses employed in IDT fabrication are within the range of 500-2000 Å, and a good design thumb rule is to keep the thickness below one tenth of the wavelength.

The deposited metal film causes acoustic wave velocity change by three different mechanisms[19]. First of all, mass loading decreases the wave velocity by

$$\left.\frac{dv}{v}\right|_m \approx -\frac{2\pi Fh}{\lambda} - \frac{0.5K^2}{(1+0.5K^2+1/\varepsilon_r)} \qquad (\text{for } h/\lambda < 0.01) \qquad (3.25)$$

where h = thickness of the metal film, λ = acoustic wavelength, v = free acoustic wave velocity and F = a constant for the substrate used, with F=0.037 for lithium niobate and F=0.01 for quartz[51,52], ε_r = substrate relative permittivity. Second, the transducer metal

film will short out the surface piezoelectric fields underneath, which also serves to decrease the acoustic wave velocity by

$$\left.\frac{dv}{v}\right|_p = -\frac{K^2}{2} \tag{3.26}$$

Third, the deposited metal film also change the effective "stiffness" of the propagating surface. The fractional velocity change $\left.\frac{dv}{v}\right|_s$ caused by this stiffness perturbation depends on both the metal and the piezoelectrics employed. This effect will increase the SAW velocity opposite to the change due to mass loading and piezoelectric field shorting out. The total fractional velocity perturbation caused by the IDT metal electrodes is the sum of these three contributions

$$\frac{dv}{v} = \left.\frac{dv}{v}\right|_m + \left.\frac{dv}{v}\right|_p + \left.\frac{dv}{v}\right|_s \tag{3.27}$$

The second term in equation (3.27) is the dominant factor for piezoelectric substrates with relatively large values of electromechanical coupling coefficient, such as lithium niobate while the other two factors are important for quartz. The results of these velocity perturbations are to cause a slight shift of the center frequency of the SAW filter and acoustic reflections from IDT fingers.

To reduce the finger reflections due to mass loading and other factors, the split finger electrodes can be employed in the IDT design. Its principle is illustrated in Figure 3.7. As shown in the figure, the electrode width and spacing both are made $\lambda_0/8$ at the

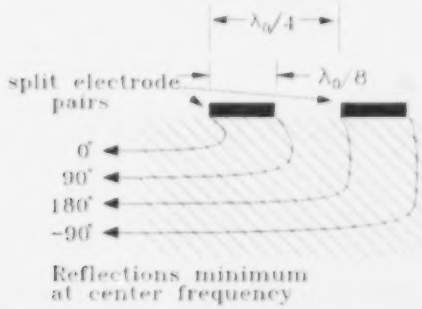

Figure 3.7. SAW reflections from fingers of split-electrode IDT give resultant minimum at center frequency[19].

center frequency so that the SAW reflections from each split-electrode pair cancel out (out of phase) at the center frequency, rather than add as for the single electrode IDTs. The disadvantage of this structure is that the center frequency is half of that of single-electrode device for the same finger width and spacing.

3.3.2 Electromagnetic Feedthrough

Electromagnetic feedthrough, also termed as crosstalk, is one of the most serious second order effects, especially for the GHz range SAW filter operation. The electromagnetic feedthrough occurs because the input and output IDTs act as the two plates of a capacitor so that the electromagnetic signal tends to be coupled directly from the input to the output at high frequencies. This feedthrough signal is coupled to the output IDT at the velocity of light to cause coherent interference with the SAW signal arriving there, and this will cause amplitude and phase ripples across the pass band at ripple frequency $f_{EM} = 1/\tau$, where τ is the time separation between the phase centers of the two IDTs. The electromagnetic coupling becomes even higher for split finger IDTs since the capacitance is 1.4 times larger than for an equivalent single electrode IDT design. This second order effect can often be minimized by improving the device packaging design and proper ground plane placement designs, etc.

3.3.3 Acoustic Attenuation

The acoustic waves undergo attenuation on their propagation paths due to several reasons, such as viscose damping, acousto-electric losses and crystal imperfections. Obviously, acoustic attenuation will increase the filter insertion loss although it is usually small enough to be neglected. However, the attenuation increases rapidly with the frequency. For example, the empirical formula for the acoustic attenuation on YZ-lithium niobate can be described as[53]

$$\alpha_t = 0.88f^{1.9} + 0.19f \quad (\text{dB}/\mu\text{s}) \tag{3.28}$$

where f is the frequency in GHz. If calculated by this equation, the acoustic attenuation for a 5 GHz filter with the IDTs separated 100 μm apart is 0.5 dB, which can still be ignored.

In addition to what is described above, there are some other second order effects worthy of mention. SAW diffraction is only troublesome with apodized IDTs. Beam steering is related to the IDT alignment with respect to the desired crystal propagation. And the bulk wave excitation problem is often solved by employing multistrip coupler (MSC) structure. Harmonics excitation is viewed as a bad effect in some places, however, it is also often used as an advantage for making GHz devices.

3.4 SAW Filter Design

3.4.1 2 GHz Filter

Since the goal of the project was to demonstrate a process feasibility of GHz SAW filter manufacturing, a simple 0.25 μm linewidth SAW filter using bidirectional IDTs was first designed, which has a center frequency close to 2 GHz. To simplify the design, the 2 GHz SAW filter consists of two identical unapodized IDTs with equal finger width and spacing. The 128^0 rotated, Y-cut ,X-propagation, lithium niobate was chosen as the piezoelectric substrate because of its high electromechanical coupling coefficient property. In order to reduce the undesirable reflections of the acoustic wave from the fingers, the split-finger IDT geometry was used in the design as shown in Figure 3.8, in which the finger width is $\lambda_0/8$, where λ_0 is the acoustic wavelength. Two important design parameters need to be changed for the split finger calculations with respect to the single

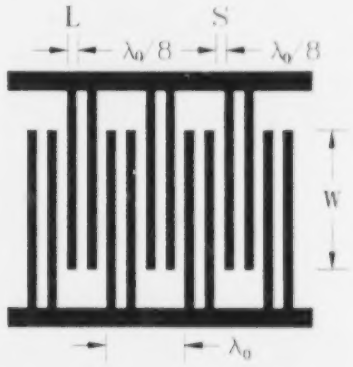

Figure 3.8. The split finger IDT with finger width and spacing of $\lambda_0/8$.

finger IDT design: the effective electromechanical coupling coefficient $K_e^2 = 0.88 \times K^2$ [48], and the IDT capacitance C_T is 1.4 times of that of an equivalent single-electrode IDT [49]. The parameters used for determining the acoustic radiation conductance are listed in Table 3.1, and the design calculations are shown as follows:

$d = 128 \times 10^{-6}$ m (the distance between the phase centers of the two IDTs)

$L = S = 0.25 \cdot 10^{-6}$ m (IDT finger width and spacing)

$v = 3992$ m / s (acoustic wave velocity for 128^0 YX – $LiNbO_3$)

$\lambda_0 = 8 \cdot L = 2 \cdot 10^{-6}$ m (acoustic wavelength)

$N = 22$ pairs (number of finger pairs for both IDTs)

$W = 80 \cdot 10^{-4}$ cm (IDT aperture)

$f_0 = \frac{v}{\lambda_0} = 1.996 \cdot 10^9$ Hz

$C_T = 1.4 \cdot C_0 WN = 1.232 \cdot 10^{-12}$ F

$G_a(f_0) = 8K_e^2 f_0 C_T N = 0.02$ mho

To cancel out the capacitive reactance caused by C_T at the center frequency f_0, a parallel or series inductor may be used. The equivalent circuits for the input IDT including these matching are shown in Figure 3.9 (a) and (b), respectively. Following the impedance matching theory, the required inductor values can be easily calculated and verified.

Table 3.1 Substrate parameters used in determination of acoustic radiation conductance[19].

Substrate	SAW Propagation Axis	velocity(m/s)	K^2(%)	C_0(pF/cm)
ST-quartz	X	3158	0.11	0.55
YZ-lithium niobate	Z	3488	4.5	4.6
128^0 YX-lithium niobate	X	3992	5.3	5.0
$LiTaO_3$	Z	3230	0.72	4.4

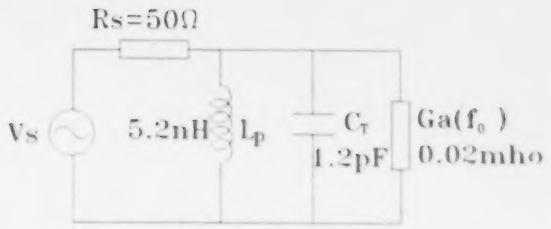

(a) Parallel inductor tuning

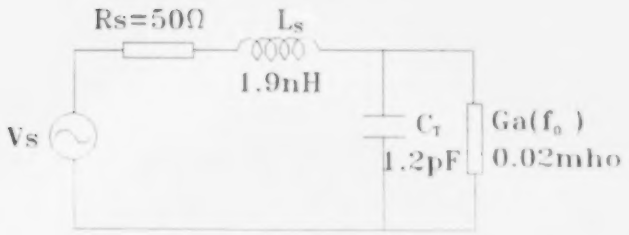

(b) Series inductor tuning

Figure 3.9. Equivalent circuit of the input IDT at center frequency showing the tuning inductor connected in (a) parallel (b) series to tune out the reactance of C_T.

For such a high frequency device, the easiest way for tuning is to use the bonding wire as the series inductor. The inductance of a cylindrical wire above a ground plane is given by[50]:

$$L = \frac{\mu}{2\pi} \ln\left(\frac{4h}{d}\right) \tag{3.29}$$

where

μ = the magnetic permeability of the wire (typically 1.257×10^{-8} H/cm)

h = the height above the ground plane (5×10^{-4} m)

d = the diameter of the wire (50×10^{-6} m)

Using this equation, the inductance of a bonding wire was calculated to be 7.38 nH/cm, so an 0.25 cm long bonding wire can approximately provide the series tuning inductance.

Due to the bidirectionality of the IDT, some of the power received by the output IDT is re-emitted back to the input IDT, and this part of the power can lead to further regeneration of a SAW wave by the input IDT. This SAW regenerative effect is called triple-transit interference (TTI). Figure 3.10 shows relative power levels associated with

the main output signal and TTI in a birectional SAW filter with matched source and load impedances. Assume the input power P_{in} = 1 W, the output power level from the main input signal is P_{out} = 1/4 W due to the bidirectinal power losses in input and output IDTs. This output signal P_{out} results in a further SAW regeneration in the input IDT, and the signal energy arriving back at the output IDT after two more traverses, i.e. the TTI signal level is P_{TTI} = 1/64 W. The ratio of the two output power levels is $P_{TTI}/P_{out} = 10\log_{10} 1/16$ = -12 dB. So, the resultant TTI signal level is 12 dB below the main output signal. Often, this 12 dB suppression is not enough for linear phase filter design because it will cause a pass-band peak-to-peak amplitude ripple of 4.4 dB and a phase ripple of 28^0 peak-to-peak.

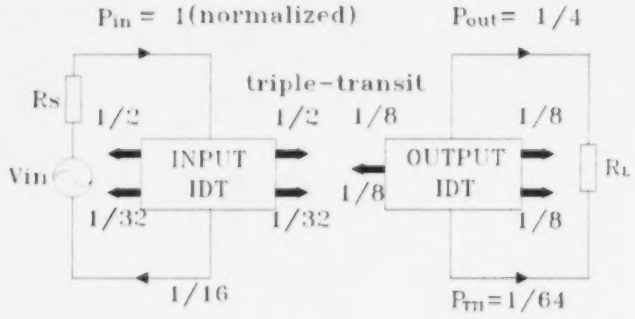

Figure 3.10. Power flow for triple-transit-interference in bidirectional IDTs[19].

The plot of these ripples vs. TTI suppression levels is shown on Figure 3.11. The amplitude ripple will appear in the passband as a periodic signal at a frequency

$$f_{TTI} = 1/2\tau \tag{3.30}$$

where τ is the time separation between the phase centers of the two IDTs.

For the bidirectional IDT configuration in this design, TTI can only be suppressed by increasing the insertion loss. Following equation (3.21) and (3.23), the insertion loss in this design is

$$IL = -10\log_{10}\left|T_{13}^{(\#1)}(f_0)\right|^2 - 10\log_{10}\left|T_{13}^{(\#2)}(f_0)\right|^2 \quad (q_a = 1, q_p = 0)$$
$$= 6 \text{ dB}$$

while the triple-transit interference suppression is

$$TTS = IL - 20\log_{10} q_a + 6$$
$$= 12 \text{ dB}$$

It is clear that the results correspond to the matched conditions for both transducers. Often, design trade-offs have to be made to increase TTS by mismatching the input or output IDT while sacrificing the insertion loss. Note that finger reflections also cause multiple transit signals, which are effectively suppressed by split finger design. However, TTI signal is a phenomenon intrinsic to the IDT bidirectionality, which can be reduced by unidirectional transducer design if low loss property is to be achieved, as will be discussed in 3.5.

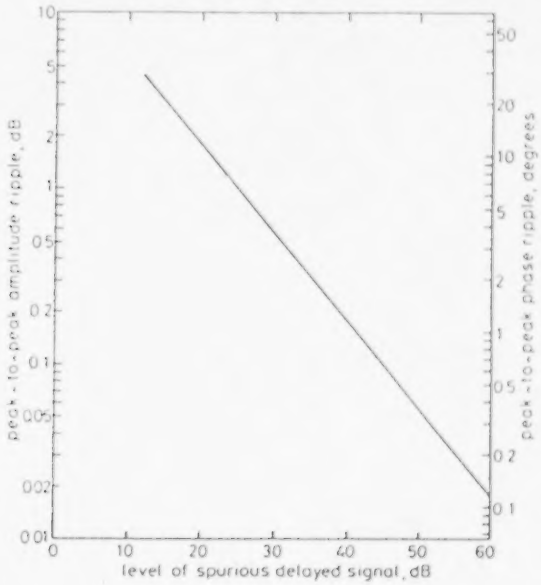

Figure 3.11. Plot of amplitude and phase ripples vs. TTI suppression level[41].

Figure 3.12 shows the calculated frequency response of the 2 GHz filter. The figure shows the relative insertion loss calculated by the delta function model while the real insertion is 6 dB if both IDTs are matched in the circuitry. The bandwidth of the filter

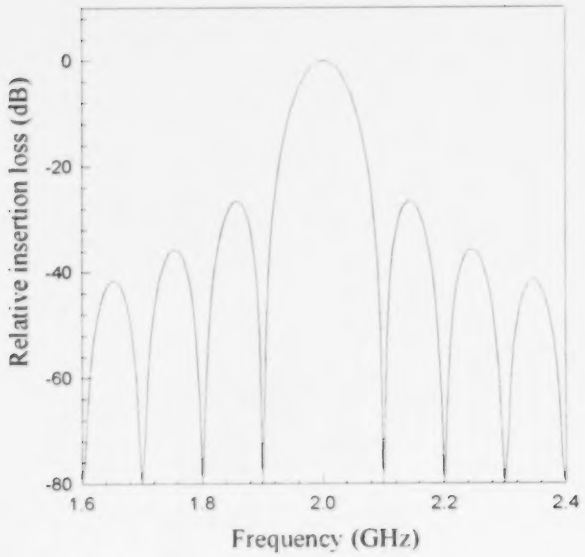

Figure 3.12. Frequency response of the 2 GHz filter with split fingers calculated by the delta function model.

is determined by the radiation Q_r and circuit Q_e defined as:

$$Q_r = \frac{f_0}{\Delta f_r} = \frac{2\pi f_0 C_T}{G_a(f_0)} = \frac{\pi}{4K^2 N} \tag{3.31}$$

and

$$Q_e = \frac{f_0}{\Delta f_e} = \frac{2\pi f_0 C_T}{G_s} \tag{3.32}$$

where Δf_r and Δf_e are the 3 dB bandwidth corresponding to the radiation Q_r and external circuit Q_e at the center frequency, respectively, and G_s is the source conductance. The bandwidth is determined by the larger Q, and there is a maximum intrinsic fractional bandwidth when they are equal. From the delta function model, the 3 dB bandwidth is $BW_3 = 0.9BW_4 \approx (0.9)1/N$. If we approximate BW_3 to 1/N, then

$$Q_r = \frac{f_0}{\Delta f} = N \tag{3.33}$$

By equating (3.31) and (3.33), we have the maximum intrinsic fractional bandwidth

$$\left.\frac{\Delta f}{f_0}\right|_I = \sqrt{\frac{4K^2}{\pi}} \tag{3.34}$$

which gives the maximum bandwidth for which the insertion loss of the SAW filter with bidirectional IDTs can be held to 6 dB. In the case of this design, the 3 dB bandwidth is

$$\Delta f \approx \frac{1}{N} \times f_0 = 92 \text{ MHz}$$

while the maximum bandwidth is about 520 MHz according to equation (3.34).

3.4.2 5 GHz Filter

To demonstrate even finer feature size SAW device technology, a 0.1 μm linewidth SAW filter was designed, which operates at a center frequency of 5 GHz approximately. This 5 GHz filter also consists of two identical split-finger unapodized IDTs with uniform finger width and spacing, and the design calculations are shown as follows:

$d = 80 \times 10^{-6}$ m (the distance between the phase centers of the two IDTs)

$L = S = 0.1 \cdot 10^{-6}$ m (IDT finger width and spacing)

$v = 3992$ m / s (acoustic wave velocity for 128° YX – $LiNbO_3$)

$\lambda_0 = 8 \cdot L = 0.8 \cdot 10^{-6}$ m (acoustic wavelength)

$N = 10$ pairs (number of finger pairs for both IDTs)

$W = 50 \cdot 10^{-4}$ cm (IDT aperture)

$f_0 = \frac{v}{\lambda_0} = 4.99 \cdot 10^9$ Hz

$C_T = 1.4 \cdot C_0 WN = 0.35 \cdot 10^{-12}$ F

$G_a(f_0) = 8K_e^2 f_0 C_T N = 0.0065$ mho

$L_s = 2.15 \cdot 10^{-9}$ H (series tuning inductor)

$L_p = 2.9 \cdot 10^{-9}$ H (parallel tuning inductor)

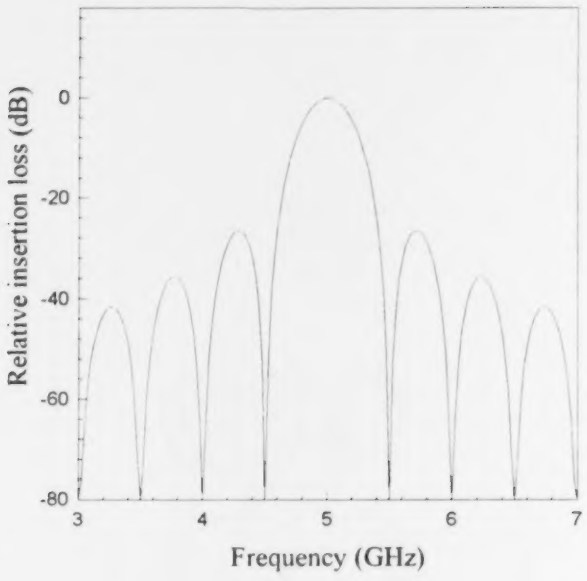

Figure 3.13. Frequency response of the 5 GHz filter with split fingers calculated by the delta function model.

Figure 3.13 shows the calculated frequency response of the 5 GHz filter with split fingers. The 3 dB bandwidth is found to be 500 MHz from the figure, and the real insertion loss and TTS are

$$IL = -10\log_{10}\left|T_{13}^{(\#1)}(f_0)\right|^2 - 10\log_{10}\left|T_{13}^{(\#2)}(f_0)\right|^2 \quad (q_a = 0.327, q_p = 0)$$

$$= 8.6\,\text{dB}$$

$$TTS = IL - 20\log_{10} q_a + 6$$

$$= 24\,\text{dB}$$

It can be seen that the insertion loss is increased due to the impedance mismatching. However, the triple transit interference signal is also efficiently suppressed at the same time. This trade-off is often made in the design of linear phase SAW filters using the bidirectional IDT configuration.

3.5 SPUDT and IIDT Configurations

As we have seen, conventional bidirectional IDTs have two disadvantages. First, the minimum insertion loss is 6 dB, which is too high for front-end applications. Second, triple-transit interference has to be suppressed at the expense of the increased insertion loss. In this section, further possible improvements on design are discussed although these are not implemented in the present project.

3.5.1 Single Phase Unidirectional Transducer (SPUDT)

As discussed earlier, triple transit interference can be caused by regenerative and/or nonregenerative reflections in IDTs. The regenerative effect means the re-excitation of a surface wave by an IDT in which a voltage has been induced by the passing surface wave. In bidirectional IDTs, the nonregenerative TTI due to finger reflections can be suppressed by the use of split-electrode geometry. The regenerative TTI can be reduced in some narrow band filters using unidirectional transducers. Unidirectionality can be achieved by three different approaches: three phase, two phase and single phase unidirectional transducers. At present, SPUDT is the most attractive one among the three.

Figure 3.14 demonstrates three different types of SPUDTs. Figure 3.14(a) shows the double-metalization type SPUDT invented by Hartmann et al[31]. Figure 3.14(b) sketches the floating-electrode type SPDUT proposed by Yamanouchi et al[33]. The focus of attention here will be the Lewis-type single-metallization SPUDT shown in Figure 3.14(c) due to versatility in structure and its couple-of-modes (COM) design approach [34].

As shown schematically in Figure 3.14(c), the SPUDT is the ladder type transducer which consists of periodically spaced groups of IDT fingers (rungs) and sets of SAW reflection gratings interleaved between them. Its principle is based on exploiting the difference between centers of transduction and reflection in IDT's and grating reflectors. Generally, the centers of transduction and reflection in a single electrode geometry IDT are coincident with the centers of the electrodes and electrode edges, respectively. By properly displacing grating elements with respect to IDT's, as is the case in SAW resonator designs, unidirectional SAW propagation can be achieved.

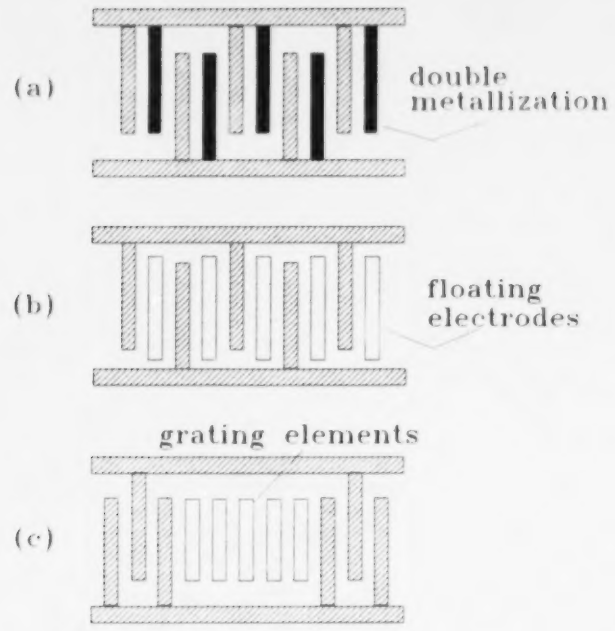

Figure 3.14. Three types of SPUDTs (a) Double-metallization type (b) Lewis-type single-metallization type (c) Floating-electrode type [from ref. 19 p.276].

In the application of Coupling-of-modes (COM) theory to the SAW device design[34], it is assumed that SAW propagation on a piezoelectric substrate can be represented by the scalar wave equation

$$(d^2\Phi / dx^2) + (\omega^2 / v^2(x))\Phi = 0 \qquad (3.35)$$

in term of quasi-static electric surface potential Φ, angular frequency ω, and SAW velocity v(x), where v(x) is considered as a sinusoidally perturbed function about free SAW wave velocity v_0 as the surface wave passes through the grating. The grating consists of a set of metal strips or etched grooves in periodic spacing Λ, then the corresponding Bragg frequency f_0 for reflection is given by $f_0 = v_0/2\Lambda$. In solving (3.35) to first order for this velocity perturbation, a set of coupled wave equations may be obtained relating to the propagation of "forward" and "backward" SAW waves, in the following derivation equation

$$-R' - j\delta R = j\kappa S$$
$$S' - j\delta S = j\kappa R \qquad (3.36)$$

where R and S and their derivatives relate the amplitudes of the forward and backward waves, respectively. And $\delta \approx 2\pi(f-f_0)/v_0$ represents frequency deviation from the Bragg frequency f_0, while κ is the grating coupling coefficient in cm^{-1}. The above COM analysis allows a general 2×2 transmission matrix **[G]** for a periodic grating to be derived. An IDT can be represented by a 3×3 admittance matrix **[T]**, which relates the input and output complex electrical and acoustic amplitudes. The third part used in the design is a 2×2 matrix **[D]**, which represents an acoustic transmission line relating to displacements between gratings and IDT's. Based on these matrixes and with boundary conditions applied, the electrical transmission characteristics of a SPUDT can be derived using an computer algorithm.

3.5.2 Interdigited Interdigital Transducer (IIDT)

At present, IIDT is the most attractive low-loss GHz filter. Figure 3.15(a) is the one track type IIDT configuration proposed by Lewis[35], in which many bidirectional input and output IDTs are connected in parallel and interleaved together to minimize the bidirectional loss. The dual track IIDT in Figure 3.15(b) was introduced by Hikita to suppress the high passband ripple caused in the one track IIDT[36]. In the latter configuration, the track-coupling is completed by a pair of two identical electrically connected IDTs each placed in different tracks. One disadvantage of IIDTs is that they take large substrate areas, but this can still be reconciled by GHz device applications since the linewidths involved are below 1 μm. The major difficulty is the design complexity for attaining a high sidelobe rejection and reducing the finger reflections. Since too many parameters are involved in the design calculations, a computer algorithm has to be developed. The details will not be discussed further here.

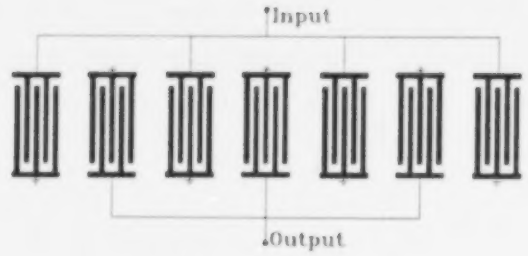

(a) One track IIDT

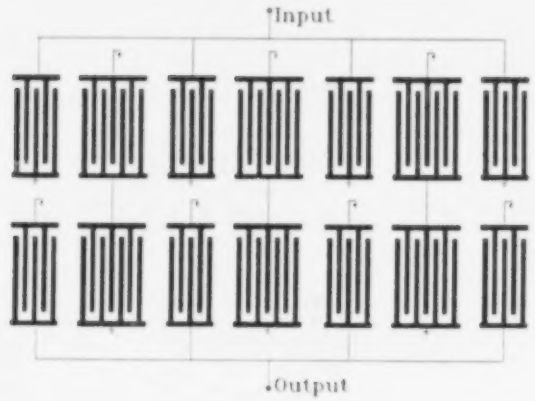

(b) Dual track IIDT

Figure 3.15. IIDT SAW filters (a) one track configuration (b) Dual track configuration.

4 Fabrication of 0.25 and 0.1 μm Linewidth SAW Filters

In this project, the fabrication of the filter includes two important processing steps: Electron Beam Lithography (EBL) for making the mask and X-ray lithography (XRL) for producing the device. The E-beam lithography was realized using the scanning electron microscope (SEM) interfaced with a personal computer scanning control system (Nanometer Pattern Generation System NPGS) at Alberta Microelectronic Centre (AMC). The X-ray lithography was completed using the laser plasma source at the Department of Electrical Engineering of the University of Alberta.

4.1 E-beam Lithography- making the mask

4.1.1 Electron Beam Lithography

It has been well known for many years that a finely focused beam of electrons can be deflected accurately and precisely over a surface. If this surface is coated with a radiation-sensitive polymeric resist, the electron beam can be used to write patterns of very high resolution. Since the wavelength of electrons is on the order of a few tenths of an angstrom, their resolution is generally not limited by diffraction considerations. As a result, the minimum linewidth that can be produced with electron beam exposure is much less than that achieved with photolithography. Structures have been made with dimensions of less than 100 nm using this technique. Currently, electron beam lithography has been used by many companies to manufacture specialty, high resolution devices. However, due to its low throughput coupled with high cost, it is more often used for the fabrications of photomasks or X-ray masks that are used with mass replication lithographic systems.

Figure 4.1 shows the simple electron beam exposure system using the Cambridge Stereoscan 250 SEM at AMC for writing the X-ray mask in this project. As shown in the figure, the mask substrate is mounted into the SEM chamber, and its position can be adjusted by the mechanical drive. A commercial e-beam lithography system, NPGS, has been installed on a personal computer and interfaced with the Cambridge Stereoscan 250 SEM controlling the scan voltages of the SEM to transfer the stored mask pattern data into the resist. The electron beam current is monitored by a Fluke Meter connected to

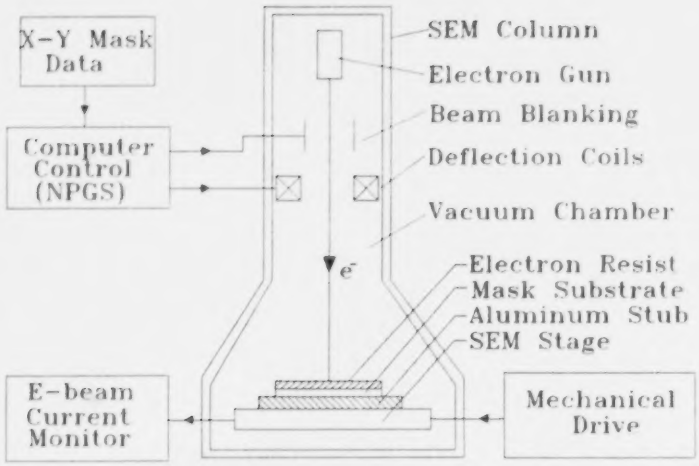

Figure 4.1. Schematic of the electron beam exposure system using the SEM at AMC.

the SEM stage, and exposure doses are controlled by NPGS.

As the incident electrons penetrate the resist, they undergo both elastic and inelastic collisions known as electron scattering. Elastic collisions result only in a change of direction of the electrons while inelastic collisions result in energy loss. These scattering processes lead to a broadening of the beam sideways, and cause exposure of the resist at points remote from the point of initial electron incidence. As a result, the developed resist images are wider than addressed. As is shown schematically in Figure 4.2 (a), there are two types of scattering that are important, forward and backscattering. Since most of the electrons are scattered in the forward direction through small angles ($<90^{0}$) relative to their original direction, this effect mainly broadens the incident beam. Some electrons experience large angle scattering (approaching 180^{0}) which causes these electrons to return to the surface. The resultant forward and backscattered absorbed energy distributions are shown in (b) of Figure 4.2, where E and σ represent absorbed energy and the standard deviation for the distributions, respectively.

The magnitude of the electron flux at any point depends upon such parameters as the atomic number and density of both the resist and substrates as well as the velocity (determined by the accelerating voltage) of the electrons. The resultant undesired exposure

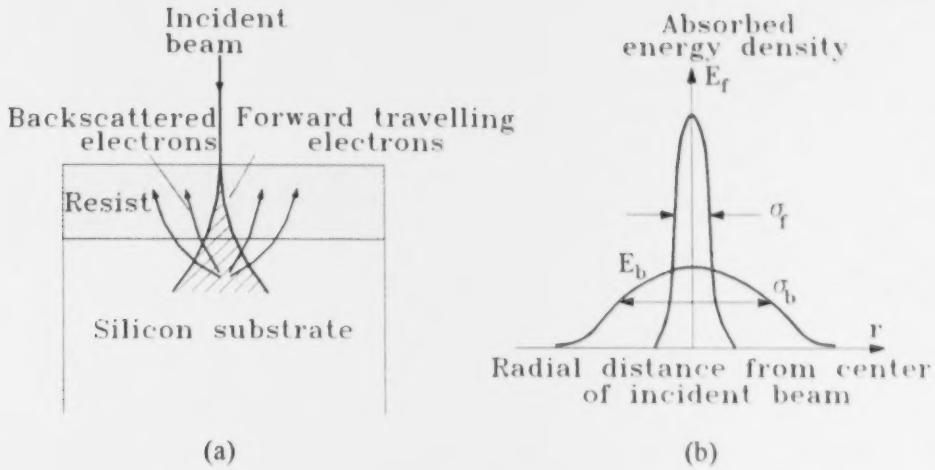

Figure 4.2. Schematic of (a) electron scattering (b) absorbed electron beam energy distribution of the incident electron beam[55].

of resist in areas not directly addressed by the electron beam is called the proximity effect, which imposes certain restrictions on the size and shape of relief structures which can be achieved in the resist, particularly for complex patterns with high packing densities and small dimensions. Figure 4.3 shows an example of the proximity effect. As shown in the figure, it is primarily variations in the background energy density which matter. A constant energy density background would give rise to no proximity effect although it would reduce resist constrast.

Due to the electron scattering effects mentioned above, a thorough understanding of the factors that affect the shape and size of the developed relief structure after exposure is important to the practical application of electron beam lithography. These factors have been the subject of extensive theoretical and experimental research. Fortunately, the simplicity of the patterns in this project allows us to optimize the exposure through trial and error only without counting on special models.

A positive chain scission resist, PMMA [poly(methylmethacrylate)], was used as the electron resist in this project[57]. The structure of PMMA is a long linear polymer:

"A-A-A-A-.....-A-A-A-A-.....-A-A-A-A"

where **A** represents a methyl methacrylate unit:

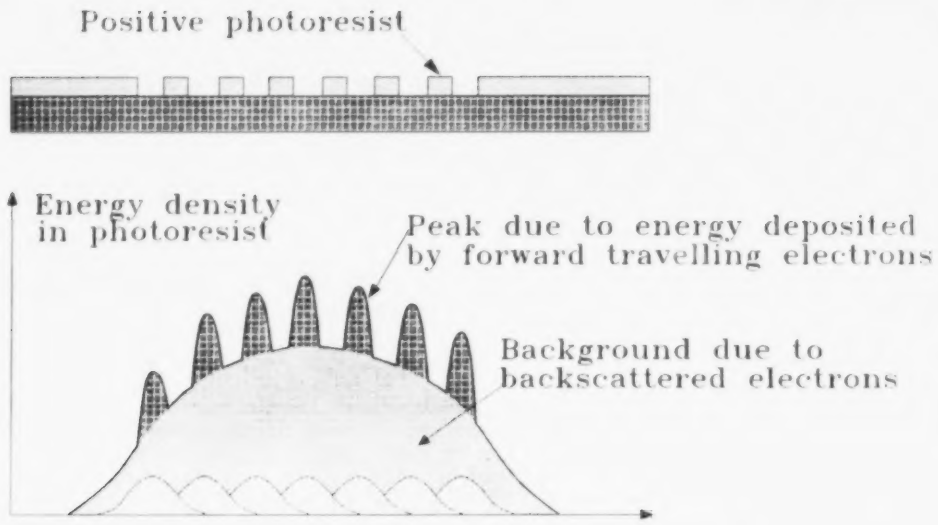
Positive photoresist
Energy density in photoresist
Peak due to energy deposited by forward travelling electrons
Background due to backscattered electrons

Figure 4.3. An example of the proximity effect [56].

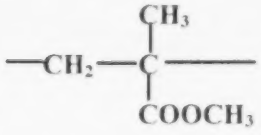

Before exposure, an "average" PMMA molecule contains about 1000 monomer units. During exposure, about 1% of the linear bonds are broken. Therefore, after exposure, an "average" molecule consists of about 100 units (about 140 eV has to be absorbed in order to break one bond). The dissolution rate of PMMA in developer (e.g. MIBK/IPA) varies approximately as the square of the molecular weight. Therefore, exposed PMMA dissolves faster than unexposed by a factor of 100. PMMA requires a high dose to expose and has excellent resolution, but has poor plasma etch resistance. Plasma etch resistance is important in many high resolution lithography schemes because the use of directional plasma in bombardment to remove the metal or oxide layers through the patterned resist leading to steep sidewalls and square features.

4.1.2 NPGS

The Nanometer Pattern Generation System (NPGS) is a commercially available computer control software and hardware system for controlling the SEM writing[58]. There are three basic steps of the pattern generation process: pattern design, parameter run file creation, and pattern writing.

1. Patterns are created using DesignCAD which is a commercial computer-aided-design program. The SAW filter layout was produced in the DesignCAD by a program in BASIC language sawf.bsc, which is included in the Appendix I. This results in a pattern file with an extension DC2.
2. Once a pattern design is created, the program MRF (Make Run File) is executed to record the exposure conditions for different drawing elements in the pattern, which generates a run file with an extention RF6.
3. After a run file has been generated , the patterns can be written using the SEM under the control of NPGS.

In E-beam writing, the pattern is scanned by the electron beam, which has a cross section of a tiny oval spot, over the pattern geometry. As shown in Figure 4.4, the beam motion is controlled by the two important parameters, center to center (CTC) distance and line spacing (LS), which has to be specified in the run file along with other parameters.

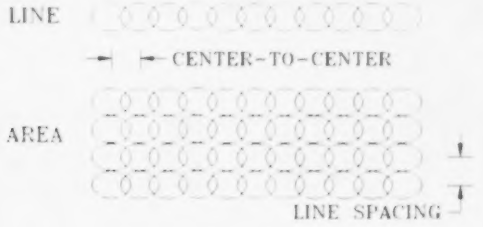

Figure 4.4. Schematic diagram showing the electron beam motion.

To write a line segment with certain width and length, the number of beam passes and points along the pass are given by:

$$\#\ \text{Beam Passes} = \text{Round}\left(\frac{\text{Pattern Line Width}}{\text{Line Spacing}}\right) \tag{4.2}$$

$$\#\ \text{Points} = \text{Round}\left(\frac{\text{Segement Length}}{\text{Center}-\text{to}-\text{center Distance}}\right) \tag{4.3}$$

More complicated patterns like polygons can be written by the function polyfill with the options of fill directions and first side fills shown in Figure 4.5. Circular arcs and curves can be written

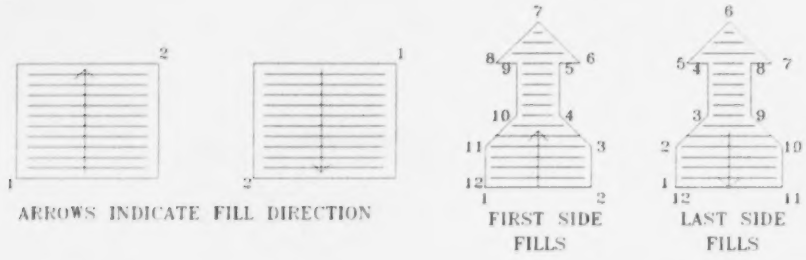

Figure 4.5. E-beam writing for filled polygons with different fill directions and first fill side.

like lines, but the calculation time for circles and circular arcs is several times longer than for lines.

The drawing elements are differentiated by drawing layers amd colors. Different writing parameters and exposures can be applied to a maximum of 19 layers and 16 colours. These parameters and exposure Time/Dose are specified in the run file. Within the make run file, each dose may be toggled between a "Line Dose" or an "Area Dose" by using the SPACE BAR when the dose menu is selected. The "Line Dose" is given in units of nC/cm and the "Area Dose" is given in units of $\mu C/cm^2$. By refering to Figure 4.4, the "Line Dose" is calculated for a single pass of the beam at an exposure point spacing given by the "Center-to-center" distance, while the "Area Dose" is calculated based on the "Center-to-Center" and the "Line Spacing" distances:

$$\text{Line dose} = \left(\frac{(\text{Beam Current}) \times (\text{Exposure Time})}{\text{Center}-\text{to}-\text{Center}}\right) \tag{4.4}$$

$$\text{Area dose} = \left(\frac{(\text{Beam Current}) \times (\text{Exposure Time})}{\text{Center}-\text{to}-\text{center} \times (\text{Line Spacing})}\right) \tag{4.5}$$

After patterns have been designed, it is important to add dump sites to them. While the beam is writing, NPGS calculates the next points. If the calculation time is longer than the exposure time, the beam will stay in the dump sites. A dump site should be far enough from the pattern area so that the burned spot will not interfere with the structure, but close enough to minimize the settling of the scan coils when the beam jumps back to the writing area.

The filter layout is shown schematically in Figure 4.6. The IDT patterns of the filter is generated using program sawf.bsc, and then the arms, pads and dump sites are added in DesignCAD. The minimum size of the IDT pads is 100×100 μm^2 since the bonding wire is 50 μm in diameter. The IDT finger is divided into several different exposure regions (not showing here) for the proximity effect corrections which will be shown later.

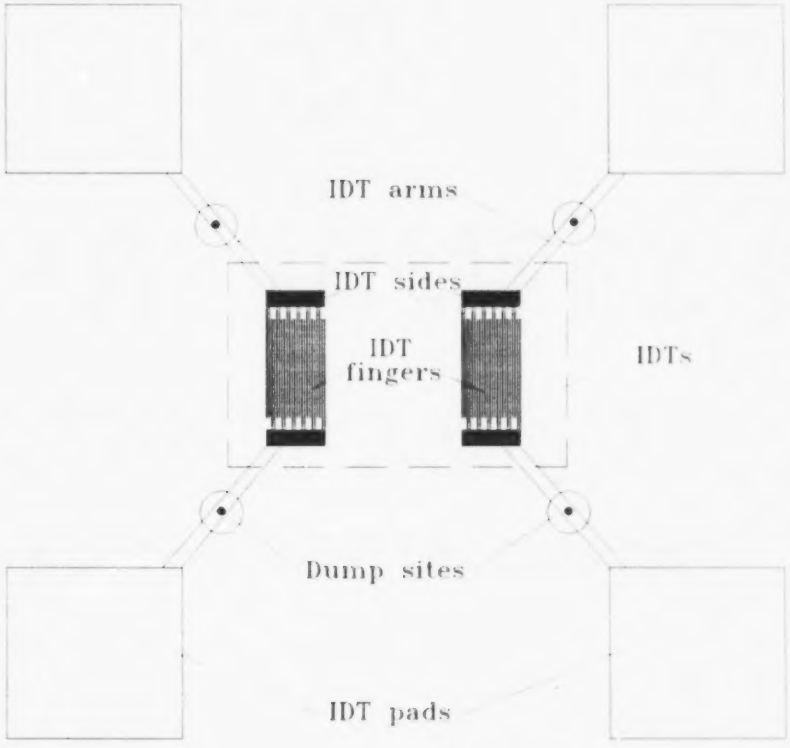

Figure 4.6. The SAW filter layout.

4.1.3 Mask Making Process

4.1.3.1 Wafer Preparation

The processing steps for the mask wafer preparation are shown in Figure 4.7[59]. The starting wafer is a double side polished p-type (100) silicon. Then, thermal oxide layers are grown on both sides of the wafer, and followed by low stress Si_3N_4 deposition using PECVD, 1.0 μm on the top, 0.5 μm on the back. Afterwards, Cr and Au thin films, 20 and 40 nm thick resepectively, are deposited onto the top surface using e-beam deposition. Next, HPR506 resist is coated on both sides of the chip, and conventional UV lithography is employed to open the backside window. Finally, the backside Si_3N_4 and SiO_2 layers in the window region are etched away in a plasma environment. After these steps, the wafers are then cut into many 8×9 mm^2 chips, which will be used as mask substrates in the next processing step.

4.1.3.2 Mask Making Process

In this project, the X-ray mask making processing steps using the E-beam lithography is illustrated in Figure 4.8. First, the mask chip is coated with 400 nm thick PMMA. Then, the patterns are written into the resist using the SEM under the control of NPGS. Next, the exposed mask is developed in MIBK (Methyl Isobutyl Ketone): IPA (Isopropyl Alcohol) = 1:3 for 1 minute, and IPA for 20 seconds, respectively, a standard KTI development process[60]. Afterwards, the mask is rinsed with de-ionized water for 20 seconds. After development, the mask may be examined under an optical microscope for correct exposures and pattern completeness. A more detailed view is possible using a SEM. The next step is gold electroplating to form the 400 nm thick metal pattern on the mask followed by resist stripping. The last step is the etching of a 1.5×1.5 mm^2 window in the silicon substrate below the gold pattern using a standard KOH wet etching technique. When completed, this results in a thin membrane, 1.0 μm thick, Si_3N_4 mask with a 400 nm thick gold pattern on top.

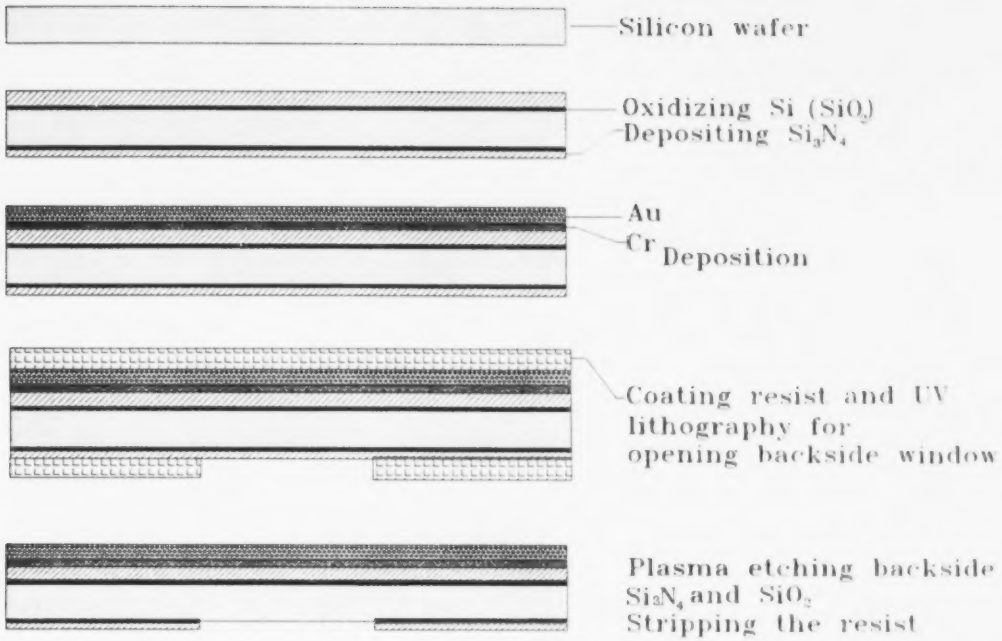

Figure 4.7. Processing steps for the mask wafer preparation.

4.1.4 Characterization of 0.25 and 0.1 μm Linewidth Mask Making Process

4.1.4.1 Resist Coating

The resist used for the E-beam lithography is PMMA from KTI, and was coated using the Solitec spinner at AMC lithography room. The initial PMMA solution is 7.5%, and should be diluted in Chlorobenzene according to the thickness requirements. The PMMA thickness depends on the feature size in the mask pattern, and is listed in table 4.1 along with its preparation. Before coating, the mask substrates should be cleaned with Acetone. The chuck was the special one used for the E-beam and X-ray lithography resist coating. The spinner was set as follows: ramp to 200, spread at 1000 rpm for 3 seconds, spin at 2500 to 3600 rpm for 25 seconds, depending on the thickness. A uniform PMMA layer with the required thickness can be achieved by controlling the spinning speed. After coated with resist, the samples were baked in an oven for 60 minutes at 150°C, and then soft-baked on a vacuum hot plate for 40 seconds at 150°C.

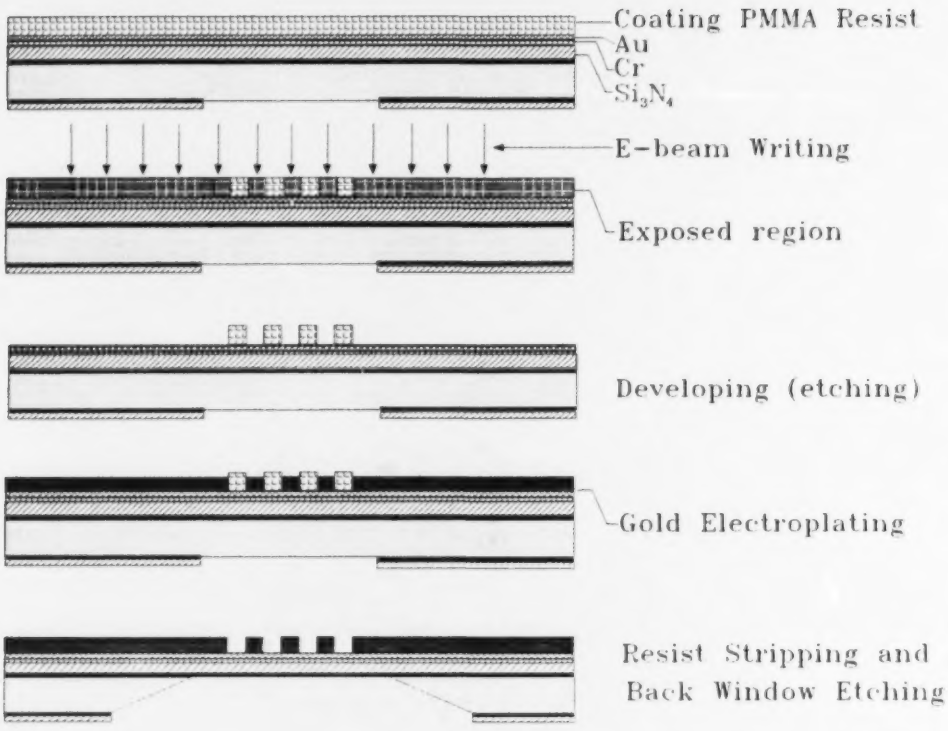

Figure 4.8. Mask making processing steps using the E-beam lithography.

It is important to check PMMA thickness during the coating process, and this was done using the Alpha-step 200 profilometer. Before measurement, the sample was scratched gently with a wafer tweezer to the gold layer surface beneath the resist. A sample of PMMA thickness measurement plot is shown in Figure 4.9.

Table 4.1. PMMA thickness and preparation for different feature size masks.

Mask feature sizes (μm)	PMMA thickness (nm)	Resist preparation (solution)
0.5	600	5% PMMA (PMMA:Chlorobenzene=5:2.5)
0.25	400	3% PMMA (PMMA:Chlorobenzene=3:4.5)
0.1	300	3% PMMA (PMMA:Chlorobenzene=3:4.5)

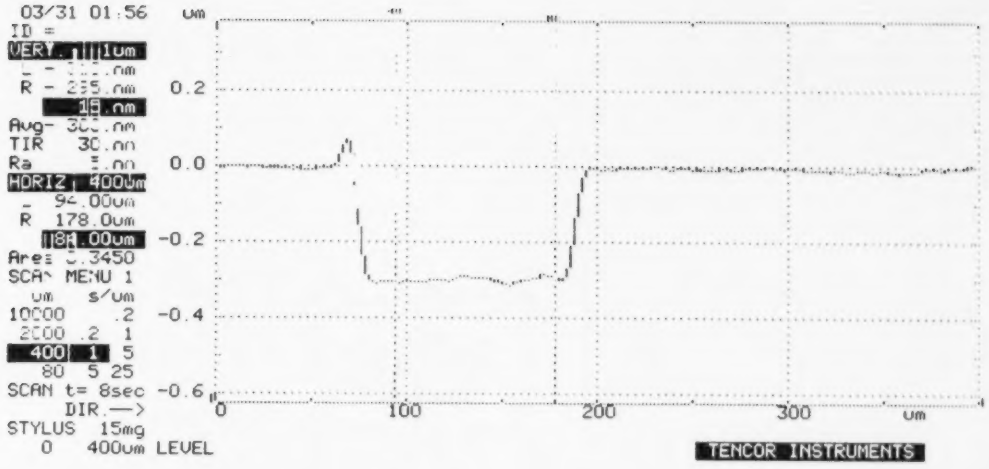

Figure 4.9. A sample plot of PMMA thickness measurement using Alpha-step 200 profilometer. The thickness and length scales are in microns.

The PMMA thickness was measured vs. the spin speed of the spinner, and the result is shown in Figure 4.10. It was found that the PMMA layer shrank during the soft baking process due to resist drying, corresponding to a thickness decrease of about 50 nm for a 350 nm resist coating as shown in the Figure 4.10. This should be taken into account since the PMMA thickness control is crucial for the exposure dose adjustment in writing masks.

4.1.4.2 SEM operation

The SEM interfaced with NPGS for E-beam lithography is a Cambridge Stereoscan 250. It is a thermionic emission type electron microscope, which can provide a maximum electron accelerating voltage of 40 keV. Each time a new filament is changed, necessary adjustments have to be made, which include: filament current, final aperture,

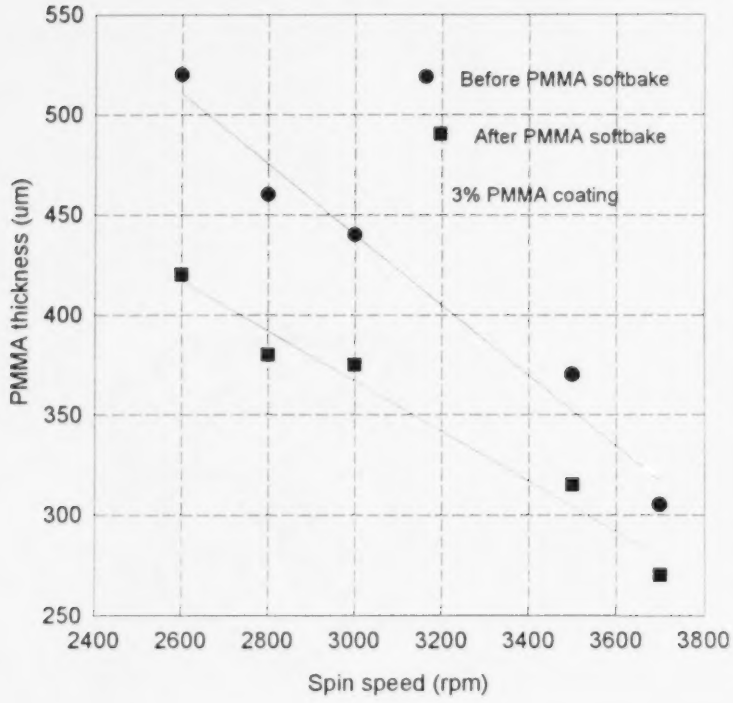

Figure 4.10. PMMA thickness vs. spin speed.

and astigmatism, etc. These adjustments are very important for the specimen examination as well as the E-beam lithography, and should be done according to the SEM operational manual[61].

The performance of the SEM was checked by writing the pattern as shown in Figure 4.11, which consists of a wheel circle with 12 spokes. The picture shows the view of the pattern in the PMMA resist. Since the circle and all the spokes received the same exposure, the line width difference vs. orientation shows that there was more noise in the horizontal than vertical direction for this SEM. As a result, the finger lines in the IDT were oriented in the vertical direction to get a better performance.

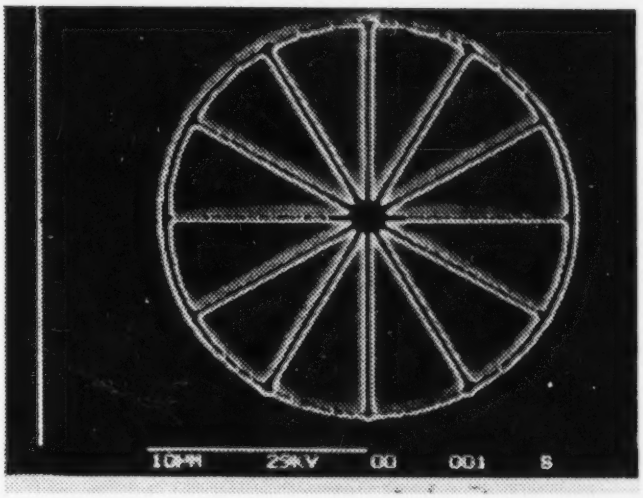

Figure 4.11. A sample test pattern written by the Cambridge Stereoscan 250 SEM[59].

As described previously, the mask substrate is a 8×9 mm^2 rectangle. The mask is mounted onto an Aluminum stub using carbon paste and placed onto the SEM stage as shown in Figure 4.11. The Aluminum stub with a cross on is used for the purpose of focusing and beam current measurement. Before writing, the edges of the mask sample

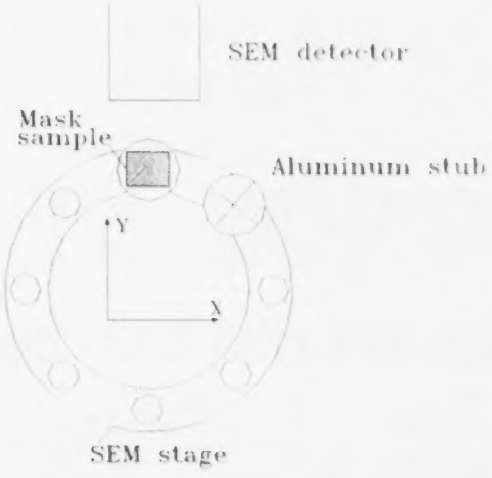

Figure 4.12. SEM stage with mask sample mounted on.

should be aligned to the stage motion directions X and Y, respectively. The stage position is indicated by the X and Y coordinates. The pattern is written in the center of the mask, and this can be done by moving the stage to the coordinate of the center. One of the problems of this SEM is that the pattern written is rotated a small angle relative to the sides of the mask even though the sides of the mask appear well aligned to the X and Y on the screen as shown in Figure 4.12. This could be a serious problem for the final device, causing the beam steering second order effect. The solution is to adjust the beam scan rotation to obtain the required angular correction. The written pattern orientation on the mask has been characterized as a function of the scan rotation, and the result is shown in Figure 4.13. It is clear that the scan rotation has to be turned 2.5° clockwise before writing after the mask sample has been aligned on the screen.

For the 0.1 μm linewidth SAW filter mask writing, it is necessary to put the IDT and contact pads in different layers and write them under different magnifications. A problem associated with this use is that the SEM patterns shift with each other under different magnifications. Fortunately, this can be compensated by adjusting the relative

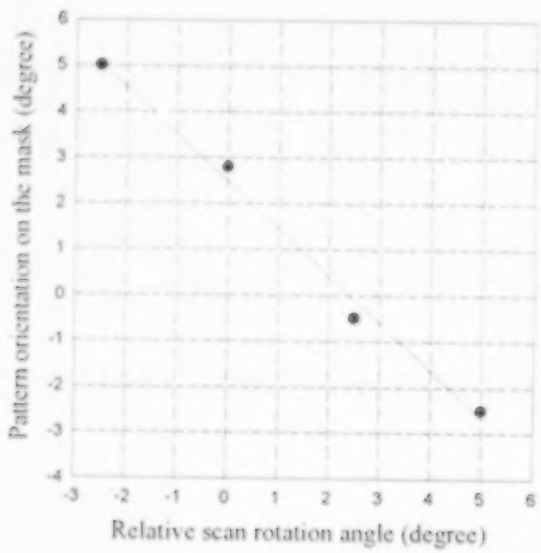

Figure 4.13. Characterization of pattern orientation vs. scan rotation of the SEM[59].

positions of patterns in different layers. After these adjustments, the SEM was found to be adequate for the E-beam lithography use. The detailed operating steps of the SEM for the E-beam writing are included in the Appendix II.

4.1.4.3 Exposures

The exposures applied to writing different feature size IDT finger patterns are summarized in Table 4.2. The experiment progressed from writing 1.0 μm and 0.5 μm linewidth masks using the Stereoscan SEM-120 working at 30 kV with filament current 60-70 pA on 600 nm PMMA[59]. The 0.25 μm linewidth mask was written initially using the Stereoscan SEM-120 with the filament current 40 pA and PMMA thickness 400 nm. The project continued with the 0.25 μm linewidth mask writing using the Stereoscan SEM-250 at 40 kV since the 400 nm was still too thick for writing at 30 kV using the Stereoscan SEM-120. Finally, The 0.1 μm linewidth mask was written successfully by the Stereoscan SEM-250 with low filament current 15-25 pA and 300 nm PMMA.

The Line Dose was used in the experiments to characterize the exposure, and the corresponding Area Dose was calculated using equation (4.5). As shown in Table 4.2, the Area Dose increases with higher electron beam energy, but doesn't change much with respect to the resist thickness for the same beam energy within the range of our experiments. Another fac: which needs to be respected is that the SEM has to work at

Table 4.2 Exposures for writing different feature size IDT finger patterns

Linewidth (μm)	0.5	0.25	0.25	0.1
PMMA thickness(nm)	600	400	400	300
Machine (Stereoscan)	SEM-120	SEM-120	SEM-250	SEM-250
E-Beam Energy (keV)	30	30	40	40
Filament current (pA)	60-70	40-70	40-70	15-25
Area Dose ($\mu C/cm^2$)	160	152	240	260
Line Dose (nC/cm)	2×4.0	4×0.95	4×1.6	4×0.65

extremely high resolution with the filament current close to 15 pA for writing the 0.1 μm linewidth mask. This is necessary to keep the exposure time not too short to be resonable for E-beam writing. Working at very high resolution makes it difficult to focus the SEM, and we have to pay more attention to the proximity effect in writing 0.1 μm linewidth mask which will be demonstrated later.

Figure 4.14 shows the linewidth vs line dose plot for writing a 0.25 μm pattern on 400 nm PMMA. It was found that many line doses had to be tried for the right exposure corresponding to a certain width line pattern. If the PMMA is too thick, it can not be etched down to the bottom. As shown in Figure 4.15, a 0.25 μm line pattern has been achieved while there is still some PMMA left at the bottom. As a result, the PMMA thickness has to be scaled down for writing a thinner width line pattern to remain below a certain aspect ratio, which is the ratio between the line depth and width.

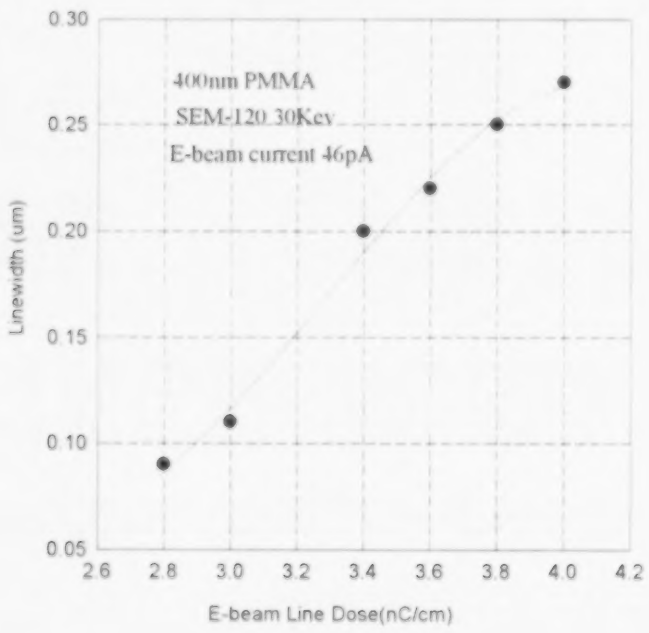

Figure 4.14. Plot of linewidth vs. E-beam line dose for writing a 0.25 μm linewidth pattern.

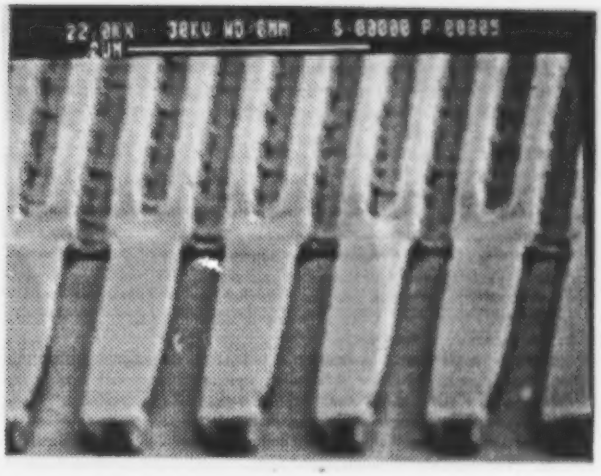

Figure 4.15. A 0.25 μm line pattern writtern not etched down to the bottom.

In E-beam writing, focusing the SEM is an important skill which needs a lot of practice, especially for patterning at very high resolution. Figure 4.16 (a) shows a granular structure pattern as a result of the SEM being out of focus. During a long period of time, the granular structure was suspected to be caused by the unknown "noise" inside or outside of the SEM. Later, it was found that focusing of the SEM was the major problem here. This problem was solved by producing some tiny dirt marks with a pencil in the vicinity of the

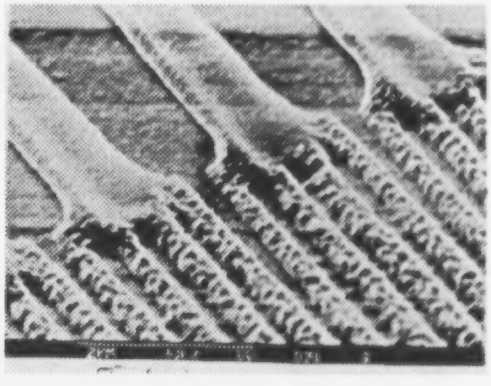

Figure 4.16. Granular structure pattern due to SEM being out of focus during E-beam writing.

pattern to be written, and focusing on them before E-beam writing. The poor quality pattern can also be discerned using an optical microscope right after being developed.

Figure 4.17 shows the SEM images of an underexposed and overexposed sample for comparision. The underexposed sample has narrower exposed lines etched away with PMMA still left in the exposed region while the overexposed sample gives exposed lines which are too wide with strong undercuts. A good exposure for a 0.25 μm mask is shown in Figure 4.18, which demonstrates a split-finger interdigital transducer pattern with uniform exposed linewidth and spacing.

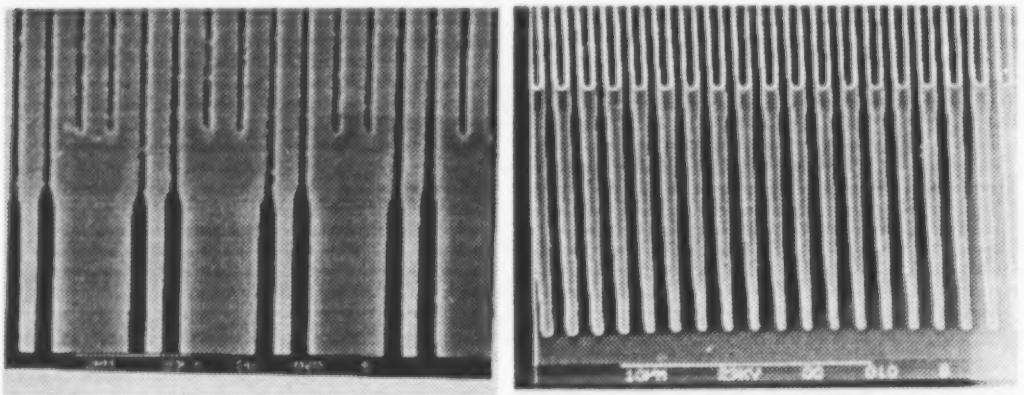

(a) (b)

Figure 4.17. SEM images showing an (a) underexposed (b) overexposed pattern.

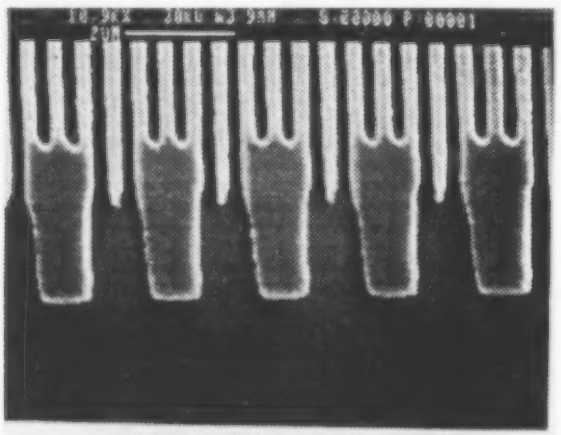

Figure 4.18. A SEM image of a well exposed 0.25 μm linewidth split finger IDT pattern.

While the 0.25 μm linewidth mask was written using the Stereoscan SEM-250 under 200X magnification, the 0.1 μm linewidth mask writing requires that the SEM works under higher magnification. As shown in Figure 4.19, the 0.1 μm pattern written under 200X was unacceptable. Figure 4.20 shows a good 0.1 μm linewidth pattern achieved with the SEM working under 1000X. When writing under higher magnification, the SEM moves the electron beam in a smaller center to center distance, so the pattern can be defined more precisely. In addition, larger voltages are required to deflect the beam for the same moving distance. Therefore, the SEM is also less susceptible to be affected by outside noise sources.

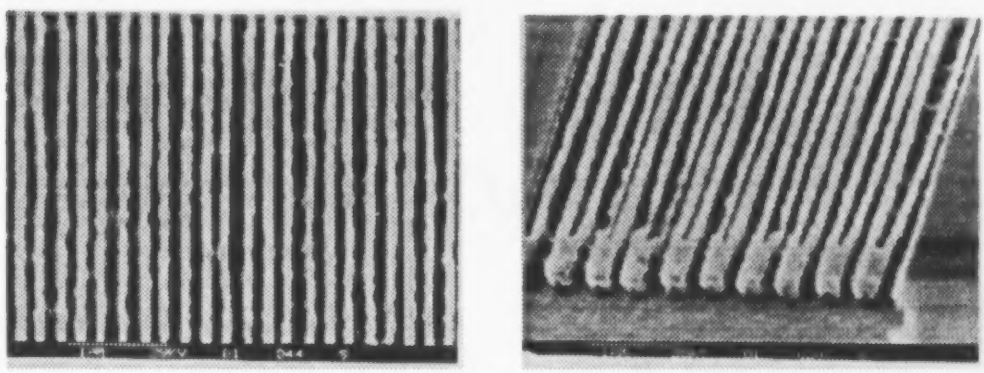

(a) top view (b) side view

Figure 4.19. A 0.1 μm linewidth mask pattern written under 200X magnification.

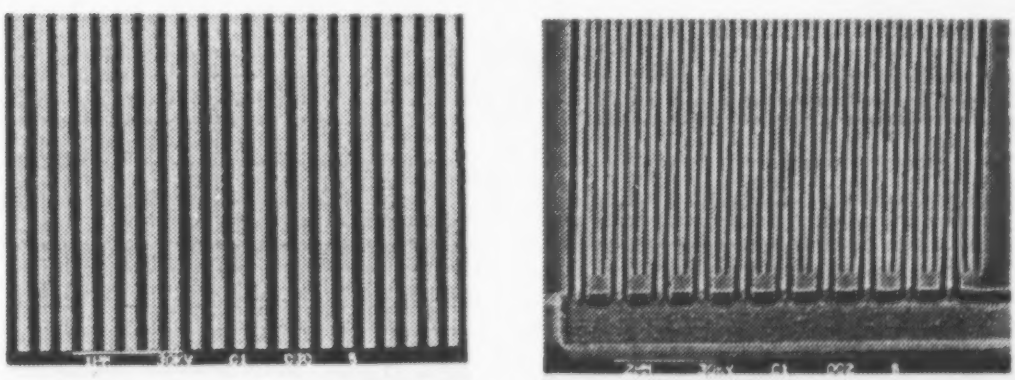

(a) top view (b) side view

Figure 4.20. A 0.1 μm linewidth mask pattern written under 1000X magnification.

4.1.5 Proximity Effect

As was described previously, when an electron beam enters a polymer film, it loses energy via electron scattering. The backscattered electrons in the resist and substrate partially expose the resist up to several micrometers from the point of impact, the well known proximity effect. Figure 4.21 gives a good demonstration of the proximity effect encountered in writing a 0.1 μm linewidth IDT. As shown in the figure, the backscattered electrons coming from the two sides of the IDT where they enter the resist traveled so far that two overexposed semi-circles result in the finger region.

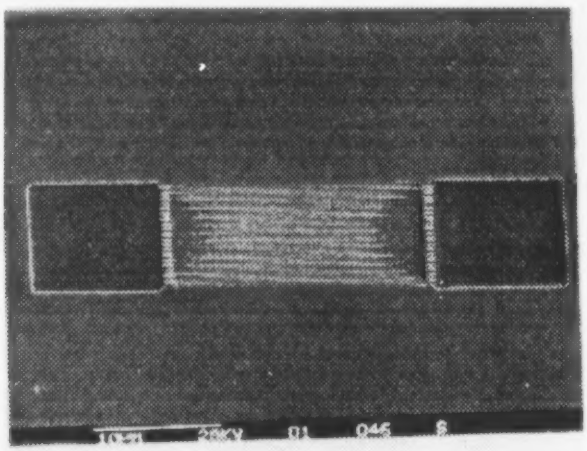

Figure 4.21. Proximity effect demonstration in writing a 0.1 μm linewidth IDT.

To compensate for proximity effects, special correction methods are needed in VLSI fabrication[62,63]. For the simple IDT patterns in this project, the proximity effect was corrected by adjusting the exposures in different regions of an IDT. As shown in Figure 4.22, the IDT pattern has been divided into three exposure regions and different doses are applied to them, respectively. Due to strong proximity effect in region 1, the dose applied there is less than those in regions 2 and 3. Figure 4.23 shows SEM pictures of a 0.25 μm linewidth mask writing before and after the proximity effect correction. In Figure 4.23 (a), the exposed lines on the edges of the IDT are narrower than those in the center. Therefore, a higher dose was applied to the lines on the edges, and the final mask after the proximity correction consists of uniform finger lines as shown in Figure 4.23 (b).

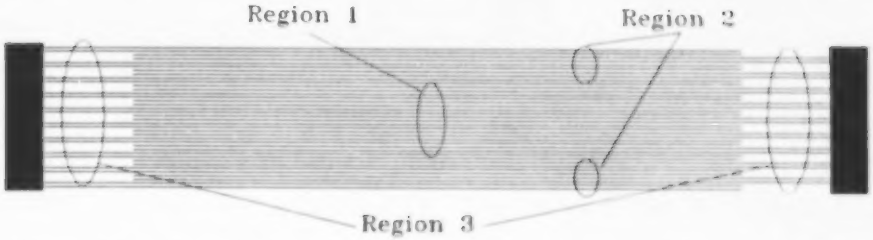

Figure 4.22. The IDT pattern has been divided into three different regions for proximity effect corrections.

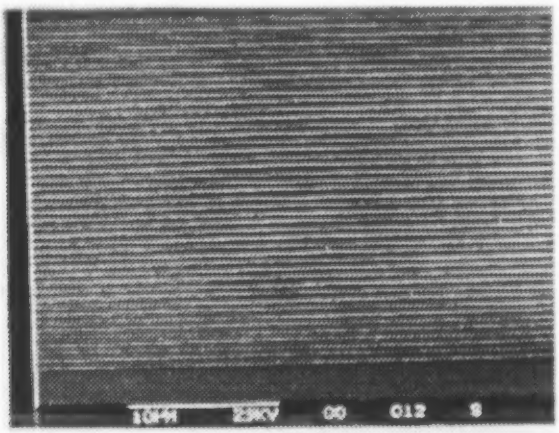

(a) pattern in PMMA before the proximity effect correction

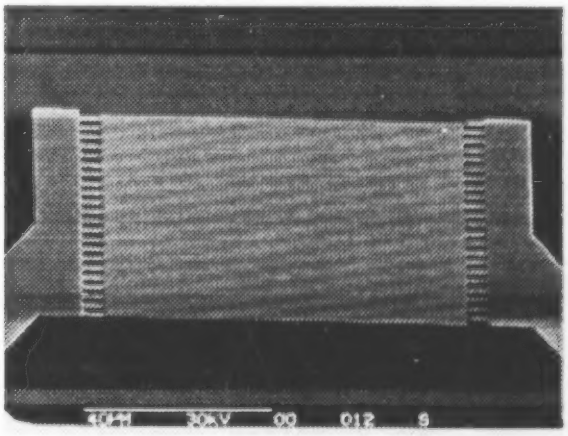

(b) mask after the proximity effect correction

Figure 4.23. The proximity effect correction for writing a 0.25 μm linewidth mask.

Figure 4.24 shows two pictures for a 0.1 μm IDT pattern written using the Stereoscan 250 SEM at 30 and 40 kV, respectively. The same doses were used in the writing of both patterns, but the finger region of the pattern written at 30 kV was apparently more seriously affected by the high exposure at the IDT side. The reason is that it is the backscattered electrons in the resist and substrate that really cause the proximity effect. Electrons injected with higher beam energy penetrate deeper into the substrate and undergo less backscattering. Therefore, the higher the electron beam energy, the less the proximity effect.

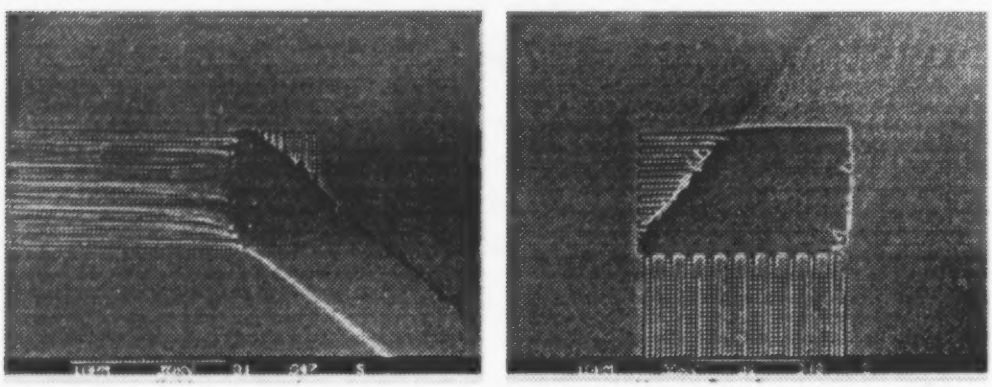

(a) (b)

Figure 4.24. A 0.1μm linewidth mask written with the same doses but the SEM working at different accelerating voltages (a) 30 kV (b) 40 kV[59].

The IDT side bar region can be formed by writing a group of lines, and this worked for the 0.25 μm linewidth mask. But a dilemma appeared in writing the 0.1 μm linewidth mask. If the dose is not enough for writing the IDT side, single lines will be formed as shown in Figure 4.25 (a). However, if the IDT side bar is exposed appropriately by applying more exposure, the IDT finger tips will be affected by the proximity effect as shown in Figure 4.25 (b). The problem was solved by writing polyfill instead of writing a group of lines, and the result is shown in Figure 4.26. In this case, the area dose applied by writing a group of lines is as high as 560 $\mu C/cm^2$ while half of the dose is enough for writing the polyfill. The conclusion is that it is better to avoid the proximity effect than to use it, especially in very fine feature size pattern definition.

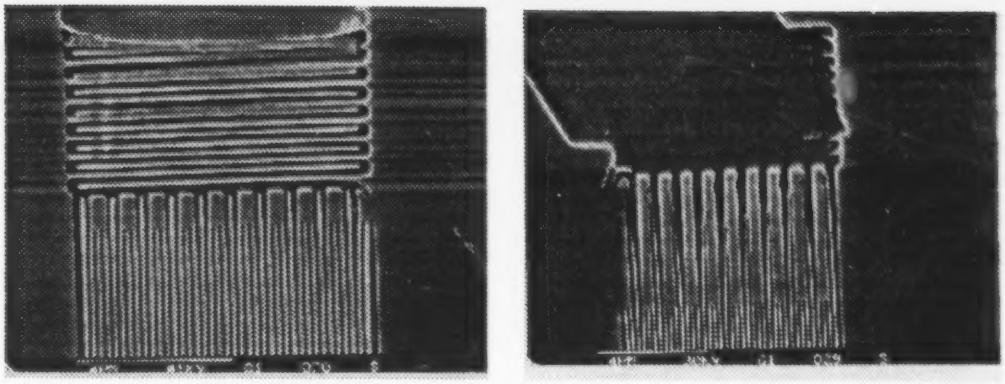

(a) (b)

Figure 4.25. The 0.1 μm linewidth mask IDT side bar region is written as a group of lines with the result that (a) single lines were formed when the dose was not enough (b) the IDT finger tips was affected although the exposure for the side was appropriate[59].

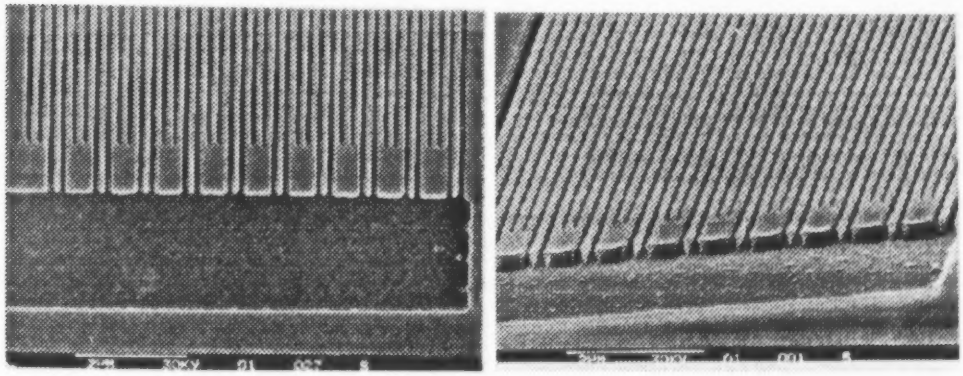

(a) top view (b) side view

Figure 4.26. The 0.1 μm linewidth mask IDT side bar region written by polyfill.

4.1.6 Masks

The SEM images of a 0.25 and 0.1 μm linewidth masks are shown in Figure 4.27. The spots on the IDT arms were caused by the electron beam sitting at those dump sites during E-beam writing. The contact pads of the 0.25 and 0.1 μm linewidth masks are 130×145 and 100×100 μm^2, respectively. To decrease the exposure time in writing the contact pads, the beam current is usually increased rapidly to about 100 pA which

decreases the resolution. To see more details of the gold fingers on these masks, SEM images are shown in Figures 4.28 and 4.29 for the 0.25 and 0.1 μm linewidth masks, respectively.

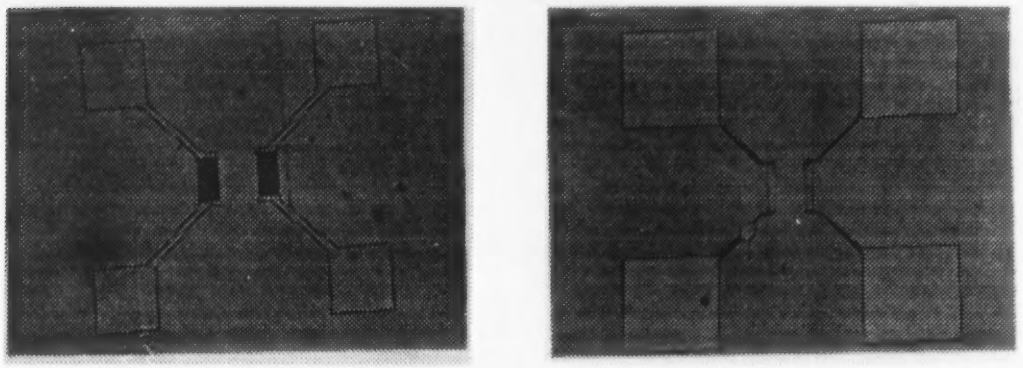

(a) (b)

Figure 4.27. SEM images of a (a) 0.25 μm and (b) 0.1 μm linewidth masks.

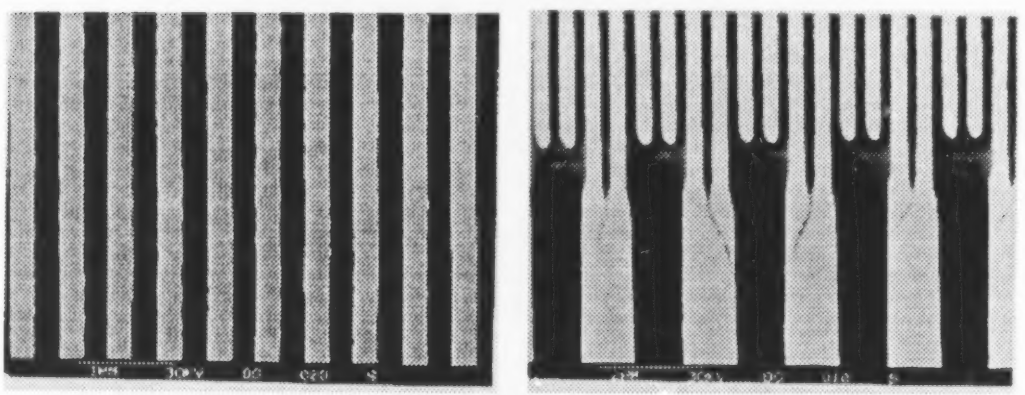

(a) top view (b) side view

Figure 4.28. SEM images of a 0.25 μm linewidth mask in gold pattern[59].

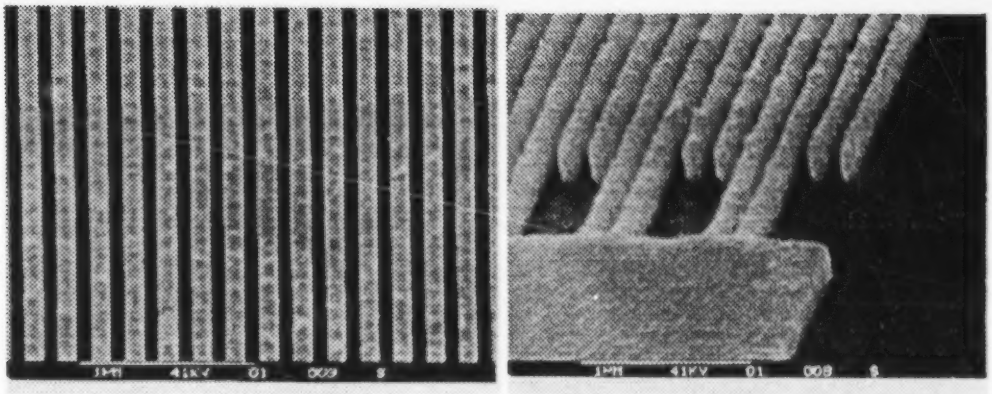

(a) top view (b) side view

Figure 4.29. SEM images of a 0.1 μm mask in gold pattern.

4.2 X-ray Lithography- Producing the Device

4.2.1 Laser Plasma X-ray Lithography

X-ray lithography is one of the main lithography techniques proposed for sub-0.25 μm line fabrication. Although photolithography technique has been continuously evolving and 193 nm deep ultra violet (DUV) lithography predicts a process development for 0.18 μm linewidth in 1998[64], X-ray lithography has its own special development target and is still an important technique under consideration for ultrahigh resolution lithography[65,66].

Laser plasma X-ray lithography provides an economic technique for producing submicron devices at a research and development level. Such a technique is potentially scalable to large scale production of devices, particularly where production runs are not so great as to justify very expensive synchrotron x-ray sources. The picosecond laser plasma developed by the Laser Plasma Group in the EE Department of the University of Alberta has successfully been used in producing the x-rays[67,68]. X-ray lithography based on this source has been well characterized[69] and has been used in producing SAW devices since 1994. The laser plasma X-ray lithography setup is shown schematically in Figure 4.30. The mask consists of an X-ray transparent membrane that supports a thin patterned film made

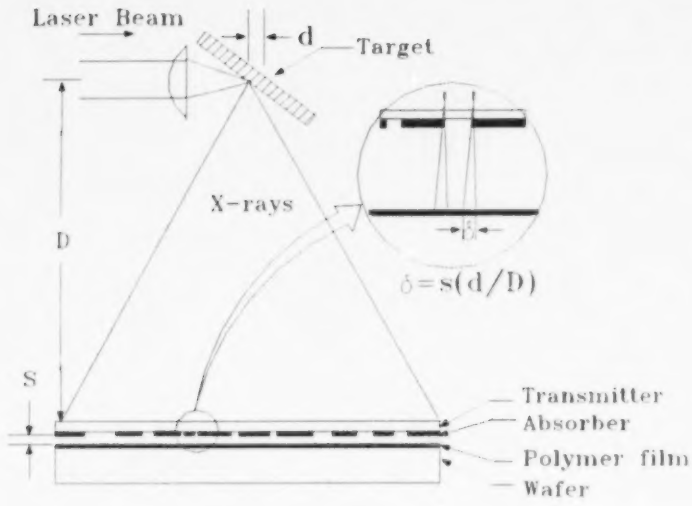

Figure 4.30. Schematic drawing of the laser plasma X-ray lithography technique.

of a material that strongly absorbs X-rays. The mask is placed over a substrate coated with a radiation-sensitive resist. A distant "point" source of ~ 1 nm wavelength X-rays from a laser produced plasma illuminates the mask, thus projecting the shadow of the X-ray absorber onto the polymer film. The inset of Figure 4.30 illustrates the penumbral distortion δ, which blurs the definition of lines in the resist and determines the minimum attainable lithographic feature resolution:

$$\delta = s(d / D) \tag{4.6}$$

where s is the spacing between the mask and the wafer, d is the source diameter, and D is the distance from the source to the mask. In any given exposure situation, the magnitude of δ can be made as small as required (such as 0.1 μm) by a proper choice of the parameters s, d and D.

In the experiment, the mask is made by the E-beam lithography process described in the last chapter, which consists of the gold pattern on Si_3N_4 membrane. The mask and substrate are mounted into the proximity printing chamber with 10 μm spacing separating them . Exposures can be made according to the previously characterized process.

4.2.2 Device Production

4.2.2.1 Wafer Preparation

The starting material is a three inch 128^0 YX-lithium niobate wafer. Before cutting the wafer into SAW substrates, impedance matching microstrip lines were first made on the wafer by conventional UV lithography using a linatronic mask. First, both sides of the wafer were coated with 1.5 μm aluminum. Then, both sides of the wafer were coated with 3 μm HPR 506 photoresist, and UV exposure was applied to the wafer top surface using the linatronic mask. Next, the resist was developed to expose the desired pattern, which was followed by the standard aluminum wet etching procedure at AMC. After etching, the impedence matching microstrip lines were left on the top surface while the aluminum on the wafer back would be used as the ground plate. After these steps, the wafer was cut into 8×9 mm^2 substrates for the device fabrication[70].

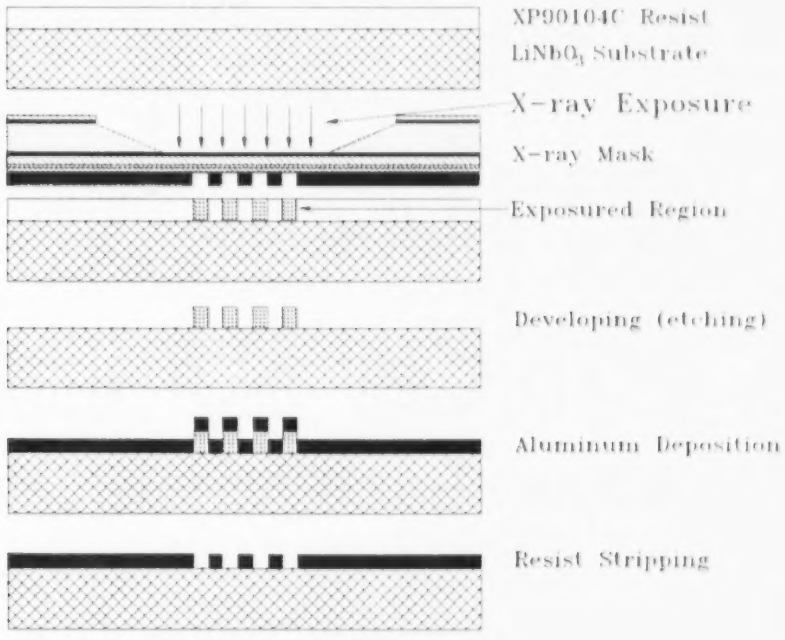

Figure 4.31. Device production processing steps by the X-ray lithography.

4.2.2.2 Device Production Process

The device production process is shown in Figure 4.31. First, the 8×9 mm^2 $LiNbO_3$ substrate is cleaned and coated with 500 nm thick Shipley XP90104C negative resist, then hexamethylenedisiloxane (HMDS) is applied to the resist and soft-baked in a vacuum hot plate for 40 seconds at 150°C. Second, the substrates and the X-ray mask are mounted into the X-ray lithography holder, and the exposure is made in the X-ray lithography chamber. Third, the exposed samples are baked in a hot plate for 60 seconds at 110 °C, then developed in Shipley MF-312 for 2 minutes, followed by water rinse for 30 seconds and dried. Next, a 150 nm aluminum layer is deposited by E-beam evaporation onto the substrate. Then, the lift-off process is carried out by stripping the resist and raised metal areas. Finally, the contact pads of the device are bonded onto the impedance matching microstrip lines by microbonding with 50 μm diameter wires.

The laser plasma X-ray lithography process has been successfully used in producing the 0.25 μm linewidth SAW filter, and the experimental details have been published recently[71]. Figure 4.32 shows the full picture of a 0.25 μm linewidth SAW filter which has been fabricated, and a SEM image of this filter in Aluminum electrodes is shown in Figure 4.33. By the time of this thesis is written, the 0.1 μm linewidth SAW device fabrication is in progress.

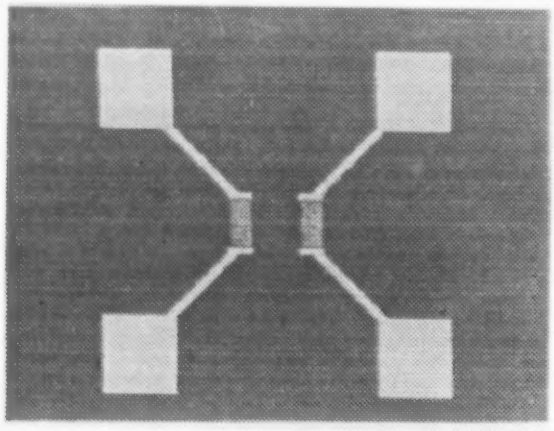

Figure 4.32. The full picture of a 0.25 μm linewidth SAW filter fabricated by the laser plasma X-ray lithography technique (contact pads dimention 130×145 μm^2)[71].

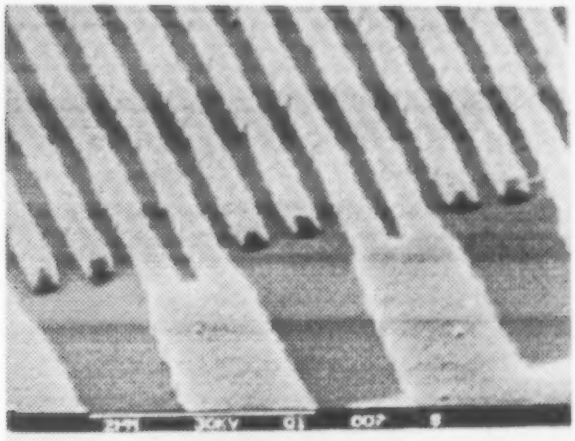

Figure 4.33. An SEM image of the 0.25 μm linewidth SAW filter showing the Aluminum electrodes[71].

5 Characterization of the 0.25 μm Linewidth SAW Filter

5.1 Filter Testing

5.1.1 Packaging Design

As is calculated, the center frequency of the 0.25 μm linewidth SAW filter is approximately 2 GHz, which is in the microwave L band range. The wavelength and frequency of an electromagnetic wave is governed by the relationship

$$\lambda = \frac{c}{f} \tag{5.1}$$

where λ = the wavelength, f = frequency, and $c = 3\times10^8$ m/s, the speed of light. By equation (5.1), the wavelength at 2 GHz is calculated to be 15 cm. Since the size of the device including its package will be comparable to the microwave signal wavelength, microstrip transmission lines have to be used in the device packaging design.

Figure 5.1 shows a SAW filter mounted on a circuit board with impedance matched microstrip lines and high frequency SMA connectors for testing. The transmission line design includes two parts: the aluminum (Al) microstrip lines on the $LiNbO_3$ substrate which was formed in the device fabrication processing, and the copper (Cu) microstrip lines on the circuit board, both are matched to 50 Ω to get the maximum power transmission. This design allowed very short (1-2 mm) bonding wires to be bonded to the Al transmission lines from the bonding pads of the transducers. Since long bonding wires (>1 cm) would act as antennas and cause strong electromagnetic wave coupling from input to output of the filter at such a high frequency, this packaging scheme has improved the filter performance. As shown in Figure 5.1, the SAW filter chip is embedded into the circuit board as a planar structure, and the connection between the Al and Cu microstrip lines is made using silver conductive adhesive.

The Cu microstrip line structure is shown in Figure 5.2. The top metal is used for the transmission line and the bottom metal is the ground plane. The material used is RT/duroid 5870 Microwave Laminate with dielectric constant $\varepsilon_r = 2.33$, h = 0.0620 inch,

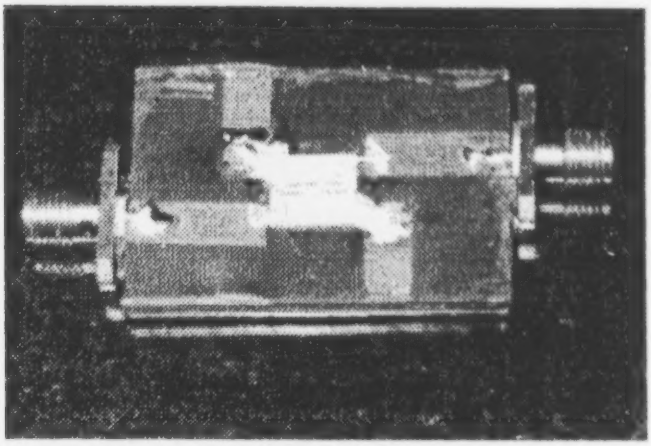

Figure 5.1. A SAW filter mounted on a circuit board with impedance matched microstrip lines and high frequency connectors.

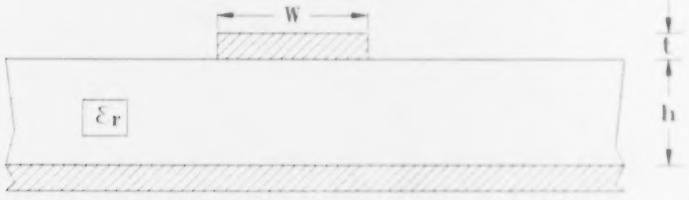

Figure 5.2. Microstrip line.

t = 0.00134 inch. To obtain a 50 Ω characteristic impedance Z_0 at 2 GHz, the microstrip line width W was found to be 0.18447 inch or 4.69 mm[72].

The Al transmission line design on $LiNbO_3$ uses the coupled stripline structure as shown in Figure 5.3. In the design calculation, a series of emperical formulas were followed to determine the characteristic impedance using the odd mode symmetry case[73]. In order to obtain a 50 Ω impedance matched microstrip line at 2 GHz, the transmission line width (w) and spacing (s) were hence determined and the results are shown as follows[74]: ε_r ($LiNbO_3$) = 30, h = 0.5 mm, t = 0.5 μm, w = 0.105 mm , and s = 1 mm.

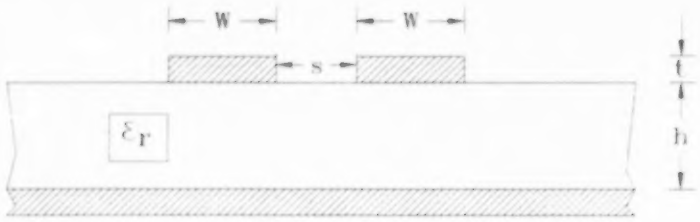

Figure 5.3. Coupled microstrip line.

5.1.2 Testing

Figure 5.4 illustrates the power flow in the SAW filter testing using the HP 8756A scalar network analyzer and HP 8350B sweep oscillator. In the figure, the input power is from HP 8350B; **R** is the reference power, and **B** and **A** are the power transmitted and reflected from the SAW filter, respectively. All these three signals enter the HP 8756A, and the transmission frequency response of the SAW filter can be analyzed and plotted out. Another network analyzer used in the testing is the HP 8510B, which not only gives direct measurement of the filter frequency transmission characteristic but also provides some advanced signal processing capabilities which enable us to remove spurious responses from the measured response using a time gating technique which is described below.

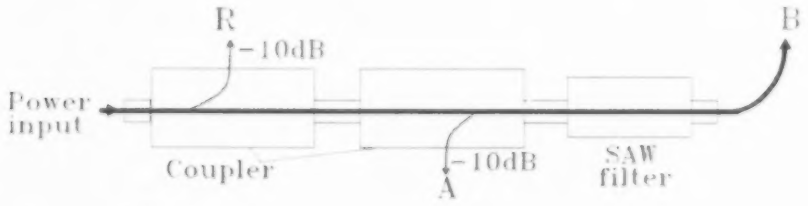

Figure 5.4. Power flow in the SAW filter testing using the scalar network analyzer HP 8756A with HP 8350B sweep oscillator.

5.2 Time Gating

As far as a filter testing is concerned, its impulse response and frequency response consist of a Fourier transform pair, and both of them contain the information to describe the performance of the filter. Therefore, the frequency response characteristics of a SAW

filter can also be analyzed by examining its impulse response. There are two approaches for doing this. First, apply an impulse input signal to the input of the filter, and observe its impulse response at the output. Second, obtain the impulse response by applying an Inverse Discrete Fourier Transform (IDFT) to the measured frequency response data. The latter provides an effective means for finding out the distortion problems in the frequency response of a SAW filter.

Time gating is a technique for removing unwanted perturbations by processing the calculated impulse response. As discussed previously, electromagnetic feedthrough (EM) and triple-transit interference (TTI) cause amplitude and phase ripples at frequencies $f_{EM} = 1/\tau$ and $f_{TTI} = 1/2\tau$ in the frequency response of a SAW filter, respectively, where the time τ is given by

$$\tau = \frac{d}{v} \tag{5.2}$$

d is the distance between the phase centers of the two IDTs, and v is the acoustic wave velocity. In the impulse response obtained from the frequency response, EM and TTI will appear as two peaks on the two sides of the main peak signal with EM arriving earlier and TTI arriving later than the main peak signal. By applying the "time gating" to this impulse response and then returning back to the frequency domain, the spurious responses caused by EM and TTI can be gated out. Time gating can be realized by using commercial softwares provided with the measurement instrumentation or implemented using algorithms. In this project, time gating was applied to the SAW filter testing using the network analyzer HP 8510B, which has built-in Fourier transform and time gating processors, so that spurious responses were easily identified in the time domain and eliminated. Therefore, the "cleaned" response transformed back to frequency domain is free of parasitic coupling and triple transit interference effects, giving the expected response for a single transit surface acoustic wave signal.

5.3 Characterization of the 0.25 μm Linewidth Filter

This project was carried out based on the previous work on the SAW filters with linewidth of 1 μm and 0.5 μm[74]. In this section, the major discussion will be devoted to

the characterization of the 0.25 μm linewidth filter. However, it is worthwhile to compare the testing results of the 1 μm and 0.5 μm linewidth SAW filters with the current 0.25 μm linewidth filter.

The configuration parameters for the 1 μm linewidth SAW filter is listed in Table 5.1. Figure 5.5 shows the frequency response of the 1 μm linewidth filter, not using split finger geometry, tested using HP 8756A, and its characteristic parameters measured and calculated are compared in Table 5.2. The measured parameters from the table are obtained from the frequency response curve of Figure 5.5 according to the definitions in section **2.5.** As shown in table 5.2, the center frequency of this filter is slightly higher than predicted. This could be caused by mass loading effect and the fabricated linewidth accuracy. The higher insertion loss results from circuit mismatches. Due to loss of active fingers in the fabrication, the bandwidth is wider than the theoretical value. The lower stop band rejection level is associated with direct feedthrough signals from the electromagnetic coupling. The most obvious distortion of this device is the high amplitude ripple in the

Table 5.1. The configuration parameters for the 1.0 μm linewidth SAW filter.

Type of IDT	Single electrode
Electrode seperation (μm)	1.0
Number of IDT finger pairs (pairs)	34
IDT finger overlap aperature (μm)	80
Seperation between two IDT centers (μm)	140
Aluminum electrode thickness (nm)	200

Table 5.2. Characteristic parameters of the 1.0 μm linewidth SAW filter.

Parameters	measured	calculated by theory
Center frequency (GHz)	1.0649	0.998
Insertion loss (dB)	11.73	6
3 dB bandwidth (MHz)	26	18
Shape factor	2.0	-
Close-in stop band rejection (dB)	15	24
Passband amplitude ripple (dB)	5	4.5
Triple-transit suppression (dB)	10	12

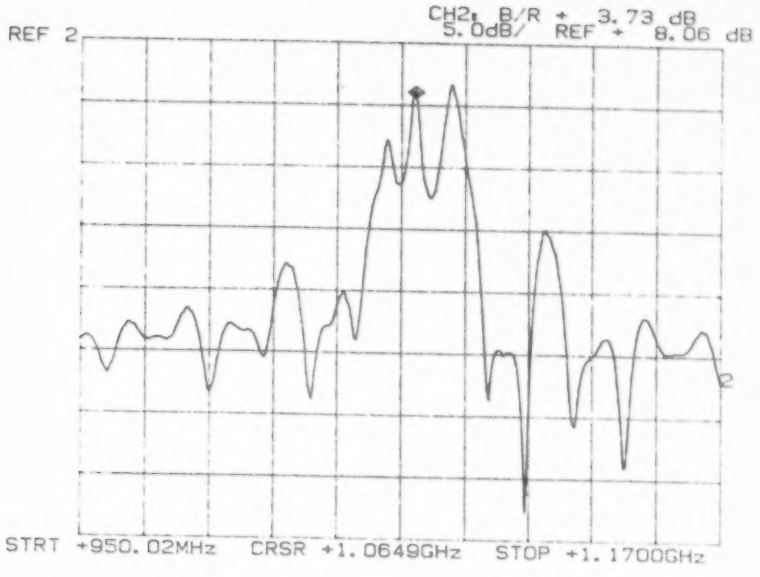

Figure 5.5. Frequency response of the 1 μm linewidth SAW filter tested using HP 8756A. The horizontal and vertical scales are 22 MHz and 5 dB per division, respectively.

passband, which has a periodic frequency of 14 MHz as seen in the measurement. In this design, the separation between the two IDTs is 140 μm, which corresponds to a time separation

$$\tau = \frac{d}{v} = \frac{140 \times 10^{-6}\,\text{m}}{3992\,\text{m/s}} = 3.5 \times 10^{-8}\,\text{s}$$

Thus, the triple transit interference ripple frequency is

$$f_{TTI} = \frac{1}{2\tau} = \frac{1}{2 \times 3.5 \times 10^{-8}} = 14.3\ \text{MHz}$$

Therefore, the passband ripple is caused by the TTI signal. Taking the finger reflections into account, the measured ripple level is higher than the ripple caused by TTI alone.

The configuration parameters for the 0.5 μm linewidth SAW filter is listed in Table 5.3. The frequency response of the 0.5 μm linewidth SAW filter, not using split fingers, is shown in Figure 5.6, and its characteristic parameters are given in Table 5.4. For the same

Table 5.3. The configuration parameters for the 0.5 μm linewidth SAW filter.

Type of IDT	Single electrode
Electrode seperation (μm)	0.5
Number of IDT finger pairs (pairs)	25
IDT finger overlap aperature (μm)	80
Seperation between two IDT centers (μm)	100
Aluminum electrode thickness (nm)	200

reason as the 1 μm linewidth device, there is still a slight center frequency shift. The insertion loss is close to 6 dB, which shows that this filter is well matched to 50 Ω at both the input and output. The most serious problem of this filter is that the frequency response has been corrupted by the electromagnetic feedthrough signal, resulting in a close-in stop band rejection of only 2 dB. In addition , the measurements of bandwidth and shape factor don't make much sense due to spurious responses in the passband. Carefully examining the passband, we can find that two types of ripples showed up: the ripple of about 2.6 dB in level at a periodic frequency of 41 MHz is caused by EM signal, and the other ripple at

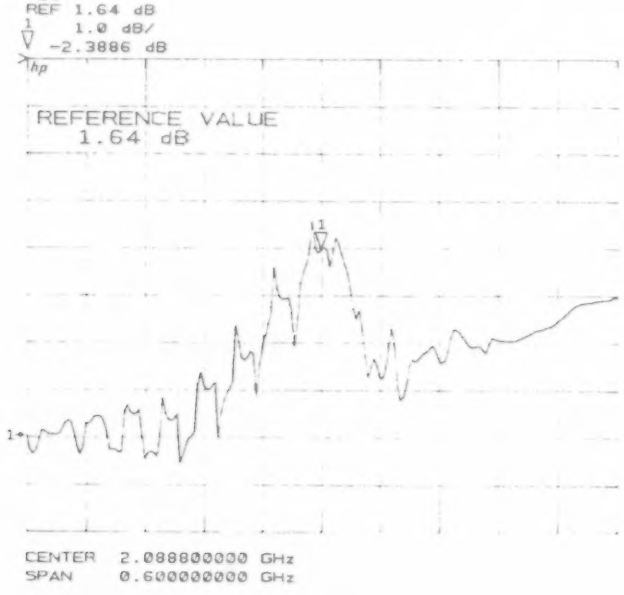

Figure 5.6. Frequency response of the 0.5 μm linewidth filter tested using HP 8510B. The horizontal and vertical scales are 60 MHz and 1 dB per division, respectively.

Table 5.4. Characteristic parameters of the 0.5 μm linewidth SAW filter.

Parameters	measured	calculated by theory
Center frequency(GHz)	2.088	1.996
Insertion loss (dB)	6.4	6
3dB bandwidth(MHz)	123	80
Shape factor	2.0	-
Close-in stop band rejection(dB)	2	24
EM passband ripple(dB)	2.6	-
TTI passband ripple (dB)	-	4.5

a periodic frequency of 20 MHz is due to TTI and finger reflections. These ripples can be verified by calculating the appropriate parameters:

$$\tau = 2.25\times10^{-8}\ \text{s}$$

$$f_{TTI} = 22\,\text{MHz}$$

$$f_{EM} = 44\,\text{MHz}$$

It is clear that electromagnetic feedthrough has become the most detrimental second order effect to the operation of filters at this high frequency - 2 GHz. Further, it is hard to distinguish the ripple levels caused by TTI and finger reflections due to the overwhelming role of the electromagnetic feedthrough signal.

Table 5.5 lists the configuration parameters of the 0.25 μm linewidth SAW filter. Figure 5.7 shows the frequency response of a 0.25 μm linewidth filter tested. Since split finger geometry was used in the design, the center frequency is still around 2 GHz although the finger linewidth has been reduced to half with respect to 0.5 μm linewidth (2 GHz) filter. As expected, there is a high frequency modulation in the passband, and the frequency of this ripple was measured to be 32 MHz. Following equation (5.2), the time separation of the two IDTs and the feedthrough ripple frequency are given by

$$\tau = 3.2\times10^{-8}\ \text{s}$$

$$f_{EM} = 31.2\ \text{MHz}$$

Therefore, the high frequency ripple is caused by electromagnetic feedthrough

Table 5.5. The configuration parameters for the 0.25 μm linewidth SAW filter.

Type of IDT	Split electrode
Electrode separation (μm)	0.25
Number of IDT finger pairs (pairs)	22
IDT finger overlap aperature (μm)	80
Seperation between two IDT centers (μm)	128
Aluminum electrode thickness (nm)	150

Figure 5.8 shows the impulse response obtained from the frequency response of Figure 5.7 using Inverse Discrete Fourier Transform provided by the HP 8510B network analyzer. In Figure 5.8, the peak at 40 ns is the main SAW signal while the peak at the left side is the spurious response due to electromagnetic feedthrough and the second peak at the right side is caused by triple transit interference since it is delayed by 2τ relative to the main peak signal, where $\tau = 32$ ns. The first right side peak delayed by τ with respect to the main peak may be associated with an unknown double transit signal.

To remove these second order effects, the time gating technique introduced in **5.2** was applied to the impulse response of Figure 5.8. Figure 5.9 shows the impulse response after time gating about the main impulse peak at 40 ns using the HP 8510B software. Figure 5.10 shows the "cleaned" frequency-domain amplitude response of the 2 GHz filter after those perturbations have been removed. It can be seen that the filter passband is now smooth without ripples.

The measured characteristic parameters of the 0.25 μm linewidth SAW filter are listed in Table 5.6 together with the theoretically expected values. The center frequency is close to the designed value because the mass loading effect has been reduced by the split finger design. The insertion loss is much higher than predicted. There are two reasons for this : first, the thickness of the finger metal layer is too high, resulting in strong acoustic attenuation in the electrode region; second, loss of active fingers in the fabrication process caused impedance mismatch and increased the insertion loss. Loss of fingers also contributes to the wider 3 dB bandwidth measured compared to expected as well. Since electromagnetic feedthrough has been removed, the sidelobe rejection is close to the design value, and less distortion is obvious in the filter response curve as is manifested by

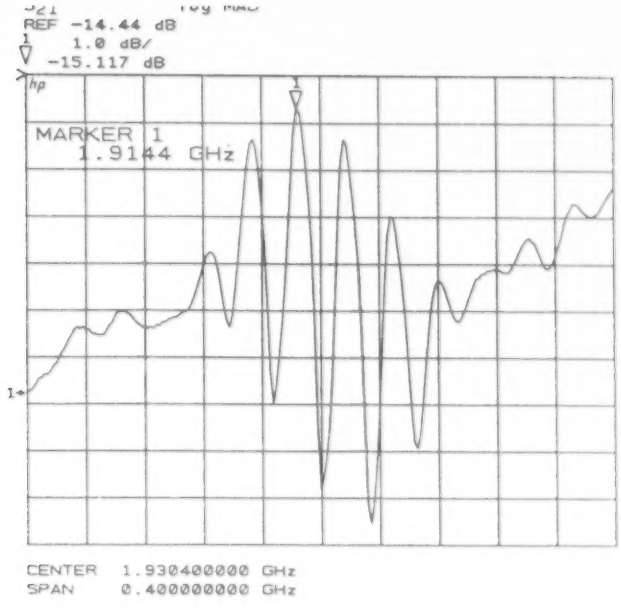

Figure 5.7. Frequency response of the 0.25 μm linewidth filter tested using HP 8510B. The horizontal and vertical scales are 40 MHz and 1 dB per division, respectively.

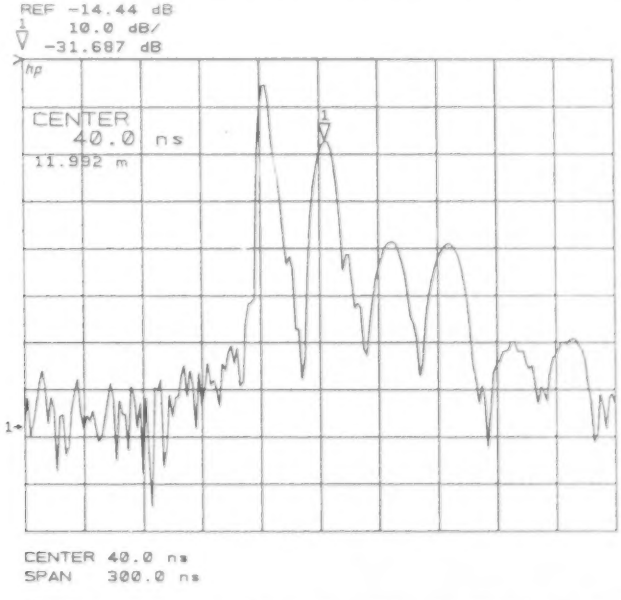

Figure 5.8. Impulse response of the 0.25 μm linewidth filter obtained from the frequency response of Figure 5.7 using HP 8510B. The horizontal and vertical scales are 30 ns and 10 dB per division, respectively.

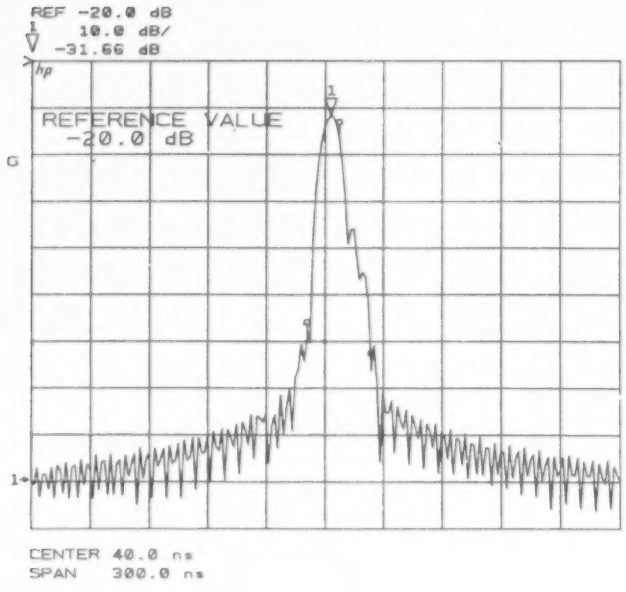

Figure 5.9. Time gating is applied to the impulse of Figure 5.8 to remove second order effects caused by electromagnetic feedthrough and triple transit interference. The horizontal and vertical scales are 30 ns and 10 dB per division, respectively.

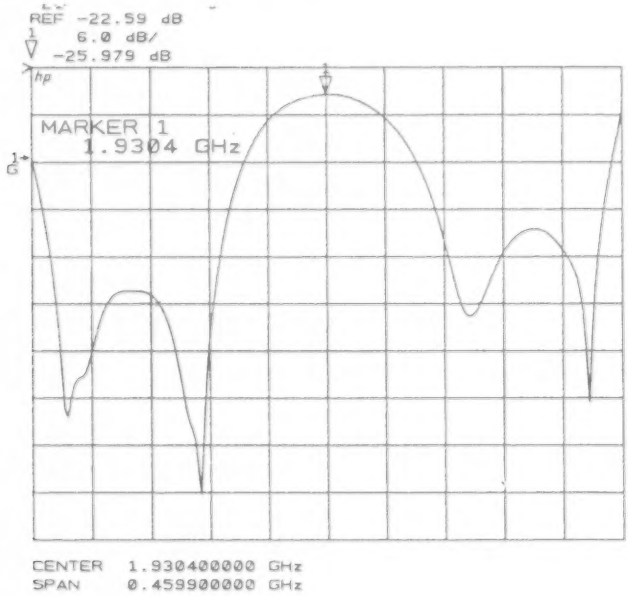

Figure 5.10. Amplitude frequency response of the 0.25 μm linewidth filter after spurious responses have been removed. The horizontal and vertical scales are 46 MHz and 6 dB per division, respectively.

Table 5.6. Characteristic parameters of the 0.25 μm linewidth SAW filter with spurious responses removed.

Parameters	measured	calculated by theory
Center frequency (GHz)	1.93	1.996
Insertion loss (dB)	29.4	6
3 dB bandwidth (MHz)	95	82
Shape factor	4.0	5.8
Close-in stop band rejection (dB)	18	24

the shape factor. Although the characteristic response of this filter is still not ideal, it shows that the filter response is close to what it should be when parasitic electromagnetic coupling and triple transit interference removed for this simple design.

In the IDT design, it is assumed that the finger width and spacing are equal, corresponding to a metalization ratio of 0.5, which is defined as the ratio of finger width to period. However, the metalization ratio of the actual 0.25 μm linewidth device was found to be 0.57, giving an error of 15% approximately. This would cause a phase shift of finger reflections since the centers of reflection are associated with the edges of the finger. As a result, the finger reflections could not be totally eliminated by the split-finger design, contributing to more ripples in the filter responses. Another effect of this fabrication inaccuracy is that it will affect the relative amplitudes of harmonics, but this effect can be ignored since foundamental response is the dominant one for this design.

As is seen above, electromagnetic feedthrough is one of the most serious problem for GHz SAW filters. In the actual device application, special techniques are required to minimize its effect. These include improved device packaging and dimension design[75,76], proper shielding, and judicious placement of ground connections. In addition, the direct through signals can also be suppressed by using specially designed circuits. For example, Figure 5.11 shows the circuitry of the balanced transformer technique for the feedthrough suppression. As shown in the figure, the balanced transformer converts the normally unbalanced input leads to a balanced arrangement to combat electromagentic feedthrough. The trade-offs made here are the increased circuit

design complexity, cost and size. This problem will not be explored further in this project, its solution is closely related to high frequency circuit design experience. It can be expected that any improvement made in this aspect will help to push these GHz filters further into practical working devices.

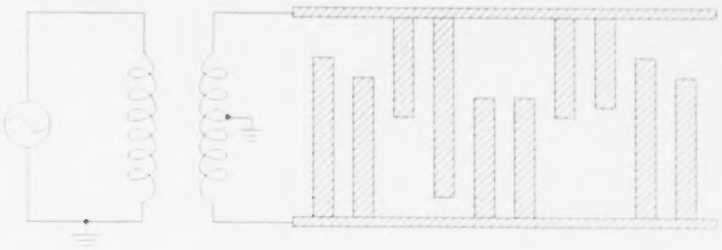

Figure 5.11. The circuitry of the balanced transformer technique for the Electro-magnetic feedthrough suppression. Ideally, the transformer converts the unbalanced input line to a balanced one[from ref. 19 p.126].

6 Conclusion

The goal of this project was to demonstrate the feasibility of the laser plasma X-ray lithography process to the manufacture of SAW devices with feature sizes from 0.25 down to 0.1 μm. The results presented were the design, fabrication and characterization of a 0.25 μm linewidth SAW filter. In addition, the first fabrication stage of the 0.1 μm linewidth SAW filter, the X-ray mask, has been completed with the results shown as well.

The SAW filters dealt with in this project are linear phase bandpass filters. Despite being over-simplified, the delta function model illustrates some important features of the SAW filter directly. The filter response can be described by either impulse response or frequency response, a Fourier transform pair. By using apodization weighting or withdrawal weighting, the frequency response could be designed to approach a required response function although this was not carried out in the present thesis project. For our simple design, the SAW filter parameters were calculated from the filter design models, and compared to the final characterization of the fabricated filters.

A basic interdigital transducer was used for the design of the present SAW filter. Based on the IDT analysis, 2 GHz and 5 GHz SAW filters with the IDT finger linewidths of 0.25 and 0.1 μm using 128^0 rot. YX $LiNbO_3$ were designed, respectively. The filter configuration consists of two identical unapodized birdirectional IDTs with uniform finger width and spacing. To eliminate the second order effect of finger reflections, a split-finger geometry was used in the IDT design. The filters were designed to be matched to 50 Ω and the series inductors provided by the boding wires in the device fabrication were judiciously used to tune out the capacitive reactances of the IDTs.

The SAW filters were fabricated by two important processing steps: EBL for making the masks, and XRL for producing the devices. The EBL was done using a stereoscan SEM-250 interfaced with the NPGS, and the whole processing was characterized, including resist coating, SEM operation, exposure and proximity effect corrections. The resist used was PMMA with the thicknesses of 400 and 300 nm for producing the 0.25 and 0.1 μm linewidth masks, respectively. The final fabricated X-ray

mask consists of gold patterns on a 1 μm thick Si_3N_4 membrane. The device production was finished by transferring the mask pattern to the $LiNbO_3$ SAW substrate using the laser plasma X-ray lithography exposure station which had been previously characterized. The processing steps also include the fabrication of Aluminum transmission lines on the SAW substrate, which enabled short bonding wires to be used for reducing the electromagnetic couplings.

The 0.25 μm linewidth SAW filter was characterized using the HP 8510B Network Analyzer. For the purpose of testing, the SAW filter was mounted onto a circuit board with impedance matched microstrip lines terminated by SMA connectors. The direct measurement of the filter power transmission characteristic showed that the filter frequency response was corrupted by the strong electromagnetic feedthrough signal. As a result, the time gating technique was applied, and the spurious responses caused by TTI and EM feedthrough were removed by this technique. The final "corrected" filter frequency response had a center frequency of 1.93 GHz with a 30 dB insertion loss and 95 MHz bandwidth at 3 dB. Except for the high value of insertion loss, the characteristic parameters were close to the expected of our simple design.

In conclusion, the fabrication of 0.25 μm linewidth SAW devices has been successfully demonstrated using x-ray lithography and the fabrication of x-ray masks for 0.1 μm linewidth devices has also been demonstrated. It is expected that the device performance could be improved considerably by using more sophisticated transducer designs, better impedance matching and layout techniques and better electromagnetic shielding of the input and output transducers from each other.

References

1. R.M. White and F.W.Voltmer, " Direct piezoelectric coupling to surface elastic waves," Appl. Phys. lett., Vol. 17, pp.314-316, 1965.

2. J.G. Gualtieri et al, " Piezoelectric materials for acoustic wave applications," IEEE Trans. UFFC , Vol. 41, No. 1, pp. 53-59, Jan.1994.

3. RFM 1995 Porduct Data Book, RF Monolitics, Inc. , Dallas, Texas.

4. Hideki Ohmori, "SAW filters hold key to creating small, portable equipment", Journal of Electronic Engineering, pp. 63-68, May,1992.

5. Kazuo Eda, "Ultra-Small SAW filter works in mobile communication", Journal of Electronic Engineering, pp. 54-57, May, 1992.

6. Satoshi Ohta, "Progress in SAW filters responds to mobilecom needs", Journal of Electronic Engineering, pp. 58-62, May,1992.

7. E.M., Biebl, et al, "High performance mobile communication front-ends in the GHZ range using low loss SAW-filters", IEEE 1991 Ultrasonics Symp. Proc., pp. 55-58, 1991.

8. P.M. Naraine and C.K. Campbell, "Gigahertz SAW filters on YZ -lithium niobate without the use of sub-micron line widths," Proc. 1984 IEEE Ultrasonics Symp., Dallas, Texas, Vol. 1, pp. 93-96, 1984.

9. Rolf Huegli, " Harmonic GHz surface-acoustic-wave filters with unidirectional transducers," IEEE Trans. Ultrason., Ferroelec., Freq. Contr., Vol. 40, No. 3, pp.177-182, May 1993.

10. K. Anemogiannis et al, " GHz low-loss SAW filters employing standard fabrication process," Proc. IEEE 1990 Ultrason. Symp., pp.129-133.

11. S. Shikata et al, " 1.5 GHz SAW bandpass filter using poly-crystalline diamond," IEEE 1993 Ultrason. Symp., pp. 277-280.

12. K.Yamanouchi, "GHz-range SAW device using nano-meter electrode fabrication technology", IEEE 1994 Ultrason. Symp., pp. 421-428, 1994.

13. W.H. Brunger et al, " Fabrication of 3.5 GHz surface acoustic wave filters by ion projection lithography," Microelectronic Engineering 17, pp. 245-248, 1992.

14. K.Tomotsune et al, "Development of quarter-micron SAW Devices using X-ray

lithography and ECR-RIBE processes", NEC Res. & Development, no.95, pp.15-20, 1989.

15. D.P. Morgan, Surface-Wave Devices for Signal Processing, pp. 15-52, Elsevier, 1985.

16. R.H. Tancrell and M.G. Holland, " Acoustic surface wave filters", Proc. IEEE 59, 393-409, 1971.

17. C.S.Hartmann, "Weighting interdigital surface wave transducers by selective withdrawal of electrodes", IEEE 1973 Ultrason. Symp., pp.423-426.

18. L.R.Rabiner and B.Gold, "Theory and Application of Digital Signal Processing", Prentice-Hall, Englewood Cliffs, pp.88-105, 1975.

19. C. Campbell, "Surface Acoustic Wave Devices and Their Signal Processing Applications", Academic Press, Inc., p.40, 1989.

20. J.H.McClellan, T.W.Parks and L.R. Rabiner, " A computer program for designing optimum FIR linear phase digital filters," IEEE Transactions on Audio and Electroacoustics, vol. AU-21, pp.506-526, 1973.

21. M.Hikita et al, " Investigation of New Low-Loss and High-Power SAW Filters for Reverse-Frequency-Allocated Cellular Radios", IEEE Trans. on Ultr., ferr. and freq. contr., Vol. 40, No.3, pp. 224-230, May, 1993.

22. K.Anemogiannis, et al, "High Performance Low-Loss SAW Filters for Mobile Radio with Improved Stopband Rejection", IEEE 1988 Ultrason. Symp. pp 77-82.

23. C.S.Hartmann, W.S.Jones, and H.Vollers, " Wide band unidirectional surface wave transducers", IEEE Trans. SU-19, pp378-381, 1972.

24. R.S.Rosenfeld, C.S.Hartmann and R.B.Brown, "Low loss unidirectional acoustic wave filters", Ann. Symp. Freq. Contr., pp.299-303, 1974.

25. K.Yamanouchi, F.M.Nyffeler, and K.Shibayama, "Low insertion loss acoustic surface wave filter using group-type unidirectional interdigital transducer", Ibid., pp. 317-321, 1975.

26. D.C. Malocha and B.J.Hunsinger, "Tuning of group type unidirectional transducers", IEEE Trans. SU-26, pp. 243-245, 1979.

27. K.Yamanochi, T.Meguro, and J.K.Gautam, " Low-loss GHz range SAW filter using group-type unidirectional transducer - new GUDT and phase shifter", IEEE 1982 Ultrason. Symp., vol.1, pp. 212-217.

28. R.C.Bray, J.P.Grubb, and W.Ishak, " SAW filters using group-type uindirectional transducers: source of problems", IEEE 1982 Ultrason. Symp., vol.1, pp. 227-232.

29. J.Ebneter, "A new design of group-type unidirectional transducers", IEEE 1984 Ultrason. Symp., vol.1, pp.22-25.

30. K.Shibayama, K.Yamanouchi, H.Sato, and T. Meguro, "GHz band SAW filter using Group-Type Unidirectional Transducer", IEEE Trans. Vol. SU-28, No.2, pp. 91-95, March 1981.

31. C.S.Hartmann, P.V.Wright, R.J.Kansy, and E.M.Garber, " An analysis of SAW IDT's with internal reflections and the application of the design to single-phase unidirectional transducers", IEEE 1982 Ultrason. Symp., pp. 40-45.

32. M.F.Lewis, "Low loss SAW devices employing single stage fabrication", IEEE 1983 Ultrason. Symp., vol. 1, pp. 104-108.

33. K.Yamanouchi and H.Furuyashki, " Low-loss SAW filters using internal reflection types of new single-phase unidirectional transducers", IEEE 1984 Ultrason. Symp., vol. 1, pp.68-71.

34. C.K.Campbell and C.B.SAW, " Analysis and design of low-loss SAW filters using single-phase unidirectional transducers", IEEE Trans. UFFC-34, pp. 357-366, 1987.

35. M.F.Lewis, "SAW filters employing interdigitated interdigital transducers, IIDT", IEEE 1982 Ultrasona. Symp., vol.1, pp. 12-17.

36. M.Hikita, et al, "High performance SAW filters with several new technologies for cellular radio", IEEE 1984 Ultrason. Symp., pp.82-92.

37. K.Anemogiannis, et al, "High performance low-loss SAW filters for mobile radio with improved stopband rejection", IEEE 1988 Ultrason. Symp., pp. 77-82.

38. H.Yatsuda, et al, "IIDT type low-loss SAW filters with improved stopband rejection in the range of 1 to 2GHz", IEEE 1992 Ultrason. Symp, pp. 67-70.

39. P.M.Smith and C.K.Campbell, "A theoretical and experimental study of low-loss SAW filters with interdigitated interdigital transducers", IEEE Trans. UFFC, vol.36, No.1, pp.10-15, 1989.

40. H.Ohnuki, et al, "Computer aided design of low-loss SAW filters employing IIDT for high performance mobile radio duplexer", IEEE 1990 Ultrason. Symp., pp. 123-127.

41. M.F.Lewis et al, "Recent developments in SAW devices", IEE proceedings, vol.131, Pt.A, No. 4, June, pp.186-216, 1984.

42. "SAW bandpass filters", Handbook of Acoustic Signal Processing, vol.1, Andersen Laboratories, Bloomfield, Connecticut, P.4.

43. W.R. Smith et al, "Analysis of Interdigital Surface Wave Transducers by Use of an Equivalent Circuit Model", IEEE Trans. MTT-17, No.11, pp. 856-864, 1969.

44. W.R. Smith et al, "Analysis and Design of Dispersive Interdigital Surface-Wave Transducers", IEEE Trans. MTT-20, No.7, pp. 458-471, 1972.

45. C.S. Hartmann et al, " Impulse response model design of acoustic surface wave filters", IEEE Trans. MTT-21, pp.162-175, 1973.

46. W.R.Smith, "Key tradeoffs in SAW transducer design and component specification", 1976 IEEE Ultra. Symp. Proc. , pp 547-552.

47. W.R.Smith, "Computer-aided design of surface acoustic wave devices", pp26-63, Elsevier scienfific pub., Co., 1976.

48. W.R.Smith and W.F.Pedler, "Fundamental and harmonic-frequency circuit model analysis of interdigital transducers with arbitrary metallization ratios and polarity sequences", IEEE Trans. MTT-23, pp.853-964, 1975.

49. S. Datta, Surface Acoustic Wave Devices, Prentice-Hall, Englewood Cliffs, P.128, 1986.

50. N.H.E. Weste and K. Eshraghian, Principles of CMOS VLSI Design, second edition, Addison-wesley pub., p 206, 1994.

51. R.H.Tancrell, "Principles of surface wave filter design", in H.Matthews (ed), Surface Wave Filters, John Wiley and Sons, New York, Chpater 3, 1977.

52. M.B.Schulz and J.H.Matsinger, "Rayleigh wave electromechanical coupling constant", Appl. Phys. Lett., Vol. 20, p.367, 1972.

53. A.J.Slobodnik, "Materials and their influence on performance", in A.A. Oliner(ed), Acoustic Surface Waves, Topics in Applied Physics, Vol.24, Speinger-Verlag, New York, Chapter 6, 1978.

54. L.F.Thompson," An introduction to lithography", ACS Symposium Series, Vol. 219, p.67, 1988.

55. Geraint Owen, "Introduction to Electron-Beam Lithography", SC01, SPIE 1996 Symposium on Microlithography, 10-15, March 1996.

56. Owen G. and Rissman P., J. Appl. Phys., 54 (6), pp. 3573-81, 1983.

57. E.D. Roberts, "Recent developments in electron resists", Solid State Technology, June, pp. pp.135-141, 1984.

58. J.C. Nabity, Nanometer pattern generation system, version 7.4, release 3/94.

59. R. Bobkowski, E-beam laboratory data book, U of A, 1995.

60. PMMA resist, KTI Chemicals, 1178 Sonora Court, Sunnyvale, CA 94086.

61. Stereoscan 250 SEM operational instructions, Cambridge Instruments Limited, Issue 2, March 1981.

62. Kenji Harafuji et al, " A novel hierarchical approach for proximity effect correction in electron beam lithography," IEEE Transactions on computer-aided design of integrated circuits and systems," Vol.12, No. 10, pp1508-1514, October 1993.

63. Geraint Owen, " Proximity effect correction in electron-beam lithography," Optical Engineering, Vol. 32, No. 10, pp2446-2451, 1993.

64. M.D. Levenson, "SEMATECH's 193nm symposium raises hopes for optical lithography", Solid State Technology, October 1995, pp54-56.

65. M. C. Peckerar, " X-ray Lithography-An overview," Proc. IEEE Vol. 81, No. 9, pp 1249-1274, 1993.

66. Franco Cerrina, "X-ray lithography", short course note, SPIE's 1996 Symposium on Microlithography, 10-15, March 1996, Santa Clara, CA, USA.

67. R. Fedosejevs, R.Bobkowski, J.N.Broughton and B.Hardwood "Kev X-ray source based on high repetition rate excimer laser-produced plasmas", SPIE Proc. Vol. 1671, pp373-382, 1992.

68. J.N.Broughton and R. Fedosejevs, "1 keV X-ray production using 50mJ KrF laser produced plasmas at 1 and 100 picoseconds", J.Appl. Phys., vol 74, pp3712-3723, 1993.

69. Raymond. K. Tam, "Characterization of a high sensitivity X-ray resist and resultant process latitude", M.Sc thesis, Department of Electrical Engineering, University of Alberta, Edmonton, Alberta, Canada, 1994.

70. R. Bobkowski, X-ray laboratory data book, U of A, 1995.

71. R. Bobkowski, Y. Li, J.N. Broughton, and R.Fedosejevs, "Fabrication of the 0.25 μm electrode width SAW filters using x-ray lithography with a laser-plasma source," SPIE Symp. on Microlithography, March 10-15, 1996, Santa Clara, US.

72. RT/duroid Microwave Laminates data book, Microwave and Circuit Materials Division, Rogers Corporation, Chandler, AZ 85226.

73. B.C. Wadell, Transmission Line Design Handbook, Artech House, pp.199-207, 1991.

74. R.B.Bobkowski, 1 μm and 0.5 μm SAW filter data book, U of A, 1995.

75. J. Gore et al, " Low-Cost Surface Mount Packaging for SAWs", 1992 IEEE Ultra. Symp., pp. 129-138.

76. Kazuo Eda, et al, " Flip-Chip Bonding Technology Fabricates GHz-Band SAW Filters", JEE, pp. 36-40, December, 1993.

Appendix 1 The SAW Filter Layout Generating Program-SAWF.BSC

```
' This program should be run in DesignCAD and will produce a submicron split-finger
'SAW filter pattern for E-beam writing. The program was modified by Yunlei Li in June,
'1996, based on Jim Hawreliak and Romuald Bobkowski's previous work.

' Please input the SAW parameters you designed.

INPUT "Width of the saw:", WIDTH
INPUT "The feature size of the filter in micron:", D
INPUT "The number of finger pairs of input IDT:", Ni
INPUT "The number of finger pairs of output IDT:", Nout
INPUT "Aperture of the IDT:", APERTURE

'Set current layer to 1, and color 1
LAYER(1) = 2
>COLOR 2

'Set a dump site at the origin
'       >SETDUMP
        >POINTXY [0,0]
        >
'As a design rule, keep the center to center spacing of the input IDT
' and the output IDT to be 100 Lamda(the wavelength)apart, so the spacing
'of the filter center to the edges of both IDTs DS, instead of 50 used in
'the previous programs.

DS=0.5*(100*4*D-0.5*Ni*8*D-0.5*Nout*8*D)

' Drawing the edge pieces of the input IDT
' Length of the input saw IDT`
Li=8*Ni*D
XVAL=-(WIDTH/2)
FOR J = 1 to 20
        >POINTXY [XVAL, Li+DS]
        >POINTXY [XVAL, DS]
        XVAL = XVAL-.25
        >POINTXY [XVAL, DS]
        >POINTXY [XVAL, Li+DS]
        XVAL=XVAL-.25
NEXT
>LINE
XVAL=WIDTH/2
FOR J = 1 TO 20
        >POINTXY [XVAL, Li+DS]
```

```
        >POINTXY [XVAL, DS]
        XVAL = XVAL+.25
        >POINTXY [XVAL, DS]
        >POINGXY [XVAL, Li+DS]
        XVAL=XVAL+.25
NEXT
>LINE

'Draw in the teeth of the input IDT'

XVAL = -WIDTH/2
YVAL = Li+DS
EXTRA = WIDTH/2 - APERATURE/2
'To compensate for the proximity effect, the outer parts on both sides of
'the IDT should receive more doses than the center fingers'

'Draw the fingers in the outer parts of IDT'
>COLOR 1
FOR J = 1 TO 4
FOR I = 1 TO 2
        XVAL = -WIDTH/2
        >POINTXY [XVAL, YVAL]
        >POINTXY [WIDTH/2-EXTRA, YVAL]
        >POINTXY [XVAL, YVAL]
        >POINTXY [WIDTH/2-EXTRA, YVAL]
        >POINTXY [XVAL, YVAL]
        >LINE
        YVAL = YVAL - 2*D
NEXT
FOR I = 1 TO 2
        XVAL = WIDTH/2
        >POINTXY [XVAL, YVAL]
        >POINTXY [-WIDTH/2+EXTRA, YVAL]
        >POINTXY [XVAL, YVAL]
        >POINTXY [-WIDTH/2+EXTRA, YVAL]
        >POINTXY [XVAL, YVAL]
        >LINE
        YVAL = YVAL - 2*D
NEXT
NEXT
'Draw the center fingers'
>COLOR 3
FOR J = 1 TO (Ni-8)
FOR I = 1 TO 2
        XVAL = -WIDTH/2
```

```
        >POINTXY [XVAL, YVAL]
        >POINTXY [WIDTH/2-EXTRA, YVAL]
        >POINTXY [XVAL, YVAL]
        >POINTXY [WIDTH/2-EXTRA, YVAL]
        >POINTXY [XVAL, YVAL]
        >LINE
        YVAL = YVAL - 2*D
NEXT
FOR I = 1 TO 2
        XVAL = WIDTH/2
        >POINTXY [XVAL, YVAL]
        >POINTXY [-WIDTH/2+EXTRA, YVAL]
        >POINTXY [XVAL, YVAL]
        >POINTXY [-WIDTH/2+EXTRA, YVAL]
        >POINTXY [XVAL, YVAL]
        >LINE
        YVAL = YVAL - 2*D
NEXT
NEXT

'Draw the other side fingers'
>COLOR 1
FOR J = 1 TO 4
FOR I = 1 TO 2
        XVAL = -WIDTH/2
        >POINTXY [XVAL, YVAL]
        >POINTXY [WIDTH/2-EXTRA, YVAL]
        >POINTXY [XVAL, YVAL]
        >POINTXY [WIDTH/2-EXTRA, YVAL]
        >POINTXY [XVAL, YVAL]
        >LINE
        YVAL = YVAL - 2*D
NEXT
FOR I = 1 TO 2
        XVAL = WIDTH/2
        >POINTXY [XVAL, YVAL]
        >POINTXY [-WIDTH/2+EXTRA, YVAL]
        >POINTXY [XVAL, YVAL]
        >POINTXY [-WIDTH/2+EXTRA, YVAL]
        >POINTXY [XVAL, YVAL]
        LINE
        YVAL = YVAL - 2*D
NEXT
NEXT
```

```
>COLOR 5
XVAL = -WIDTH/2
YVAL = Li+DS
EXTRA = WIDTH/2 - APERATURE/2
FOR J = 1 TO Ni
FOR I = 1 TO 2
        XVAL = -WIDTH/2
        >POINTXY [XVAL,YVAL]
        >POINTXY [XVAL+(EXTRA-1), YVAL]
        >POINTXY [XVAL, YVAL]
        >POINTXY [XVAL+(EXTRA-1),YVAL]
        >POINTXY [XVAL, YVAL]
        >LINE
        YVAL = YVAL - 2*D
NEXT
FOR I = 1 TO 2
        XVAL = WIDTH/2
        >POINTXY [XVAL,YVAL]
        >POINTXY [XVAL-(EXTRA-1), YVAL]
        >POINTXY [XVAL, YVAL]
        >POINTXY [XVAL-(EXTRA-1),YVAL]
        >POINTXY [XVAL, YVAL]
        >LINE
        YVAL = YVAL - 2*D
NEXT
NEXT

' Drawing the edge pieces of the output IDT
' Length of the output saw IDT'
Lout=8*Nout*D
XVAL=-(WIDTH/2)
>COLOR 2
FOR J = 1 TO 20
        >POINTXY [XVAL,-(Lout+DS)]
        >POINTXY [XVAL,-DS]
        XVAL = XVAL-.25
        >POINTXY [XVAL,-DS]
        >POINTXY [XVAL,-(Lout+DS)]
        XVAL=XVAL-.25
NEXT
>LINE
XVAL=WIDTH/2
FOR J = 1 TO 20
        >POINTXY [XVAL,-(Lout+DS)]
        >POINTXY [XVAL,-DS]
```

```
        XVAL = XVAL+.25
        >POINTXY [XVAL,-DS]
        >POINTXY [XVAL,-(Lout+DS)]
        XVAL=XVAL+.25
NEXT
>LINE

' Draw in the teeth of the output IDT'

XVAL =-WIDTH/2
YVAL = -(Lout+DS)
EXTRA = WIDTH/2 -APERATURE/2
 'To compensate for the proximity effect, the outer parts on both sides of
'the IDT should receive more doses than the center fingers'

'Draw the fingers in the outer parts of IDT'
>COLOR 1
FOR J = 1 TO 2
FOR I = 1 TO 2
        XVAL = -WIDTH/2
        >POINTXY [XVAL, YVAL]
        >POINTXY [WIDTH/2-EXTRA, YVAL]
        >POINTXY [XVAL, YVAL]
        >POINTXY [WIDTH/2-EXTRA, YVAL]
        >POINTXY [XVAL, YVAL]
        >LINE
        YVAL = YVAL + 2*D
NEXT
FOR I = 1 TO 2
        XVAL = WIDTH/2
        >POINTXY [XVAL, YVAL]
        >POINTXY [-WIDTH/2+EXTRA, YVAL]
        >POINTXY [XVAL, YVAL]
        >POINTXY [-WIDTH/2+EXTRA, YVAL]
        >POINTXY [XVAL, YVAL]
        >LINE
        YVAL = YVAL + 2*D
NEXT
NEXT
'Draw the center fingers'
>COLOR 3
FOR J= 1TO (Nout-4)
FOR I = 1 TO 2
        XVAL = -WIDTH/2
        >POINTXY [XVAL, YVAL]
```

```
        >POINTXY [WIDTH/2-EXTRA, YVAL]
        >POINTXY [XVAL, YVAL]
        >POINTXY [WIDTH/2-EXTRA, YVAL]
        >POINTXY [XVAL, YVAL]
        >LINE
        YVAL = YVAL + 2*D
NEXT
FOR I = 1 TO 2
        XVAL = WIDTH/2
        >POINTXY [XVAL, YVAL]
        >POINTXY [-WIDTH/2+EXTRA, YVAL]
        >POINTXY [XVAL, YVAL]
        >POINTXY [-WIDTH/2+EXTRA, YVAL]
        >POINTXY [XVAL, YVAL]
        >LINE
        YVAL = YVAL + 2*D
NEXT
NEXT
'Draw the other side fingers'
>COLOR 1
FOR J = 1 TO 2
FOR I = 1 TO 2
        XVAL = -WIDTH/2
        >POINTXY [XVAL, YVAL]
        >POINTXY [WIDTH/2-EXTRA, YVAL]
        >POINTXY [XVAL, YVAL]
        >POINTXY [WIDTH/2-EXTRA, YVAL]
        >POINTXY [XVAL, YVAL]
        >LINE
        YVAL = YVAL + 2*D
NEXT
FOR I = 1 TO 2
        XVAL = WIDTH/2
        >POINTXY [XVAL, YVAL]
        >POINTXY [-WIDTH/2+EXTRA, YVAL]
        >POINTXY [XVAL, YVAL]
        >POINTXY [-WIDTH/2+EXTRA, YVAL]
        >POINTXY [XVAL, YVAL]
        >LINE
        YVAL = YVAL + 2*D
NEXT
NEXT

XVAL =-WIDTH/2
YVAL = -(Lout+DS)
```

```
EXTRA = WIDTH/2 -APERATURE/2
>COLOR 5
FOR J = 1 TO Nout
FOR I = 1 TO 2
        XVAL = -WIDTH/2
        >POINTXY [XVAL,YVAL]
        >POINTXY [XVAL+(EXTRA-1), YVAL]
        >POINTXY [XVAL, YVAL]
        >POINTXY [XVAL+(EXTRA-1),YVAL]
        >POINTXY [XVAL, YVAL]
        >LINE
        YVAL = YVAL + 2*D
NEXT
FOR I = 1 TO 2
        XVAL = WIDTH/2
        >POINTXY [XVAL,YVAL]
        >POINTXY [XVAL-(EXTRA-1), YVAL]
        >POINTXY [XVAL, YVAL]
        >POINTXY [XVAL-(EXTRA-1),YVAL]
        >POINTXY [XVAL, YVAL]
        >LINE
        YVAL = YVAL + 2*D
NEXT
NEXT

REGEN
>ZOOM 0
END
```

Appendix 2 Stereoscan SEM 250 Operating Procedures for E-beam Writing

A2.1 Initial Preparation

1. Pattern run file: draw the pattern layout using DesignCAD, and then run MRF to create the pattern run file, and set run file parameters.

2. SEM adjustment: adjust the filament current, final aperture and astigmatism of the SEM following the Cambridge Stereoscan SEM 250 Manual.

3. E-beam writing tools: a clean Aluminum stub with a scratch cross, a sample box containing clean Aluminum stubs, tweezers, pencils, a bottle of carbon paste, Aluminum foil, a screw driver for mounting the sample onto the SEM stage.

A2.2 E-beam Writing Procedures

1. Enter E-beam lithography room at AMC, close the door, fluorescent light off, and yellow light on. Turn on the computer and printer.

2. Paste mask substrates onto Aluminum stubs with the carbon paste. Make pencil marks on the samples to produce small dirt marks for the purpose of the SEM focusing.

3. SEM vacuum off, close the isolation valve, unlock SEM chamber door and wait till the SEM chamber can be opened.

4. Mount the Aluminum stub with the scratched cross first, then mount the samples to the left of the Aluminum stub.

5. Close SEM door, vacuum on, and open the isolation valve till the chamber vacuum light is on (green).

6. Press DAY (SEM on), open the detector interlock (forward to open), then press FILAMENT button on (green), and EHT button on (green).

7. Check SEM setting: SEM voltage-40 kV, filament current -3.2 A, magnification-200X, spot size (resolution)-11, beam mode-focus normal, beam scanning-TV mode.

8. Adjust the stage flatness: rotate the stage to bring a hole on the stage into the center of the screen, move the stage all the way up, turn coarse focus and fine focus to get a clear view of the hole. Adjust the stage tilt knob until the hole appears circular and symmetric.

9. SEM focusing: rotate the stage to bring the Aluminum stub with the cross into view, find a small object with a sharp edge and focus on it. Increase the magnification and keep on focusing. You will find that it is difficult to focus under a very high magnification. In this case, switch the beam scanning from TV mode to normal raster to get a more clear view, adjust the fine focus knob to focus again. Get good focusing of the small object under a magification of 30K or higher.

10. E-beam current measurement: turn on the Fluke Meter and push the "grey" button to increase its accuracy. With the SEM still focusing on that small object under 30K or higher, adjust the E-beam current by turning the fine spot size knob. The current is related to the Fluke Meter voltage by:

$$I\,(pA) = \text{voltage}\,(mv)*100 / 0.994 - 34.53$$

Or, you can read the table pasted on the SEM panel to find out the current values corresponding to the voltages. Set the E-beam current which you want.

11. Align the sample on the screen: rotate the stage and move it in X and Y directions to bring the mask sample into view, and adjust its sides parallel to the sides of the monitor screen, and focus on some dirt marks on the four edges to check if the sample is flat. If not , go back to step 8.

12. Coordinate measurement: Move the corners of the sample to the center of the screen and measure their X and Y coordinates, respectively. Calculate the mask center position, which is where the pattern will be written.

13. Move the stage to somewhere in the vicinity of the sample center, find a very small object and focus on it. This is to ensure the SEM is well focused in the center region, and this is very important because it will directly affect the quality of the pattern on the mask. If it is very difficult to find a focusing object under a high resolution, decrease the resolution to find one and increase the resolution back and focus. It is suggested that it is better to move the beam to approach the center from the Y direction.

14. Ready for writing: set the beam scanning to TV mode, VIDEO switch off, SEM/NPGS switch to NPGS. Run DAC0 4 on the computer to move the electron beam out of the center. Set the magnification to the value under which the pattern will be

written (e.g. 1000X), rotate the scan rotation knob 2.5^0 clockwise to correct the pattern orientation.

15. Writing the pattern: Move the stage to the mask center. Run MRF and check or set the parameters in the pattern run file: Center to center distance, Line spacing, magnification, beam current, exposure doses, etc. When everything is ready, keep yourself comfortable and not moving, and press the space bar to start writing.

16. When the pattern writing has been finished, move the beam to the sample edge. Switch SEM/NPGS to SEM, VIDEO switch on. Turn off the EHT and FILAMENT (both yellow), close the detector interlock. Turn off the SEM by pressing DAY.

17. Open the SEM door following step 3. Take the samples out of the SEM chamber and put them into the sample box, wrap the box with a piece of Aluminum foil. Before you leave for developing the samples, turn the SEM chamber vacuum on following step 5, and turn off the computer.